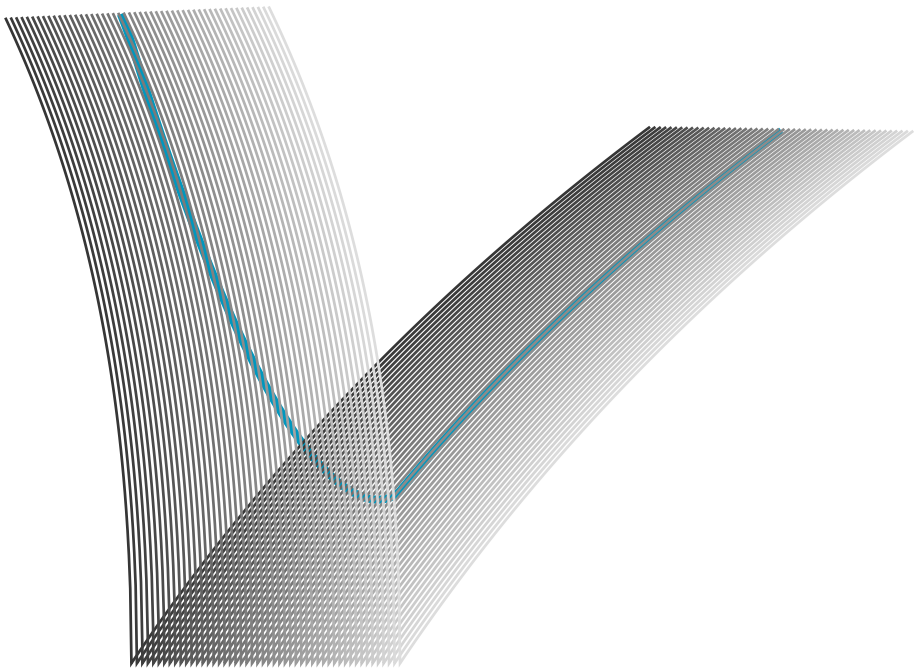


Looking for Stability

Advances on spectrum-based stability and stabilization of uncertain linear time-delay systems

Luca Fenzi



Dissertation presented in partial fulfillment of the requirements for the degree of Doctor of Engineering Science (PhD): Computer Science

February 2020

LOOKING FOR STABILITY

*Advances on spectrum-based stability and stabilization of
uncertain linear time-delay systems*

Luca Fenzi

February 2020

*Dissertation presented in partial fulfillment of the requirements for
the degree of Doctor of Engineering Science (PhD): Computer Science*

Supervisor:

Prof. dr. ir. W. Michiels

Members of the Examination Committee:

Prof. dr. ir. O. Van der Biest (chairman)

Prof. dr. ir. D. Nuyens

Prof. dr. ir. G. Pipeleers

Prof. dr. T. Vyhldal

Dr. rer. nat. M. Voigt

© 2020 KU Leuven – Faculty of Engineering Science
Uitgegeven in eigen beheer, Luca Fenzi, Celestijnenlaan 200A box 2402, B-3001 Leuven (Belgium)

Alle rechten voorbehouden. Niets uit deze uitgave mag worden vermenigvuldigd en/of openbaar gemaakt worden door middel van druk, fotokopie, microfilm, elektronisch of op welke andere wijze ook zonder voorafgaande schriftelijke toestemming van de uitgever.

All rights reserved. No part of the publication may be reproduced in any form by print, photoprint, microfilm, electronic or any other means without written permission from the publisher.

«Io non ho la minima idea di cosa possano essere la bellezza o l'eleganza in una formula matematica, ma so riconoscere queste qualità nelle montagne e nelle linee che si possono seguire per scalarle.»

ERMANNNO SALVATERRA
In Insieme in Vetta. Le cordate famose e le loro imprese,
of A. Gogna and A. Raggio

ACKNOWLEDGEMENTS

The work behind this PhD thesis would not have been possible without the support, the guidance, and the help that I received from many people. In these few lines I would like to thank the most important.

Wim, thank you for guiding me through the PhD, demanding a high quality of work and assisting me in writing this thesis. I will always remember your enthusiasm in doing research and our meetings, when you taught me how to tackle problems in a structured way. I am grateful for your support, your advice, and for carefully proofreading all my papers, also in the weekends.

I would like to thank all the jury members for accepting to take part in the examination committee, for carefully reading my PhD thesis, and for all the questions, feedback and suggestions. I thank *Prof. O. Van der Biest* for chairing the defense, *Dirk* and *Goele* for their assistance during my PhD, *Tomas* and *Matthias* for the extensive discussion during the preliminary defense. I would also like to thank *Tomas* together with *Dan* for their collaboration, and for finding interesting engineering applications.

I am grateful to my research team, *Koen*, *Pieter*, *Deesh*, *Libo*, *Haik*, *Kirill*, *Dan*, *Alexey*, *Marco*, *Yanling*, and *Francesco*. Thanks for sharing your expertises and ideas during our weekly group lunch, and also for the spare time spent together. I will always remember the running and cycling activities with *Koen* and *Pieter*, the driving lessons with *Libo*, and the teaching duties shared with *Deesh*. Thank you, *Francesco*, for standing by me through thick and thin.

I would like to express my gratitude to the time-delay group in Udine. *Rossana*, thank you for motivating me pursuing the research on time-delay systems, for your excellent guidance during the master thesis, and for introducing me to the polynomial chaos theory. *Francesca* and *Davide*, thanks to enlighten me on the more abstract aspects of the time-delay system theory and for the joyful moments at the workshops.

I would like to thank the *NUMA group* and *SIAM student chapter KU Leuven* for organizing interesting activities. I am grateful for the discussions at the coffee breaks and the enjoyable dinners with all of you. In particular, I would like to thank my office mates. *Adrian* and *Francesco*, thank you for your research advice and for your lessons on the Football tournaments. *Julian*, thank you for your precious advice on how to present.

Thanks to all the people who made my stay in Belgium enjoyable. I would like to thank *KU Leuven Photography group* and *Principiæ* for stimulating my creativity. Special thanks go to my Italian family in Leuven *Steve*, *Dario*, *Greta*, and *Monica*, who made me feel at home; quoting *Steve's* PhD thesis: "during these years, we shared fun and exciting times as well as less-positive moments, which have allowed us to build a solid friendship."

I would like to thank the friends spread around Europe, who supported me even if we rarely see each other. I would like to thank *la compa* and the friends from Udine University for being a fixed point when I passed by Italy. Special mentions go to *Simonetti* and to *Grasso*. *Simonetti*, thank you for carefully proofreading my first articles, and for always remembering me how beautiful the mountains are, especially the ones near Moggio. *Grasso*, thanks for comforting me in the academic life and to always showing me how useful mathematics is in applications.

I would like to thank *my family*, *Valentina's parents* and my officially cohabiting *girlfriend*, for always being near me in the difficult and joyful moments. You are very important to find my balance again, especially in periods of high pressure and stress. In particular, this thesis would not have been possible without the loving care of *Vale*, who moved to Belgium with me.

Luca
Lovanio
January 2020

To my stability, Valentina.

ABSTRACT

Time-delay systems model widespread phenomena, ranging from life sciences and economics to natural sciences and engineering. We focus on linear time-delay systems of time-invariant and periodic type, whose stability properties can be inferred from the spectrum of infinite-dimensional operators. Indeed, the asymptotic growth or decay rate of the solutions towards zero can be determined by the spectral radius of the monodromy operator, or the spectral abscissa of the infinitesimal generator associated with the time-invariant time-delay system. The optimization of these stability measures with respect to system parameters permits to stabilize an unstable system and/or to increase the decay rate of the solutions towards zero.

This thesis aims to develop and analyze accurate and reliable numerical methods for the stability assessment and stabilization of linear time-delay systems, validating the efficiency of the novel methodologies on numerical examples and engineering applications. The main contributions follow two research directions. First, we consider linear time-invariant time-delay systems, whose parameters are affected by uncertainties, modeled by a random vector. Second, we present stability assessment and stabilization methods for linear periodic time-delay systems, where the period and delays are commensurable.

The spectral abscissa of a time-invariant time-delay system, whose uncertainties are modeled by a random vector, is a random variable, and admits a polynomial chaos expansion. Other than explaining the parallelism between the polynomial chaos and the polynomial approximation theories, we systematically demonstrate that the lack of smoothness properties of the spectral abscissa heavily affects polynomial approximation methods. The insights on the behavior of the spectral abscissa, which can be generalized to the behavior of the spectral radius of periodic time-delay systems, also play a role in the development of novel stability optimization methods.

The novel stability optimization method, handling the uncertainty, considers as objective function the mean of the spectral abscissa with a variance penalty. Compared to the optimization of the spectral abscissa for the nominal model, the novel approach shows better robustness properties, and, in contrast to worst-case analysis, furnishes more realistic results, exploiting a probabilistic description of the uncertainties.

Moreover, we develop novel stability assessment and stabilization methods for time-delay systems, whose delays and period are commensurate numbers. For these systems, the spectral radius can be not only inferred from the monodromy operator but also from the eigenvalues of a characteristic matrix, whose evaluation involves solving an initial value problem. The exploitation of this characteristic matrix provides three main contributions. Firstly, we propose a novel two-stage approach for the stability assessment, which iteratively refines the accuracy of the spectral radius obtained by the discretization of the monodromy operator. Secondly, we prove a

characterization of left eigenvectors of the characteristic matrix in terms of right eigenfunctions of the monodromy operator associated with a dual periodic time-delay system. As a third contribution, we derive from the characteristic matrix a formula to compute the derivatives of the spectral radius with respect to parameters, which is adopted in a spectrum-based stabilization method.

SAMENVATTING

Tijdsvertragingssystemen model wijdverspreide fenomenen, variërend van life sciences en economie tot natuurwetenschappen en engineering. We richten ons op lineaire tijdvertragingssystemen van het tijdinvariante en periodieke type, waarvan de stabiliteitseigenschappen kunnen worden afgeleid uit het spectrum van oneindig-dimensionale operatoren. Inderdaad, de asymptotische stijging of daling van de oplossingen dichtbij nul kan worden bepaald door de spectrale straal van de monodromie-operator, of de spectrale abscis van de infinitesimale generator geassocieerd met het tijdinvariante tijdvertragingssysteem. De optimalisatie van deze stabiliteitsmaatregelen met betrekking tot systeemparemeters maakt het mogelijk om een onstabiel systeem te stabiliseren en/of de vervalsnelheid van de oplossingen naar nul te verhogen.

Dit proefschrift beoogt de ontwikkeling en analyse van nauwkeurige en betrouwbare numerieke methoden voor de stabiliteitsbeoordeling en stabilisatie van lineaire tijdvertragingssystemen, waarbij de efficiëntie van de nieuwe methoden met numerieke voorbeelden en technische toepassingen wordt gevalideerd. De belangrijkste bijdragen volgen twee onderzoeksrichtingen. Eerst beschouwen we lineaire tijdinvariante tijdvertragingssystemen, waarvan de parameters worden beïnvloed door onzekerheden, gemodelleerd door een willekeurige vector. Ten tweede presenteren we stabiliteitsbeoordeling en stabilisatiemethoden voor lineaire periodieke tijdvertragingssystemen, waarbij de periode en vertragingen evenredig zijn.

De spectrale abscis van een tijdinvariant tijdvertragingssysteem, waarvan de onzekerheden worden gemodelleerd door een willekeurige vector, is een willekeurige variabele en laat een polynomiale chaosbenadering toe. Anders dan het verklaren van het parallelisme tussen de polynomiale chaos en de polynomiale benaderingstheorieën, tonen we systematisch aan dat het gebrek aan gladheidseigenschappen van de spectrale abscis de polynoombenaderingsmethoden sterk beïnvloedt. De inzichten over het gedrag van de spectrale abscis, die kunnen worden gegeneraliseerd naar het gedrag van de spectrale straal van periodieke tijdvertragingssystemen, spelen ook een rol bij de ontwikkeling van nieuwe methoden voor stabiliteitsoptimalisatie.

De nieuwe stabiliteitsoptimalisatiemethode, die omgaat met de onzekerheid, beschouwt als objectieve functie het gemiddelde van de spectrale abscis met een term die het hebben van een hoge variantie afstraft. Vergeleken met de optimalisatie van de spectrale abscis voor het nominale model, vertoont de nieuwe benadering betere robuustheidseigenschappen en levert, in tegenstelling tot de worst-case-analyse, realistischere resultaten, waarbij gebruik wordt gemaakt van een probabilistische beschrijving van de onzekerheden.

Bovendien ontwikkelen we nieuwe stabiliteitsbeoordelings en stabilisatiemethoden voor tijdvertragingssystemen, waarvan de vertragingen en periode evenredig zijn. Voor deze systemen kan de spectrale straal niet alleen worden afgeleid uit de monodromie-operator, maar ook uit de eigenwaarden van een karakteristieke matrix, waarvan de evaluatie het oplossen van een beginwaardeprobleem inhoudt. De exploitatie van deze karakteristieke matrix levert drie belangrijke bijdragen. Ten eerste stellen we een nieuwe tweetrapsbenadering voor de stabiliteitsbeoordeling voor, die iteratief de nauwkeurigheid van de spectrale straal verfijnt die wordt verkregen door de discretisatie van de monodromie-operator. Ten tweede bewijzen we een karakterisering van linker eigenvectoren van de karakteristieke matrix in termen van rechter eigenfuncties van de monodromie-operator geassocieerd met een dubbel periodiek tijdvertragingssysteem. Als derde bijdrage leiden we uit de karakteristieke matrix een formule af om de afgeleiden van de spectrale straal met betrekking tot parameters te berekenen, die wordt gebruikt in een op spectrum gebaseerde stabilisatiemethode.

NOTATIONS

Related to time-delay system

r	System dimension
h	Number of delays
τ_j	j -th delay
T	Period
ω	Uncertain parameters, realization of the random vector ω
K	Controller parameters

Sets

\mathbb{N}	Natural numbers (zero included)
\mathbb{R}	Real numbers
\mathbb{R}_+	Non-negative real numbers
\mathbb{C}	Complex numbers
X	Time-delay system state space

Inner products and norms

$ \cdot $	Absolute value
$\langle \cdot, \cdot \rangle$	Euclidean inner product on a vector space
$\ \cdot\ _2$	2-norm, or Euclidean norm, on a vector space
$\ \cdot\ _1$	1-norm on a vector space
$\ \cdot\ _\infty$	Infinity norm on a vector space
$\langle \cdot, \cdot \rangle_w$	w-inner product
$\ \cdot\ _w$	w-norm
$\ \cdot\ _s$	Supremum norm, also known as L^∞ norm

Letter-based symbols

$\bar{\mu}$	Conjugate of a complex scalar μ
v^T, A^T	Transpose of a vector v and of a matrix A
v^*, A^*	Conjugate transpose of a vector v and of a matrix A
$\dot{x}(t)$	Derivative of x with respect to time
$\ddot{x}(t)$	Second derivative of x with respect to time
$\alpha'(\omega)$	Derivative of the function α at the point ω
$\alpha^{(k)}(\omega)$	k -th derivative of the function α at the point ω
$\tilde{\mathcal{A}}, \check{\mathcal{N}}$	Transposed characteristic matrices

Operators, spectral quantities and stability measures

$\mathcal{T}(t, t_0)$	Solution operator, with $t \geq 0$ and $t_0 \in \mathbb{R}$
\mathcal{U}	Monodromy operator
\mathcal{A}	Infinitesimal generator of the solution operators $\{\mathcal{T}(t, 0)\}_{t \geq 0}$
$\sigma(\cdot)$	Spectrum
μ	Floquet multipliers
λ	Eigenvalue/characteristic roots
ρ	Spectral radius of the monodromy operator, <i>stability measure</i>
α	Spectral abscissa of the infinitesimal generator, <i>stability measure</i>
\mathcal{A}	Characteristic matrix of autonomous time-delay system
\mathcal{N}	Characteristic matrix of periodic time-delay system

Related to the probabilistic framework

ω	Random vector
$\mathcal{U}(a, b)$	Random variable uniformly distributed in the real interval $[a, b]$
D	Stochastic dimension
w	Probability density function of the random vector ω (In chapter 2, denotes the polynomial basis weighting function)
Ω	Support of the random vector ω (In chapter 2, denotes the support of the weighting function w)
$\mathbb{E}(\omega)$	Expected value of the random vector ω
$\mathbb{V}(\omega)$	Variance of the random vector ω
κ	Trade-off parameter quantifying the variance penalty

Special constants

i	Imaginary unit
e	Euler's number
π	Archimedes' constant
I_n	Identity matrix of size $n \times n$
0	All-zero matrix of appropriate size
$0_{n \times m}$	All-zero matrix of size $n \times m$

Other

\otimes	Kronecker product
$\text{Re}(\cdot)$	Real part
$\text{Im}(\cdot)$	Imaginary part
$\lceil v \rceil$	Integer obtained by rounding $v \in \mathbb{R}$ towards infinity
$\lfloor v \rfloor$	Integer obtained by rounding $v \in \mathbb{R}$ towards minus infinity
$k \bmod N$	Remainder after division of the integer k by $N \in \mathbb{N} \setminus \{0\}$
\mathcal{O}	Landau notation

CONTENTS

1	INTRODUCTION	1
1.1	Preliminaries	2
1.2	Contributions	19
1.3	Outline	24
2	SMOOTHNESS PROPERTIES OF THE STABILITY MEASURE	27
2.1	Behavior of the spectral abscissa	28
2.2	Polynomial (chaos) expansion	31
2.3	Univariate polynomial approximation	34
2.4	Multivariate polynomial approximation	40
2.5	Beyond polynomial (chaos) approximations	49
3	PROBABILISTIC STABILITY OPTIMIZATION	53
3.1	Objective function, analysis & evaluation	56
3.2	Optimization problem	63
3.3	Numerical examples and applications	65
4	STABILITY AND STABILIZATION FOR PERIODIC DELAY SYSTEMS	81
4.1	Spectral properties	82
4.2	Stability assessment	87
4.3	Characterization of the left eigenvectors	95
4.4	Stability optimization	99
4.5	Numerical examples	101
4.6	Further remarks	109

5	CONCLUSIONS	115
5.1	Research results	115
5.2	Future perspectives	118
	BIBLIOGRAPHY	130
	CURRICULUM VITAE	131
	PUBLICATIONS AND SOFTWARES	132

INTRODUCTION

The PhD thesis starts presenting to the non-specialists the main motivation to study spectrum-based stability and stabilization for time-delay systems. Then, the preliminaries introduce the results and numerical methods on the stability of linear time-delay systems of periodic and time-invariant type, providing the basis for the development of the following sections and chapters. Based on these preliminaries, the main contributions of this thesis are briefly summarized, and compared with the state-of-the-art. This chapter ends schematically describing the overall structure of the thesis.

The experience helps us to find a long-lasting equilibrium, stable against the uncertainty that we will face in the future. In a similar way, this thesis analyzes systems, whose present action depends on past events; and aims at improving the stability conditions of such systems.

Systems, for which the future is not only determined by the present but also by the past, model widespread phenomena, where a delay occurs between the cause and its effect. These *time-delay systems* provide a reliable mathematical description of maturation periods in life sciences and in economics, or the non-instantaneous transfer of material, energy and information in chemistry, physics, engineering, and communication [20, 81]. Even washing our hands can be modeled by a time-delay system; indeed, when we adjust the faucet, the water temperature does not instantaneously change.

We consider time-delay systems for which the stability properties are characterized by whether every solution will remain close to zero or be repelled away. In this context, the stability optimization drives every solution to decay to zero as fast as possible. The stability assessment and optimization methods for these time-delay systems are fundamental for the construction of reliable machines, or to quantify parameters in mathematical models. However, analyzing the behavior of every solution is infeasible, and therefore, we describe all the possible solutions by operators, so that the stability conditions are determined by intrinsic quantities, the eigenvalues, of these operators.

More precisely, we focus on zero-solution stability of linear time-delay systems of time-invariant and periodic type, which respectively determine the stability of an equilibrium and periodic solution for a nonlinear time-invariant delay system, by the principle of linearized stability. In a linear time-delay system, the asymptotic growth or decay rate of the solutions towards zero depends on eigenvalues of an

infinite-dimensional operator. Hence, the system stability can be inferred from the location of these eigenvalues, and their relocation might provide a faster convergence to the zero-solution.

This thesis aims to develop accurate and reliable numerical methods for the stability assessment and stabilization of linear time-delay systems, testing these novel approaches on numerical examples and engineering applications. To this end, two main research directions are followed. First, disturbances, affecting the parameters of time-delay systems, are considered and exploited by novel stability and stabilization methods in a probabilistic framework, assuming that the time-delay system uncertainties are described by random variables. Second, we present novel computational methods for the stability analysis and optimization of linear time-periodic delay systems, which permit to iteratively refine the accuracy of the eigenvalues obtained by the discretization of infinite-dimensional operators.

This chapter is organized as follows. First, section 1.1 briefly reviews the stability properties for time-delay systems, setting the necessary basis for the development of the next chapters. Next, section 1.2 summarizes the contributions, reviewing the state of the art. Finally, we give an overview of the thesis in section 1.3.

1.1 PRELIMINARIES

This section provides a brief overview on the stability assessment and stability optimization methods for linear time-delay system, introducing the main definitions, properties and notations. We start analyzing the stability properties of the general periodic linear time-delay systems in section 1.1.1. Then, we analyze the special case of time-invariant linear time-delay systems in section 1.1.2, describing a well-established method to compute its associated stability measure in section 1.1.3. Hence, section 1.1.4 analyzes the stability optimization approach, considering time-invariant delay systems. The stability assessment and optimization for the general periodic linear time-delay system represents a main contribution of this work, as discussed in section 1.2.3 and chapter 4. For a more extensive treatise on the stability of time-delay system we refer to the monographs [33, 59, 8], from which we heavily borrow.

1.1.1 Stability measure for linear periodic time-delay systems

Let us consider the following linear periodic time-delay system

$$\dot{x}(t) = \sum_{j=0}^h A_j(t)x(t - \tau_j), \quad t \geq t_0 \in \mathbb{R}, \quad (1.1)$$

where

- there are $h + 1$, $h \in \mathbb{N}$, non-negatives delays, sorted, without loss of generality, in increasing order $0 \leq \tau_0 < \dots < \tau_h$;
- $x(t) \in \mathbb{R}^r$ represents the state at time $t \geq t_0 - \tau_h$;
- for $j = 1, \dots, h$, the system matrix $A_j : \mathbb{R} \rightarrow \mathbb{R}^{r \times r}$, $t \mapsto A_j(t)$ is a continuous and T -periodic function, with $T \in \mathbb{R}_+ \setminus \{0\}$.

If all system matrices are constant, $A_j(t) \equiv A_j$, being periodic for any period $T > 0$, then the time-delay system is called *autonomous* or *time-invariant*.

Since the present is influenced by the past events, $x(t - \tau_j)$ with $\tau_j > 0$, the solution of (1.1) cannot be specified by a single event at the starting time $x(t_0)$, yet a piece of trajectory over a time-interval of length τ_h is needed. More precisely, for any initial function $\varphi \in X$, where X is the set of continuous functions from $[-\tau_h, 0]$ to \mathbb{C}^r , the initial value problem

$$\begin{cases} \dot{x}(t) = \sum_{j=0}^h A_j(t)x(t - \tau_j), & t \in [t_0, \infty), \\ x(t) = \varphi(t - t_0), & t \in [t_0 - \tau_h, t_0], \end{cases} \quad (1.2)$$

admits a unique forward solution, denoted by $x(t; t_0, \varphi)$. In order to retrieve the solution at every time $t \geq t_0$, we need to know the solution in the previous interval of length τ_h , this state is denoted by $x_t(\cdot; t_0, \varphi) \in X$ and is defined by

$$x_t(\theta; t_0, \varphi) = x(t + \theta; t_0, \varphi), \quad \theta \in [-\tau_h, 0].$$

A linear system generally presents only one equilibrium point, the zero-solution $x \equiv 0$. We focus on the stability properties of (1.1), analyzing the convergence of the solutions to the zero-solution. In order to quantify the distance of a solution from the zero-solution, we equip the state space X with the supremum norm, also known as the L^∞ norm,

$$\|\varphi\|_s = \sup_{\theta \in [-\tau_h, 0]} \|\varphi(\theta)\|_2, \quad \varphi \in X,$$

where $\|\cdot\|_2$ is the Euclidean vector norm.

The zero-solution is *stable* if and only if for any $\varepsilon > 0$ there exists $\delta > 0$ such that $\|x_t(\cdot; t_0; \varphi)\|_s < \varepsilon$ for all $t \geq t_0$ and for any $\varphi \in X$ with $\|\varphi\|_s \leq \delta$. In addition, if $\lim_{t \rightarrow \infty} \|x_t(\cdot; t_0, \varphi)\|_s = 0$ also holds, then the zero-solution is *asymptotically stable*. If a system is not stable, then it is called *unstable*. For reasons of conciseness, we often refer the (asymptotic) stability and instability directly to the system (1.1) instead of the more precise formulation, which refers to the zero-solution.

The stability of system (1.1) can be inferred from the spectrum of infinite-dimensional operators linearly mapping the infinite-dimensional state space X into itself. By the

existence and uniqueness of the forward solution, we define the *solution operator*, $\mathcal{T}(t, t_0)$, which translates the solution along its trajectory, associating the state at time $t_0 \in \mathbb{R}$ to the state at time $t + t_0$ with $t \in \mathbb{R}_+$; in formula $\mathcal{T}(t, t_0) : X \rightarrow X$ such that

$$\mathcal{T}(t, t_0)\varphi = x_{t+t_0}(\cdot; t_0, \varphi), \quad \varphi \in X.$$

Since the solution operator associates the solution at time t_0 to the one at time $t + t_0$, its spectrum suggests the decay or growth rate of the solution between these two instances. By the system matrices periodicity T , it is natural to consider the solution operators $\mathcal{T}(T, t_0)$ describing the variation of the solutions after a period. The spectrum of $\mathcal{T}(T, t_0)$, denoted by $\sigma(\mathcal{T}(T, t_0))$, is an at most countable compact set in the complex plane with zero as only possible accumulation point; in other words, it admits a finite number of elements outside any ball around the origin. This spectrum is independent of the starting time $t_0 \in \mathbb{R}$, and all its non-zero elements are eigenvalues. Operator $\mathcal{T}(T, 0)$ is called *monodromy operator* and is denoted by \mathcal{U} ; therefore, the monodromy operator is defined as $\mathcal{U} : X \rightarrow X$ such that for any $\varphi \in X$

$$\mathcal{U}\varphi = x_T(\cdot; 0, \varphi).$$

The non-zero eigenvalues of the monodromy operator are called *Floquet multipliers*. By definition, they satisfy the infinite-dimensional linear eigenvalue problem

$$\mathcal{U}\varphi = \mu\varphi, \quad \mu \in \mathbb{C} \setminus \{0\}, \quad \varphi \in X \setminus \{0\}. \quad (1.3)$$

The Floquet multipliers determine the asymptotic growth/decay of solution of (1.2) in the time-interval of length T . The largest modulus of the Floquet multipliers, the so-called *spectral radius*

$$\rho = \max_{\mu \in \sigma(\mathcal{U})} |\mu|,$$

represents a stability measure for the system (1.1), as stated in the following theorem.

PROPOSITION 1.1 *The zero-solution of (1.1) is asymptotically stable if and only if all the Floquet multipliers are strictly contained in the complex unit circle, or*

$$\rho < 1.$$

The zero-solution is unstable if there is at least one Floquet multiplier with modulus larger than 1, i.e. $\rho > 1$.

In the linear autonomous time-delay system, we have an uncountable number of stability conditions induced by Proposition 1.1. Indeed, since constant system matrices can be interpreted as periodic for any period $T \in \mathbb{R}_+ \setminus \{0\}$, then we can define infinitely many monodromy operators, whose spectral radius permits to infer the stability properties of the autonomous system. However, the autonomous case admits an additional stability measure whose computation and optimization are well-established, as described in the following sections.

1.1.2 Another stability measure for linear autonomous time-delay systems

Since the system matrices do not depend on time, the initial time t_0 can be set to zero without loss of generality. Hence, the autonomous time-delay system is

$$\dot{x}(t) = \sum_{j=0}^h A_j x(t - \tau_j), \quad t \in \mathbb{R}_+. \quad (1.4)$$

In a similar way, the solution operators depend only on a single parameter, $\mathcal{T}(t, 0)$. The family of solution operators $\{\mathcal{T}(t, 0)\}_{t \in \mathbb{R}_+}$ permits to reformulate system (1.4) into an infinite-dimensional ordinary differential equation over the state space X . Indeed, taking the right-hand derivative of $\{\mathcal{T}(t, 0)\}_{t \in \mathbb{R}_+}$ in $t = 0$, we get

$$\frac{d}{dt} x_t = \lim_{\delta \rightarrow 0^+} \frac{x_{t+\delta} - x_t}{\delta} = \lim_{\delta \rightarrow 0^+} \frac{T(\delta, 0) - T(0, 0)}{\delta} x_t = \mathcal{A} x_t, \quad (1.5)$$

where $x_t = x_t(\cdot; 0, \varphi)$ for any $\varphi \in X$ and \mathcal{A} is the *infinitesimal generator* of $\{\mathcal{T}(t, 0)\}_{t \in \mathbb{R}_+}$, characterized as the operator $\mathcal{A} : \mathcal{D}(\mathcal{A}) \subset X \rightarrow X$ such that

$$\begin{cases} \mathcal{D}(\mathcal{A}) = \left\{ \varphi \in X : \dot{\varphi} \in X \text{ and } \dot{\varphi}(0) = \sum_{j=0}^h A_j \varphi(-\tau_j) \right\}, \\ \mathcal{A} \varphi = \dot{\varphi}. \end{cases} \quad (1.6)$$

Since autonomous delay system can be seen as linear infinite-dimensional ordinary differential equations, the following example briefly reviews the terminology and the results shown until now in the simpler case of linear finite-dimensional ordinary differential equations.

Example 1.1. Let us take a step back, and consider an ordinary differential equation

$$\dot{x}(t) = Ax(t), \quad t \in \mathbb{R}, \quad x(t) \in \mathbb{R}^r \text{ and } A \in \mathbb{R}^{r \times r}. \quad (1.7)$$

There exists a unique solution of system (1.7), for any given state at time $t_0 = 0$, $x(0) \in \mathbb{R}^r$; this solution is defined forward and also backward in time, and admits an explicit expression

$$x(t) = \exp(At) x(0), \quad \text{for any } t \in \mathbb{R}.$$

Therefore, the solution operator $\mathcal{T}(t, 0)$, translating a solution from the state at time 0 to the time $t \in \mathbb{R}$, is the matrix exponential of At ,

$$\mathcal{T}(t, 0) = \exp(At). \quad (1.8)$$

The infinitesimal generator of $\{\mathcal{T}(t, 0)\}_t$ is the matrix A , which defines system (1.7),

$$\left. \frac{d \exp(At)}{dt} \right|_{t=0} = A.$$

If λ is an eigenvalue of A , then $e^{\lambda t}$ is an eigenvalue of $\mathcal{T}(t, 0)$, by (1.8). Since system (1.7) is asymptotically stable if and only if all the eigenvalues of A are in the complex left half-plane, we can retrieve the results of Proposition 1.1. Indeed, system (1.7) is asymptotically stable if and only if all the eigenvalues of $\mathcal{T}(t, 0)$ for $t > 0$ are contained in the complex unit circle.

Analogously to Example 1.1, the spectra of the solution operator $\mathcal{T}(t, 0)$ and of the infinitesimal generator \mathcal{A} are related by

$$\sigma(\mathcal{T}(t, 0)) \setminus \{0\} = \exp(t\sigma(\mathcal{A})). \quad (1.9)$$

Therefore, the spectrum of \mathcal{A} is at most countable compact set in the complex plane with minus infinity as only possible accumulation point; in other words, it admits finitely many elements in any right half-plane. All the elements of $\sigma(\mathcal{A})$ are eigenvalues, and they satisfy the following infinite-dimensional eigenvalue problem

$$\mathcal{A}\varphi = \lambda\varphi, \quad \lambda \in \mathbb{C}, \quad \varphi \in X \setminus \{0\}. \quad (1.10)$$

Let us recall that every solution operator $\mathcal{T}(t, 0)$ for $t > 0$ can be interpreted as monodromy operator for the autonomous system (1.4). Therefore, by the previous Proposition 1.1 and the relation on spectra (1.9), the autonomous systems (1.4) admit another stability measure, the real part of the rightmost eigenvalues of the infinitesimal generator, the so-called *spectral abscissa*

$$\alpha = \max_{\lambda \in \sigma(\mathcal{A})} \operatorname{Re}(\lambda).$$

PROPOSITION 1.2 *The zero-solution of (1.4) is asymptotically stable if and only if all the eigenvalues of the infinitesimal generator are contained in the left half-plane or equivalently if and only if*

$$\alpha < 0.$$

The zero-solution is unstable if there is an eigenvalue of the infinitesimal generator with positive real part, $\alpha > 0$.

Since the infinitesimal generator permits to rewrite system (1.4) into an infinite-dimensional ordinary differential equations (1.5), its eigenvalues express the asymptotic exponential growth/decay rate of the solutions of (1.4) towards zero, similarly to the finite-dimensional case presented in Example 1.1.

Moreover, substituting into (1.4) an exponential solution $x(t) = e^{\lambda t}v$, we get the following finite-dimensional nonlinear eigenvalue problem

$$\left(\lambda I_r - \sum_{j=0}^h A_j e^{-\lambda \tau_j} \right) v = 0, \quad \lambda \in \mathbb{C}, \quad v \in \mathbb{C}^r \setminus \{0\},$$

which is equivalent to the infinite-dimensional linear eigenvalue problem (1.10) as stated in the following theorem.

THEOREM 1.3 *Let $\hat{\lambda} \in \mathbb{C}$. If the pair $(\hat{\lambda}, \hat{\varphi})$ is a solution of the infinite-dimensional linear eigenvalue problem*

$$\mathcal{A}\varphi = \lambda\varphi, \quad \lambda \in \mathbb{C}, \quad \varphi \in X \setminus \{0\}, \quad (1.11)$$

then $(\hat{\lambda}, \hat{v})$ is a solution of the finite-dimensional nonlinear eigenvalue problem

$$\left(\lambda I_r - \sum_{j=0}^h A_j e^{-\lambda\tau_j} \right) v = 0, \quad \lambda \in \mathbb{C}, \quad v \in \mathbb{C}^r \setminus \{0\}, \quad (1.12)$$

where $\hat{v} = \hat{\varphi}(0)$.

Conversely if the pair $(\hat{\lambda}, \hat{v})$ is a solution of (1.12) then $(\hat{\lambda}, \hat{\varphi})$ is a solution of (1.11), where $\hat{\varphi}(\theta) = e^{\hat{\lambda}\theta}\hat{v}$ for $\theta \in [-\tau_h, 0]$.

The eigenvalues of the nonlinear eigenvalue problem (1.12) are also called *characteristic roots*, since they solve the following scalar equation, named *characteristic equation*

$$\det(\mathcal{A}(\lambda)) = 0, \quad (1.13)$$

where $\mathcal{A}(\lambda)$ denotes the *characteristic matrix* defined as

$$\mathcal{A}(\lambda) := \lambda I_r - \sum_{j=0}^h A_j e^{-\lambda\tau_j}.$$

Before analyzing how to compute and minimize the spectral abscissa of the infinitesimal generator, the next example illustrates the spectrum-based stability properties of a simple scalar time-delay system: the *hot shower problem* a didactic example often encountered in the literature [52, 20, 38].

Example 1.2. Let us consider the simplified model of a human adjusting the water temperature by swinging the faucet handle,

$$\dot{x}(t) = -Kx(t-1), \quad (1.14)$$

where $x(t)$ denotes the difference between the water temperature at time t and the desired one, and $-Kx(t-1)$ represents the reaction of the person in adjusting the faucet, occurring with a delay $\tau = 1$ s, due to the propagation of the water in the pipes.

A person, reacting forcefully to a wrong temperature, is modeled by a large value of K . In this case, the temperature may oscillate with increasing amplitude, leading to repeated burns or frostbite until the faucet breaks. For example, for $K = 2$ system (1.14) is unstable due to a positive spectral abscissa of the infinitesimal generator, which present eigenvalues in the right half-plane, Figure 1.1a; or equivalently due to a spectral radius of the solution operator $\mathcal{T}(1, 0)$ larger than one, since there are Floquet

multipliers outside the complex unit disc, Figure 1.1b. If the initial condition of the water temperature is hotter 1°C than the desired one, then the temperature oscillates with growing amplitude, where the asymptotic exponential growth rate is determined by the spectral abscissa, as illustrated in Figure 1.1c.

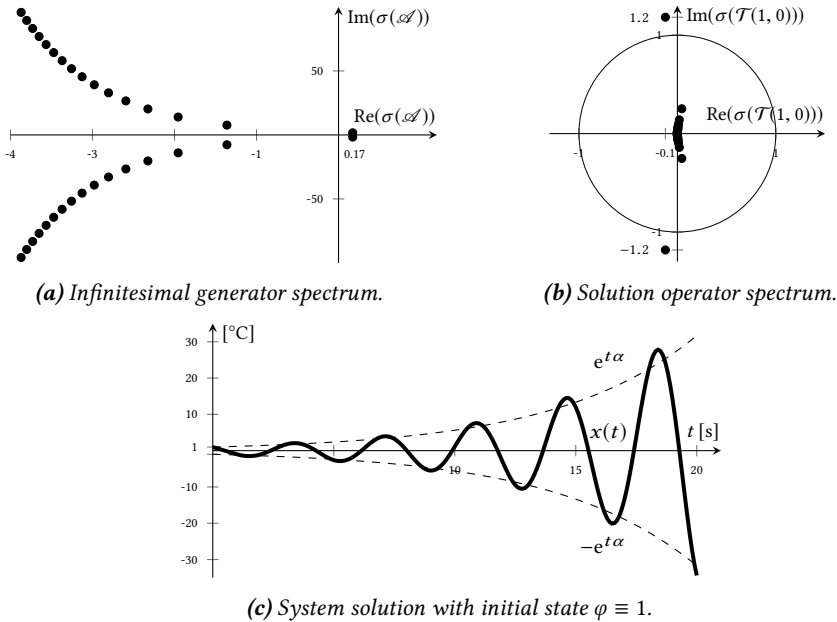


Figure 1.1 Analysis of the hot shower problem (1.14) with reaction parameter $K = 2$.

A more gentle person, with a small value of K , can find the desired temperature to wash its hands. However, if the time required to reach a temperature close to the desired one is long, then the water bill will be costly. For example, for $K = 1$ the stability of system (1.14) can be inferred from the negative value of the spectral abscissa, Proposition 1.2, or by the spectral radius of the solution operator $\mathcal{T}(1, 0)$ smaller than one, Proposition 1.1. Indeed, all the eigenvalues are contained in the left half-plane and all the Floquet multipliers are in the complex unit circle, as respectively depicted in Figures 1.2b and 1.2a. For an initial condition $x(t) \equiv 1$ with $t \in [-1, 0]$ the settling time of the solution to reach the desired water temperature is long as illustrated in Figure 1.2c.

1.1.3 Spectrum based stability assessment for autonomous delay systems

The dual interpretation of the eigenvalues in Theorem 1.3, either as infinite-dimensional and linear or finite-dimensional and nonlinear, lies at the basis of efficient stability assessment methods as [51] and the package DDE-BIFTOOL [78]. In

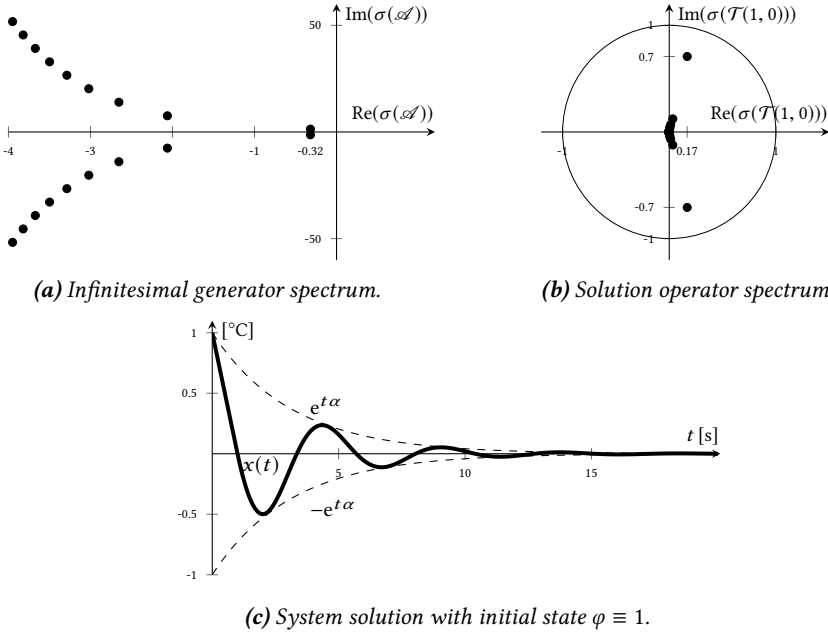


Figure 1.2 Analysis of the hot shower problem (1.14) with reaction parameter $K = 1$.

these methods, a spectral discretization of the infinite-dimensional linear eigenvalue problem (1.11) furnishes a global view of the infinitesimal generator spectrum, permitting to detect a guess of the rightmost eigenvalues. Then, the accuracy of these guesses is refined by Newton’s method based on the finite-dimensional nonlinear eigenvalue problem (1.12). Hence the stability assessment, relying on the spectral abscissa, considers only the real part of the rightmost eigenvalue.

Remark 1.1. Other methodologies permit to compute the characteristic roots of linear autonomous time-delay systems. For example, the advanced quasi-polynomial mapping [97] relies on splitting the real and imaginary parts of the characteristic equation (1.13) into two surfaces, such that the characteristic roots are determined by the intersections between these two surfaces. The interested reader is referred to [38, Chapter 2], for an overview on numerical methods to compute the characteristic roots for an autonomous linear time-delay system.

We briefly review the computation of the characteristic roots following the approach in [59, Section 2.2]. We first describe the discretization of the infinite-dimensional eigenvalue problem into a finite-dimensional linear eigenproblem, which presents the same underlying ideas of [8, Chapter 5]. Then, we present a local method to compute the characteristic roots by the finite-dimensional nonlinear eigenvalue

problem. Finally, we sketch a two-stage approach which combines the previous results.

Discretization of the infinite-dimensional linear eigenvalue problem

We derive a finite-dimensional linear eigenvalue problem, whose eigenvalues approximate some elements of the infinitesimal generator spectrum. Given a positive integer M , we approximate any element of the state space $\varphi \in X$ by M -degree polynomial, φ_M . Given a polynomial basis $\{p_i\}_{i \in \mathbb{N}}$ in the interval $[-\tau_h, 0]$, the polynomial approximation is uniquely determined by the coefficients $c = (c_0^T \dots c_M^T)^T \in (\mathbb{C}^r)^{M+1}$ such that

$$\varphi_M(t) = \sum_{i=0}^M c_i p_i(t), \quad t \in [-\tau_h, 0]. \quad (1.15)$$

We determine the discretization of the infinite-dimensional linear eigenvalue problem, $\mathcal{A}\varphi = \lambda\varphi$ with $\varphi \in X \setminus \{0\}$ and $\lambda \in \mathbb{C}$, by the characterization (1.6) of the infinitesimal generator, $\mathcal{A}\varphi = \dot{\varphi}$, with $\dot{\varphi}(0) = \sum_{j=0}^h A_j \varphi(-\tau_j)$. Indeed, we impose the collocation requirements in 0

$$\lambda\varphi_M(0) = \sum_{j=0}^h A_j \varphi_M(-\tau_j). \quad (1.16)$$

and in M distinct points $\{\xi_m\}_{m=1}^M$ over the interval $[-\tau_h, 0)$

$$\lambda\varphi_M(\xi_m) = \dot{\varphi}_M(\xi_m), \quad m = 1, \dots, M. \quad (1.17)$$

Hence, the discretization of the infinite-dimensional linear eigenvalue problem (1.11) is expressed in terms of the coefficients $c \in \mathbb{C}^{r(M+1)}$ of the M -degree polynomial, φ_M by a matrix formulation of conditions (1.16)-(1.17).

If we express the polynomial φ_M in the Chebyshev basis

$$\varphi_M(t) = \sum_{i=0}^M c_i T_i \left(2 \frac{t}{\tau_h} + 1 \right), \quad t \in [-\tau_h, 0],$$

with T_i the i -degree Chebyshev polynomial of the first kind, then its derivative is

$$\dot{\varphi}_M(t) = \sum_{i=0}^M c_i \frac{2}{\tau_h} i U_{i-1} \left(2 \frac{t}{\tau_h} + 1 \right), \quad t \in [-\tau_h, 0],$$

where U_i is the i -degree Chebyshev polynomial of the second kind. If $\{\zeta_m\}_{m=1}^M$ are the normalized grid-points, scaled and shifted to the interval $[-1, 1]$,

$$\zeta_m = 2 \frac{\xi_m}{\tau_h} + 1,$$

The convergence of the eigenvalues of (1.19) to the characteristic roots is fast. More precisely, spectral accuracy, *i.e.* a convergence rate faster than $O(M^{-k})$ for every $k \in \mathbb{N}$, can be proven [8, Section 5.3], since the asymptotic distribution of the chosen collocation points is asymptotically equal to the distribution of zeros of Chebyshev polynomials scaled and shifted in $[-\tau_h, 0]$.

Newton's method for nonlinear eigenvalue problem

The finite-dimensional nonlinear eigenvalue problem (1.12) allows us to compute the eigenpairs by applying an iterative solver for nonlinear equations to

$$\begin{cases} \mathcal{A}(\lambda)v = 0, \\ w^*v = 1, \end{cases}$$

where the second equation, with $w \in \mathbb{C}^r \setminus \{0\}$ and $*$ denoting the conjugate transpose, is a normalization constraint. If $y = (v^T \lambda)^T$, we can rewrite the system in the form $F(y) = 0$. The application of Newton's method leads us to the basic iteration

$$y_{i+1} = y_i - J(y_i)^{-1}F(y_i), \quad i \in \mathbb{N}, \quad (1.20)$$

where $J(y_i)$ denotes the Jacobian of $F(y)$ at $y = y_i$, and is given by

$$J(y_i) = \begin{pmatrix} \mathcal{A}(\lambda_i) & \frac{d\mathcal{A}(\lambda_i)}{d\lambda}v_i \\ w^* & 0 \end{pmatrix} = \begin{pmatrix} \lambda_i I_r - \sum_{j=0}^h A_j e^{-\lambda_i \tau_j} & v_i + \sum_{j=0}^h \tau_j A_j e^{-\lambda_i \tau_j} v_i \\ w^* & 0 \end{pmatrix}.$$

Characteristic roots computation

The previous results lead us to the following algorithm for computing (part of) the spectrum of the infinitesimal generator.

Algorithm 1.1. *Two-stage approach for computing characteristic roots.*

1. Fix M and compute eigenvalues and eigenvectors of (1.19).
2. Correct the individual characteristic roots approximation, and extracted eigenvector of (1.12), by applying Newton's iteration (1.20).

In the initialization of the second stage, we extract an approximation of the right eigenvector of the nonlinear eigenvalue problem (1.12). By (1.15), and the construction of the finite-dimensional linear eigenvalue problem (1.19), $c \in \mathbb{C}^{r(M+1)}$ parametrizes the polynomial approximation corresponding to an eigenfunction of the infinitesimal generator \mathcal{A} . Hence, by Theorem 1.3, the eigenvector approximation of (1.12) can be extracted by an eigenvector $c = (c_0^T \cdots c_M^T)^T$ of (1.19),

$$v = \sum_{i=0}^M p_i(0)c_i.$$

Remark 1.2. The number of collocation points M should not be too large, since the eigenvalue computation of (1.19) has complexity $\mathcal{O}((rM + r)^3)$ by a direct method. On the other hand, the eigenvalues of (1.19) should be in the basin of attraction of the rightmost characteristic roots, so that the Newton’s method converges to the desired solution. We refer to [59, Section 2.2.2] for an empirical method to determine the number of collocation points M , so that the eigenvalues of (1.19) approximates the characteristic roots of (1.4) in a given right half-plane.

Example 1.3. For the simple scalar system (1.14), the characteristic roots can be analytically obtained by solving the characteristic equation (1.13),

$$\lambda + Ke^{-\lambda} = 0 \text{ if and only if } \lambda = W_k(-K),$$

where for any integer k , W_k denotes the k -th branch of the Lambert W function.

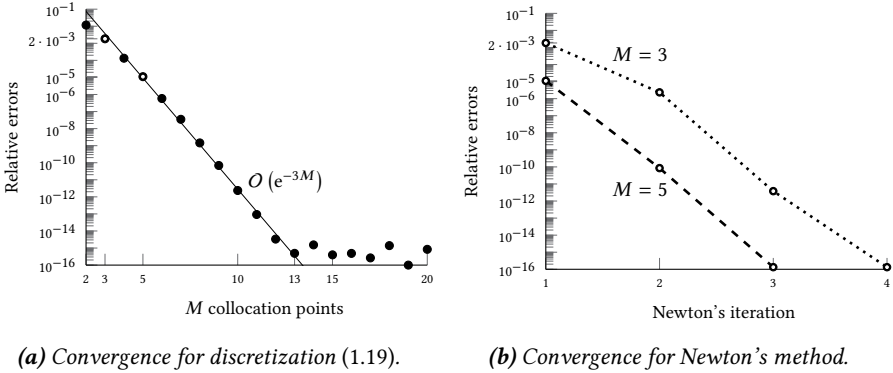


Figure 1.3 Relative errors to evaluate the rightmost characteristic root with Algorithm 1.1, for system (1.14) with $K = 2$. Newton’s method is initialized on the rightmost eigenvalues of (1.19), considering $M = 3$ and $M = 5$ collocation points.

For $K = 2$ the rightmost characteristic root is $\lambda = -0.3181 + 1.3372i$ and its approximation by Algorithm 1.1 is illustrated in Figure 1.3. In Figure 1.3a, the rightmost eigenvalue obtained by spectral collocation in the first stage of Algorithm 1.1 spectrally converges to the rightmost characteristic root. In Figure 1.3b, few Newton’s iteration permits to refine the accuracy up to machine precision of coarse estimates of the rightmost characteristic root, obtained by spectral collocation.

For large dimension of the system matrices $r \gg 1$, solving the eigenvalue problem (1.19) in the first stage of Algorithm 1.1 becomes computationally infeasible. However, for this large scale problem specific software have been implemented, like the infinite Arnoldi’s method [41, 40] and Compact Rational Krylov method [92].

1.1.4 Spectrum based stability optimization for autonomous delay systems

In this section, we consider time-delay system whose matrices are functions of system or controller parameters $\mathbf{K} = (K_1 \cdots K_k) \in \mathbb{R}^k$. More precisely, we consider the following linear autonomous time-delay system

$$\dot{x}(t) = \sum_{j=0}^h A_j(\mathbf{K})x(t - \tau_j), \quad t \in \mathbb{R}_+, \quad (1.21)$$

under the assumption that $A_j : \mathbb{R}^k \rightarrow \mathbb{R}^{r \times r}$, $\mathbf{K} \mapsto A_j(\mathbf{K})$ are smooth functions, for $j = 1, \dots, h$. Analogously, its associated characteristic matrix is denoted by $\mathcal{A}(\lambda; \mathbf{K})$. However, to simplify the notations, we omit the parametric argument if it is not essential for the discussion and in particular, we do not explicitly state \mathbf{K} in the infinite-dimensional operators and their eigenvalues.

In this work, we focus on spectrum-based methods for stabilizing an unstable system or for improving the decay rate of solutions to equilibrium based on minimizing the stability measures as a function of controller parameter, similarly to [59, Chapter 7] for autonomous systems, and [77, 63] for periodic systems. For periodic time-delay system the (squared) spectral radius is minimized, shrinking the spectrum of the monodromy operator towards zero. For autonomous time-delay systems (1.21), this optimization problem can be recast as minimizing the spectral abscissa of the infinitesimal generator, shifting the characteristic roots to the left. Hence the stability optimization objective functions are

$$\begin{aligned} \min_{\mathbf{K}} \rho^2, & \quad \text{with } \rho = \max_{\mu \in \sigma(\mathcal{U})} |\mu|; \\ \min_{\mathbf{K}} \alpha, & \quad \text{with } \alpha = \max_{\lambda \in \sigma(\mathcal{A})} \operatorname{Re}(\lambda); \end{aligned}$$

where the first one holds for periodic time-delay system, while the latter one only holds for autonomous time-delay systems.

The stabilization of time-delay systems is a challenging problem, since it requires shaping the spectrum of an infinite-dimensional operator, minimizing a dominant element of this infinite (but countable) spectrum, by tuning a finite number of degrees of freedom, the controller parameters \mathbf{K} . By Propositions 1.1-1.2, the stabilization of an autonomous time-delay system can be equivalently stated in terms of spectral radius and spectral abscissa. In particular, the minimization of the spectral radius minimizes the largest in modulus Floquet multipliers, while the spectral abscissa stability optimization minimizes the real part of the rightmost characteristic roots.

The objective function of the spectrum-based stability optimization problems is in general non-convex, as illustrated in Figure 1.4, and is also non-smooth, as analyzed, more in detail, in the next chapter 2. Except for degenerate examples, non-differentiable points, due to multiple dominant elements of the spectrum (counted

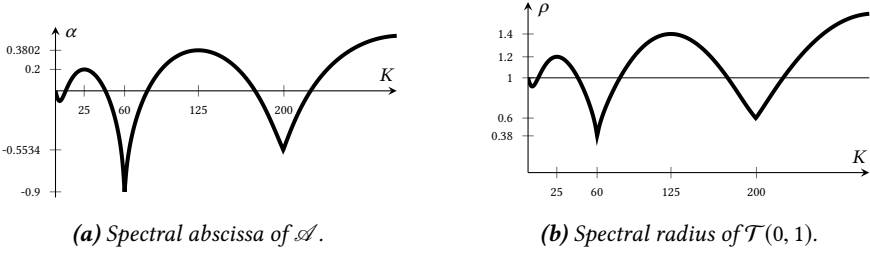


Figure 1.4 The stability measures for the time-delay system $\dot{x}(t) = -Kx(t) + 0.1Kx(t-1)$, varying the parameter $K \in [0, 300]$, present multiple local minima, therefore they are non-convex.

with multiplicity), occur on a set with measure zero in the parameter space. Therefore, the previously defined objective functions are differentiable almost everywhere. Based on these properties, the optimization is handled by the MATLAB code HANSO (Hybrid Algorithm for Non-Smooth Optimization), described in [64].

HANSO is a two-phase process, based on BFGS algorithm with weak Wolfe condition in the line search and on the gradient sampling method. Due to the non-convexity of the problem, the BFGS phase is run from multiple starting points, often randomly chosen, and with a rapid convergence leads to a reasonably good approximation of the optimum [48]. Then, the gradient sampling, a generalization of the steepest descent method for non-smooth problems, starts from the minimum point found by BFGS. Since in this minimum the objective function is often non differentiable, the sampling gradient samples a number of gradients in the near neighborhood of the iteration point, hence considers as a descent direction the vector with the smallest norm in the convex hull of these sampled gradients, and finally a new iteration is found along this direction with a standard line search [9, 93].

The underlying optimization process with HANSO only requires the evaluation of the objective function and its gradient with respect to controller parameters, whenever the objective function is differentiable. The objective function is differentiable and hence its gradient exists, if the dominant element of the spectrum is isolated and simple; in this case the gradient can be evaluated as¹

$$\nabla_{\mathbf{K}} (\rho^2) = 2 \operatorname{Re} (\bar{\mu}_D \nabla_{\mathbf{K}} \mu_D), \quad \text{and} \quad \nabla_{\mathbf{K}} \alpha = \operatorname{Re} (\nabla_{\mathbf{K}} \lambda_D),$$

where μ_D denotes the *dominant Floquet multipliers*, which are Floquet multipliers with modulus equal to the spectral radius, $\rho = |\mu_D|$ and non-negative imaginary part, $\operatorname{Im}(\mu_D) \geq 0$; while λ_D denotes the *dominant characteristic roots*, which are

¹ The gradient of the squared spectral radius follows from

$$\nabla_{\mathbf{K}} (|\mu|^2) = \nabla_{\mathbf{K}} \bar{\mu} \mu = 2 (\operatorname{Re}(\mu \nabla_{\mathbf{K}} \mu) - \operatorname{Im}(\mu \nabla_{\mathbf{K}} \mu)) = 2 \operatorname{Re} (\bar{\mu} \nabla_{\mathbf{K}} \mu).$$

characteristic roots with real part equal to the spectral abscissa $\alpha = \text{Re}(\lambda_d)$ and non-negative imaginary part, $\text{Im}(\lambda_d) \geq 0$.

Remark 1.3. Since we only consider real-valued time-delay systems, the non-real characteristic roots and non-real Floquet multipliers always occurs in complex conjugate pairs. For this reason, the dominant eigenvalues, *i.e.* the dominant Floquet multipliers and the dominant characteristic roots, are chosen with non-negative imaginary part.

Since the evaluation of the gradient of the objective function depends on the gradient of dominant eigenvalues, $\nabla_{\mathbf{K}}\lambda_d$ and $\nabla_{\mathbf{K}}\mu_d$, the following proposition provides an explicit expression for the eigenvalues derivatives of a general finite-dimensional eigenvalue problem $\Lambda(\lambda; \mathbf{K})v = 0$ with respect to parameters \mathbf{K} .²

PROPOSITION 1.4 *Given $\mathbf{K} \in \mathbb{R}^k$, let λ be a simple eigenvalue of a finite-dimensional eigenproblem $\Lambda(\lambda; \mathbf{K})$ with $u, v \in \mathbb{C}^r \setminus \{0\}$ its left and right eigenvectors, such that $\Lambda(\lambda; \mathbf{K})v = 0$, and $u^*\Lambda(\lambda; \mathbf{K}) = 0$. Then for each $i \in \{1, \dots, k\}$ we can express*

$$\frac{\partial \lambda(\mathbf{K})}{\partial K_i} = \frac{-u^* \frac{\partial \Lambda(\lambda; \mathbf{K})}{\partial K_i} v}{u^* \frac{\partial \Lambda(\lambda; \mathbf{K})}{\partial \lambda} v}, \quad \text{for } i = 1, \dots, k.$$

Proof. To prove the proposition, we left-multiply by u^* the partial derivative of $\Lambda(\lambda; \mathbf{K})v = 0$ with respect to a parameter K_i , for every $i = 1, \dots, k$. Refer to [76, Lemma 2.7] for further details. \square

An eigenvalue $\hat{\lambda}$ of a finite-dimensional nonlinear eigenvalue problem $\Lambda(\lambda)v = 0$ with $v \in \mathbb{C}^r \setminus \{0\}$ is *simple* when its algebraic and geometric multiplicity are equal to 1, where the *algebraic multiplicity* equals the number of times $\hat{\lambda}$ appears as a root of the characteristic equation $\det(\Lambda(\lambda)) = 0$, while the *geometric multiplicity* is equal to the null space dimension of $\Lambda(\hat{\lambda})$.

Proposition 1.4 applied to the nonlinear eigenvalue problem (1.12), permits to compute the gradient of a simple characteristic roots with respect to a parameters vector \mathbf{K} .

Algorithm 1.2. *Computing the gradient of a characteristic roots.*

1. Compute the targeted characteristic root λ and its right eigenvector v by Algorithm 1.1.
2. Compute $u \in \mathbb{C}^r \setminus \{0\}$, the corresponding left eigenvector.

² The proposition is stated considering a general finite-dimensional eigenvalue problem $\Lambda(\lambda; \mathbf{K})v = 0$, since it will not only be applied to the characteristic matrix eigenproblem $\mathcal{A}(\lambda; \mathbf{K})v = 0$ but also to other finite-dimensional eigenvalue problems, in the upcoming sections 2.5 and 4.4.

3. Compute the partial derivative of the Floquet multiplier with respect to the elements of \mathbf{K} by

$$\frac{\partial \lambda}{\partial K_i} = \frac{u^* \left(\sum_{j=0}^h \frac{\partial A_j(\mathbf{K})}{\partial K_i} e^{-\tau_j \lambda} \right) v}{u^* \left(I_r + \sum_{j=0}^h \tau_j A_j(\mathbf{K}) e^{-\tau_j \lambda} \right) v}, \quad \text{for } i = 1, \dots, k.$$

For a small problem, the left eigenvector $u \in \mathbb{C}^r \setminus \{0\}$ can be computed as singular vector corresponding to the smallest singular value of the characteristic matrix $\mathcal{A}(\lambda; \mathbf{K})$. However, for large scale problems, the singular value decomposition becomes computationally infeasible. In this case, the left eigenvector, $u \in \mathbb{C}^r \setminus \{0\}$, of the characteristic matrix $\mathcal{A}(\lambda)$ is evaluated as right eigenvector of the “transposed” nonlinear eigenvalue problem

$$\check{\mathcal{A}}(\lambda)u = 0, \quad \text{where } \check{\mathcal{A}}(\lambda) = \lambda I_r - \sum_{j=0}^h A_j^T e^{-\lambda \tau_j}, \quad \text{for } \lambda \in \mathbb{C}, \quad (1.22)$$

as proved in the following proposition.

PROPOSITION 1.5 *Let $u \in \mathbb{C}^r \setminus \{0\}$ and $\lambda \in \mathbb{C}$. Vector u is the left eigenvector of (1.12) corresponding to eigenvalue λ if and only if it is a right eigenvector of (1.22) corresponding to eigenvalue $\bar{\lambda}$.*

Proof. Since for any $\lambda \in \mathbb{C}$ we have $\mathcal{A}(\lambda) = (\check{\mathcal{A}}(\bar{\lambda}))^*$, $u^* \mathcal{A}(\lambda) = 0$ if and only if $\check{\mathcal{A}}(\bar{\lambda})^* u = 0$, which concludes the proof. \square

The matrix valued function $\check{\mathcal{A}}(\lambda)$ can be interpreted as the characteristic matrix associated with the dual time-delay system of (1.4),

$$\dot{x}(t) = \sum_{j=0}^h A_j^T x(t - \tau_j). \quad (1.23)$$

In this view, a characteristic root and its associated left and right eigenvectors can be hence computed by applying Algorithm 1.1 to the original system (1.4) and to its dual system (1.23), followed by a pairing of eigenvalues and associated eigenvectors induced by Proposition 1.5.

Example 1.4. In Example 1.2, not only the stability of system (1.14) is important, so that the modeled person does not repeatedly get burns and frostbites, but also a fast decay of the solution towards zero, in order to reduce the water bill. Therefore, in this example, we are looking for the best reaction parameters by means of stability optimization, considering the reaction parameter K as a controller \mathbf{K} of system (1.21).

An application of the stability optimization, with $M = 10$ collocation points, yields the stabilizing reaction parameter $K = 0.3680$, for which the spectral abscissa is

$\alpha = -0.9989$. The final controller parameter is very close to the minimizer $K = e^{-1}$ for which the rightmost characteristic roots $\lambda = -1$ corresponds to a double non-semi-simple eigenvalue, Figure 1.5.

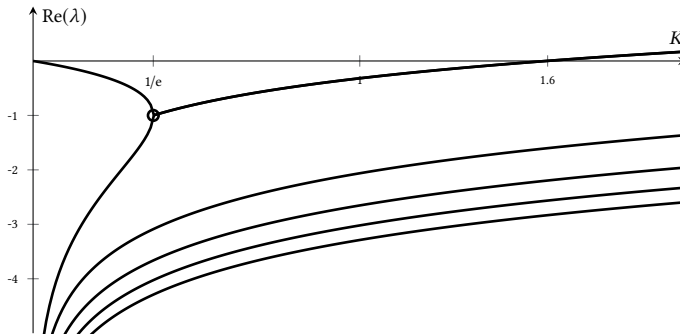


Figure 1.5 Real part of the 10 rightmost characteristic roots varying the parameter K . For $K \in [1/e, 2]$ the depicted rightmost characteristic roots are complex conjugate. The spectral abscissa corresponds to the maximum real part of the rightmost eigenvalue. The final iteration of the optimization process is indicated by a circle.

Analogously to Example 1.2, the spectra of the infinitesimal generator \mathcal{A} and of the solution operator $\mathcal{T}(1, 0)$ are respectively illustrated in Figures 1.6a and 1.6b. In particular, Figure 1.6a shows the approximation of the rightmost characteristic roots by the discretization with $M = 10$ collocation points. If the initial water temperature is 1°C warmer than the desired one, then the person modeled by the designed reaction parameter adjusts in few seconds the faucet in such a way that the water temperature is close to the desired one, as illustrated in Figure 1.6c. This latter figure also highlights the asymptotic convergence rate of the solution, determined by the spectral abscissa.

Remark 1.4. Other spectrum-based techniques for the stabilization of autonomous time-delay system are based on the direct assignment of multiple characteristic roots [6, 7, 49, 68, 69, 96]. These analytic control design techniques are really difficult to apply to the general case (1.21), since the imposition of multiple characteristic roots does not guarantee that these multiple eigenvalues are dominant, determining hence the stability of the system. Moreover, analogously to the minimization of the spectral abscissa in Example 1.4, the stability induced by these spectrum-based techniques is sensitive to perturbation of the system parameters, as further discussed in section 1.2.1 and in the following chapter 2.

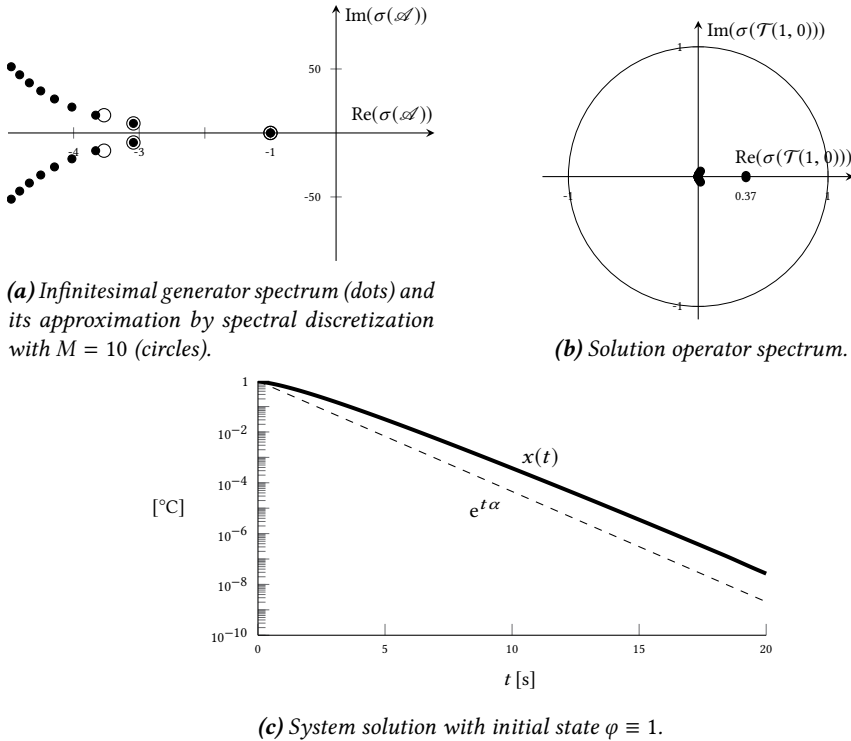


Figure 1.6 Analysis of the hot shower problem (1.14) with reaction parameter $K = 0.3680$, designed by stability optimization method.

1.2 CONTRIBUTIONS

In this section, the main contributions of the work are highlighted and compared with the state of the art. These contributions are presented following the chronological order of the author’s research work. Section 1.2.1 considers the generalization of the stability assessment and stability optimization in a probabilistic setting, where the system’s uncertainties are described by a random vector. Then, section 1.2.2 describes the behavior of the stability measures as function of system parameters, and the effects of this behavior on polynomial approximation methods. The last main contribution of this thesis concerns the stability assessment and stabilization for periodic time-delay system whose delays and period are commensurate numbers, as described in section 1.2.3.

1.2.1 Probabilistic stability and stabilization approach

The mathematical approximation of natural phenomena and engineering applications necessarily introduces uncertainties, since we are not able to determine with full precision all the parameters and interactions. Therefore, a high level of uncertainty is often contained in reliable mathematical models, related to specific physical parameters, and affects the stability properties. For example, in the hot shower problem (1.14), we cannot expect to accurately set the reaction parameter K . Therefore, we add to a given value of the reaction parameter K a disturbance ω , which describes the uncertainty, or the lack of precision. In this way, the model is given by

$$\dot{x}(t) = -(K + \omega)x(t - 1), \quad (1.24)$$

and its stability measures, its associated characteristic roots and Floquet multipliers, are functions of the uncertainty ω .

Traditionally, the robustness of the stability analysis against uncertainties is handled by bifurcation analysis or within a pseudo-spectral approach. The former, implemented in the software package DDE-BIFTOOL [78], analyzes the functions of the rightmost eigenvalues and largest Floquet multipliers varying a small number of (controller and uncertain) parameters; for further information refer to the book [59] and reference therein. The latter considers the supremum of the stability measures obtained for any possible perturbation with a given upper bound [30, 57, 70]. This worst-case analysis may lead to conservative results, in particular if the dependence on these uncertain parameters is nonlinear.

In order to fully exploit the uncertainty structure, we consider the uncertainties as realizations of a random vector with a given probability density function. In this way, a time-delay system, whose parameters are perfectly known, can be interpreted as a realization of an associated uncertain time-delay system, where some parameters are determined by a random vector. For this uncertain system, the stability measure is a random variable whose probability density function provides a probabilistic measure of the stability assessment. The mean and the variance of the spectral abscissa random variable permit to quantify the main properties of the probability density function, and therefore they can be linked to the stability assessment of the uncertain time-delay system. Moreover, minimizing the mean with a variance penalty of this random spectral abscissa with respect to controller parameters provides a stability optimization method which is more robust against uncertainties than the deterministic approach described in section 1.1.4 and less conservative with respect to the worst-case minimization, *e.g.* the pseudospectral minimization [30, 4].

In order to motivate the proposed approach and highlight the contributions, we consider the hot shower problem (1.24) with controller parameter K and uncertainty ω , where ω is a realization of a random variable uniformly distributed in the interval $[-0.1, 0.1]$. Table 1.1 compares the results obtained by designing the reaction parameter with a deterministic approach, considering $\omega = 0$, or by the minimization

of the mean and of the mean with a variance penalty, considering ω a realization of a uniform random variable in $[-0.1, 0.1]$. Even though for the deterministic problem we get a smaller value of the spectral abscissa, the mean, and in particular, the variance are bigger compared to the probabilistic approach. The large value of the variance highlights the sensitivity of the deterministic approach, indeed a small perturbation might heavily affect the asymptotic exponential decay rate of the solutions, since the designed reaction parameter is close to a non-Lipschitz behavior of the spectral abscissa. On the other hand, the proposed approach presents a small variance ensuring the robustness of the system stability against uncertainties. In addition, increasing the variance penalty in the objective function, the probabilistic stabilization further decreases the sensitivity of the spectral abscissa with respect to the disturbances.

Table 1.1 Spectral abscissa ($\omega = 0$), its mean and variance for system (1.24) considering $\omega \sim \mathcal{U}[-1, 1]$ with designed reaction parameter K . The second column furnishes the results for the deterministic control design, obtained by minimizing the spectral abscissa for the deterministic model (1.14), while the second and third columns show the results of the probabilistic control design, obtained by minimizing respectively the mean and the mean plus variance of the spectral abscissa of system (1.24), with ω realization of a uniform random variable in $[-0.1, 0.1]$.

Control design	Deterministic	Probabilistic	
		Mean	Mean+ κ Variance, $\kappa = 1$
Designed parameter K	0.3680	0.4550	0.4510
Spectral abscissa $\alpha(\omega)$	-0.9998	-0.8577	-0.8635
Mean of $\alpha(\omega)$	-0.7487	-0.8516	-0.8518
Variance of $\alpha(\omega)$	$3.8459 \cdot 10^{-2}$	$6.1633 \cdot 10^{-3}$	$6.0837 \cdot 10^{-3}$

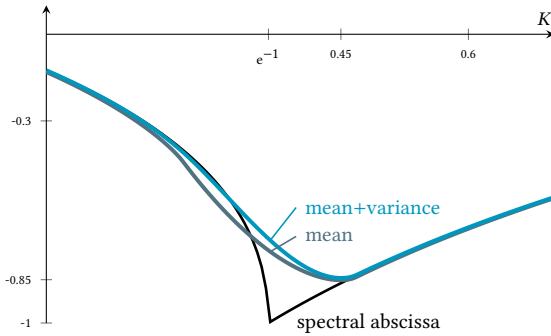


Figure 1.7 Objective functions comparison. The spectral abscissa for system (1.14) presents a non-Lipschitz behavior, illustrated also in Figure 1.5, while the mean and the mean with a variance penalty of the spectral abscissa behave smoothly for system (1.24), where ω is a realization of a uniform random variable in $[-0.1, 0.1]$.

The introduction of probabilistic uncertainties has, in addition, a smoothing effect on the stability optimization as illustrated in Figure 1.7. The non-Lipschitz behavior close to the optimal point for the objective function of the deterministic system (1.14) does not occur for the probabilistic model (1.24); indeed, in this latter case, the objective function involves an integral (mean and variance) of the stability measure, which smooths the integrand behavior.

1.2.2 Polynomial approximation of maximum eigenvalue function

Approximating a function by a polynomial is a widely used approach [90], and we have already applied it in section 1.1.3 to approximate the infinitesimal generator eigenvalue problem into a finite-dimensional one. Moreover, polynomial approximation is the core of the polynomial chaos method used in uncertainty quantification to approximate a quantity of interest as a function of uncertain parameters and then extract statistical information, like mean and variance [47, 103, 50].

In the last decades, applications of the polynomial chaos method to approximate eigenvalue functions has acquired more and more interest in the scientific community, as shown by the publications on standard eigenvalue problems [19, 27, 32, 46, 67, 74, 100] and on eigenvalue problems associated with autonomous time-delay systems [94]. However, the accuracy of the polynomial approximation crucially depends on the smoothness properties of the function to be approximated, and a maximum eigenvalue function, like spectral abscissa, is not always differentiable, as illustrated in Figures 1.5 and 1.7.

The second main contribution of this work stresses how the lack of smoothness properties of stability measure functions affects the polynomial approximation and polynomial chaos methods. To this end, the parallelism between polynomial chaos theory and polynomial approximation is exposed, and the convergence results of the latter framework are applied into the former context. These results represent a novelty especially in the uncertainty quantification literature, where the specific smoothness properties of eigenvalue function are rarely considered [19, 27, 32, 46, 67, 74, 100, 94].

The focus on maximum eigenvalue functions, despite the widespread usage of polynomial approximations, is motivated by the applications in control design. Indeed, as briefly introduced in the previous section, the stability optimization techniques provide, in general, non-smooth behavior of the stability measure for the controlled system and the corresponding literature often overlooks the robustness against parameter variations. In this context, where non-smooth behavior often occurs, the accuracy of polynomial and polynomial chaos approximations might be highly affected.

1.2.3 Stability and stabilization for periodic time-delay systems

Several methods explicitly or implicitly discretize the monodromy operator eigenvalue problem (1.3) into a generalized finite-dimensional eigenproblem, providing an approximation of the stability measure of the periodic time-delay system (1.1). For example, the semi-discretization approach [37] is based on approximating the delays by sawtooth functions, in such a way that the stability of the approximated system can be inferred from the stability of a higher order differential equation in discrete time. Analogously to the infinitesimal generator discretization in section 1.1.3, the monodromy operator and the solution operator are respectively discretized into a matrix by collocation methods in the software package DDE-BIFTOOL [78] and in the approach [8]. These methods rely on a discretize-first approach, where the accuracy of the Floquet multipliers cannot be iteratively refined, as in the second stage of Algorithm 1.1 for time-invariant system, discussed in section 1.1.3.

We propose a novel two-stage approach for periodic time-delay systems whose delays τ_j and period T are assumed commensurate numbers. This latter assumption is essential to alternatively characterize the Floquet multipliers by the solutions of a finite-dimensional nonlinear eigenvalue problem, where the product of the proposed characteristic matrix with a vector is implicitly defined by the solution of an initial value problem for an ordinary differential equation. The considered characteristic matrix generalizes the result of [42, Appendix A.2] and [80, Theorem 2.1], analyzing a scalar system with a single delay, and the characterization in [84, 71, 39], considering periodic systems with only one delay equal to the period, and expressing the nonlinear eigenvalue problem in terms of Floquet exponents, rather than Floquet multipliers. Refer to [85, 79] and reference therein for an overview on characteristic matrices for periodic time-delay system.

The novel stability assessment method first solves an eigenvalue problem obtained by the discretization of the monodromy operator, furnishing multiple approximations of the Floquet multipliers, and then iteratively refines these approximations, based on a nonlinear eigenvalue problem formulation. This efficient and reliable method for the computation of dominant Floquet multipliers is conceptually similar to Algorithm 1.1, since it exploits the dual interpretation of the Floquet multipliers arising from either the infinite-dimensional linear and the finite-dimensional nonlinear eigenvalue problem.

As a second contribution, we prove that the left eigenvectors of the characteristic matrix can be characterized in terms of right eigenvectors of a “transposed” nonlinear eigenvalue problem, analogously to the Proposition 1.5 for time-invariant systems. Moreover, we characterize the left eigenvector in terms of right eigenfunctions of the monodromy operator associated with a dual periodic time-delay systems, analogously to the transposition of the autonomous system (1.4), given by (1.23). These characterizations permit to extend the method for computing right eigenvectors to left eigenvectors, avoiding the construction of the full characteristic matrix, in

order to compute a left eigenvector corresponding to an already computed Floquet multiplier.

As a third contribution, we develop a novel method for stability optimization of periodic time-delay systems. Indeed, Proposition 1.4 applied to the characteristic matrix permits to compute the derivatives of simple Floquet multipliers with respect to (control) parameters, similarly to Algorithm 1.2. This result furnishes a good initialization for the iterative solver, based on the nonlinear eigenvalue problem, and can be applied in a stability optimization method, to minimize the spectral radius. The proposed stability optimization method improves in two ways existing techniques as [77, 63], where the monodromy operator is respectively discretized by semi-discretization and by spectral collocation. First, the objective function, and its gradient, whenever they exist, are at the level of the nonlinear eigenvalue problem, used for local corrections in the proposed method, while the existing techniques are based on a priori fixed discretization of the monodromy operator. Second, the efficiency and reliability of the optimization routine is improved by the explicit computation of the gradient.

1.3 OUTLINE

Based on the previously introduced preliminaries, chapter 2 analyzes the smoothness properties of the stability measure functions, and the effects of these behaviors on the polynomial approximation. The analyses of the stability measure smoothness properties play a major role in the context of spectrum-based stability analysis and stabilization, and is relevant for the following chapters 3-4. In particular, the stability assessment and optimization for autonomous time-delay systems with uncertain parameters, modeled as realizations of a random vector, is considered in chapter 3. Chapter 4 deals with periodic time-delay systems, whose delay and period are commensurable, and provides accurate and reliable methods for the computation of the spectral radius and its minimization. An overview of the chapters and their connections is illustrated in Figure 1.8.

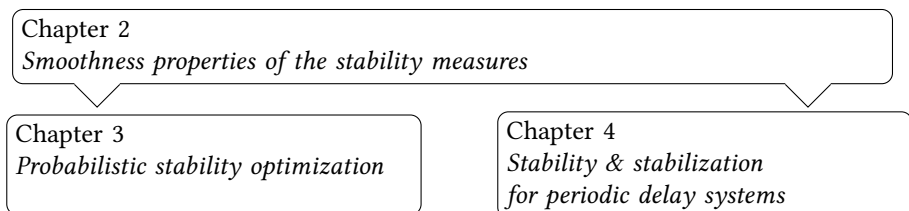


Figure 1.8 Overview of the different chapters.

Chapter 2 is mainly based on the paper [24] published in Numerical Algorithms, and contains the taxonomy of the spectral abscissa behaviors, associated with an autonomous time-delay system, presented in the paper [22] and in the conference proceeding [26]. Paper [22], published in Linear Algebra and its Applications, and the conference proceeding [26], presented at the European Nonlinear Dynamics Conference 2017 ground chapter 3. Chapter 4 is based on the manuscript [55] submitted to SIAM Journal on Matrix Analysis and Applications.

SMOOTHNESS PROPERTIES OF THE STABILITY MEASURES

This chapter first analyzes the smoothness properties of the spectral abscissa as function of system parameters. Even if the system matrices are analytic functions of the parameters, the stability measure may not be differentiable and even non-Lipschitz continuous, due to multiple dominant eigenvalues counted with multiplicity. This first analysis constitutes the basis for the stability optimization methods presented in the following chapters 3–4. Moreover, the chapter analyzes the effects of the lack of smoothness properties on the asymptotic convergence rate of polynomial approximations, which are closely related to the polynomial chaos approximations, if the parameters corresponds to realizations of random variables. The non-differentiable behaviors heavily affect not only the approximation errors of Galerkin and collocation based polynomial approximations, but also the numerical errors to evaluate the coefficients in the Galerkin approach with integration methods.

The behavior of the stability measures, introduced in section 1.1, as a function of system parameters is determined by the dominant eigenvalues. In particular, the smoothness properties of the spectral abscissa and of the spectral radius are respectively determined by the behavior of the dominant characteristic roots (in the sense of being rightmost) and of the dominant Floquet multipliers (in the sense of having maximal modulus). The elements of an operator spectrum, which are dominant eigenvalues in a compact parameter space, are finite in number, due to properties of the infinite-dimensional operator spectrum. The following analysis on the smoothness properties and polynomial (chaos) approximation can be extended to real-valued functions determined by a finite number of dominant eigenvalues for a general parametrized eigenvalue problem. Hence, even though the results can be trivially generalized to the spectral radius of the monodromy operator for periodic time-delay systems, for simplicity, we restrict to analyze the spectral abscissa function for autonomous time-delay systems

$$\dot{x}(t) = \sum_{j=0}^h A_j(\omega)x(t - \tau_j(\omega)), \quad (2.1)$$

where $\omega \in \Omega \subset \mathbb{R}^D$ models $D \in \mathbb{N}$ parameters subject to uncertainties, the parameter space Ω is a compact subset of \mathbb{R}^D , and for every $j \in \{0, \dots, h\}$, $A_j : \Omega \rightarrow \mathbb{R}^{r \times r}$ and $\tau_j : \Omega \rightarrow \mathbb{R}_+$ are smooth functions.

The spectral abscissa associated with system (2.1) is a function of the uncertainties ω ,

$$\alpha : \Omega \subset \mathbb{R}^D \rightarrow \mathbb{R}, \text{ such that } \omega \mapsto \alpha(\omega) := \max_{\lambda \in \mathbb{C}} \{\operatorname{Re}(\lambda) : \det(\mathcal{A}(\lambda; \omega)) = 0\}, \quad (2.2)$$

where $\mathcal{A}(\lambda; \omega)$ is the characteristic matrix depending on the eigenvalue $\lambda \in \mathbb{C}$ and the uncertainty ω ,

$$\mathcal{A}(\lambda; \omega) = \lambda I_r - \sum_{j=0}^h A_j(\omega) e^{-\lambda \tau_j(\omega)}.$$

The chapter is organized as follows. In section 2.1, we briefly review the behavior of the spectral abscissa function furnishing test-cases, which are then analyzed in the following two sections. Section 2.2 focuses on the polynomial expansion of the spectral abscissa function, explaining the parallelism between polynomial approximation and polynomial chaos theory. In section 2.3, the polynomial approximation for the parametric eigenvalue problem with $D = 1$ is investigated. Then, in section 2.4, the multivariate polynomial approximation (with $D > 1$) is analyzed through some numerical experiments. The chapter ends in section 2.5 furnishing novel perspective on future research directions to approximate the stability measure functions. The numerical experiments of this chapter, performed using the software Chebfun [16], are publicly available along with the tutorial [23].

2.1 BEHAVIOR OF THE SPECTRAL ABCISSA

In general, the spectral abscissa function (2.2) is smooth almost everywhere in the parameter space Ω . However, even if the system matrices are analytic functions of the parameters, the spectral abscissa is in general not differentiable everywhere due to the presence of the maximum operator in (2.2) and due to the presence of multiple dominant characteristic roots. Indeed, in a set of measure zero, more than one dominant characteristic root, counted with multiplicity, can present the same real part; in these points, the spectral abscissa function might be non-differentiable and even non-Lipschitz continuous.

We distinguish the different qualitative behavior of the spectral abscissa function by considering the dominant characteristic roots, which are characteristic roots $\lambda \in \mathbb{C}$ satisfying $\operatorname{Re}(\lambda) = \alpha(\omega)$ and $\operatorname{Im}(\lambda) \geq 0$. Indeed, relevant results on the behavior of eigenvalues of parametrized eigenvalue problems [44, 53] allow us to characterize the smoothness properties of the spectral abscissa function as follows.

Smooth behavior The spectral abscissa is smooth on the entire parameter space Ω , if for all $\omega \in \Omega$, there is only one dominant characteristic root, whose algebraic and geometric multiplicity is equal to 1, *i.e.* the dominant characteristic root is simple

in Ω . In this case, the partial derivative of the dominant characteristic root and of the spectral abscissa function with respect to a system parameter can be computed by the explicit formula stated in Proposition 1.4.

Example 2.1. The following parametric eigenvalue problem with $\omega \in [-1, 1]$

$$\left(\lambda I_2 - \begin{pmatrix} e^\omega & 0 \\ 0 & -1 \end{pmatrix} \right) v = 0, \quad v \in \mathbb{C}^2 \setminus \{0\},$$

presents a smooth behavior of the spectral abscissa function

$$\alpha(\omega) = e^\omega, \quad \omega \in [-1, 1],$$

as illustrated in Figure 2.1.

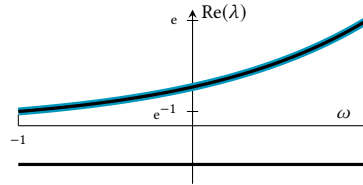


Figure 2.1 Real part of the spectrum, where the spectral abscissa is highlighted.

Lipschitz behavior The spectral abscissa may not be differentiable but it is Lipschitz continuous in Ω , if the dominant characteristic root is simple in the domain Ω , except in a set of measure zero, where the rightmost eigenvalues are multiple but their algebraic multiplicity is always equal to the geometric one, *i.e.* the rightmost eigenvalues are semi-simple. In this situation, the dominant characteristic roots can cross but not overlap each other or, if they overlap, then their algebraic multiplicity equals the geometric one.

Example 2.2. The following parametric eigenvalue problem with $\omega \in [-1, 1]$

$$\left(\lambda I_2 - \begin{pmatrix} \omega & 0 \\ 0 & 0 \end{pmatrix} \right) v = 0, \quad v \in \mathbb{C}^2 \setminus \{0\},$$

presents a Lipschitz continuous spectral abscissa function

$$\alpha(\omega) = \begin{cases} 0, & \text{if } \omega \in [-1, 0), \\ \omega, & \text{if } \omega \in [0, 1]. \end{cases}$$

Indeed, the spectral abscissa is a piecewise linear function, as shown in Figure 2.2, and in $\omega = 0$ there is a multiple semi-simple characteristic root.

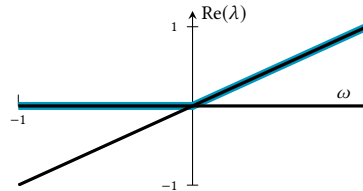


Figure 2.2 Real part of the spectrum, where the spectral abscissa is highlighted.

Continuous behavior The spectral abscissa is continuous but typically not Lipschitz continuous if there exists $\omega \in \Omega$ where there is a dominant characteristic root with algebraic multiplicity greater than the geometric one, *i.e.* this dominant characteristic root is non-semi-simple.

Example 2.3. The following parametric eigenvalue problem with $\omega \in [-1, 1]$

$$\left(\lambda I_2 - \begin{pmatrix} 0 & \omega \\ 1 & 0 \end{pmatrix} \right) v = 0, \quad v \in \mathbb{C}^2 \setminus \{0\},$$

presents a continuous spectral abscissa function

$$\alpha(\omega) = \begin{cases} 0, & \text{if } \omega \in [-1, 0), \\ \sqrt{\omega}, & \text{if } \omega \in [0, 1]. \end{cases}$$

Indeed, the spectral abscissa is not Lipschitz continuous at $\omega = 0$, where there is a double non-semi-simple characteristic root.

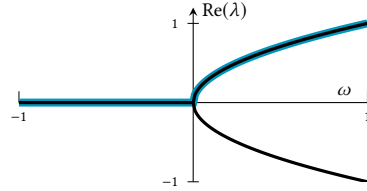


Figure 2.3 Real part of the spectrum, where the spectral abscissa is highlighted.

The non-smooth behaviors of the spectral abscissa function often occur in the stabilization of time-delay systems. The minimization of the dominant characteristic roots analyzed in section 1.1.4 leads to multiple (and, in general, non-semi-simple) dominant characteristic roots. In the minimum, the dominant characteristic roots counted with multiplicity are mainly equal to the dimension of the controller plus one, $k + 1$. Indeed, we can intuitively think that each controller parameter can shift to the left a single rightmost characteristic root, when all the k controller parameters are designed so that the k rightmost characteristic roots, counted with multiplicity, have the same real part as the $k + 1$ th rightmost characteristic root, then a minimum of the stability optimization is reached. This situation occurs in Example 1.4, where the minimal spectral abscissa is attained when there is a double non-semi simple dominant characteristic root.

Additional novel control design techniques, introduced in Remark 1.4, directly impose multiple non-semi-simple dominant characteristic roots in the spectrum of the controlled time-delay system [68, 96, 49, 69, 6, 7]. These design techniques are simple but they provide, in general, non-smooth behaviors of the spectral abscissa for the controlled system, yet in the corresponding literature no attention is paid to robustness against parameter variations, while the usage of the polynomial chaos expansion may become questionable. Therefore, we are going to systematically show through numerical examples, how the non-smooth behaviors of the spectral abscissa affect the polynomial approximation, which is strictly connected to the polynomial chaos theory as explained in the following section.

2.2 POLYNOMIAL (CHAOS) EXPANSION

Let $\{p_i(\omega)\}_{i \in \mathbb{N}}$ be a degree graded polynomial basis orthogonal with respect to a smooth non-negative function $w : \Omega \rightarrow \mathbb{R}_+$, $\omega \mapsto w(\omega)$ defined and normalized on the compact support $\Omega \subset \mathbb{R}^D$, i.e. $\int_{\Omega} w(\omega) d\omega = 1$. The spectral abscissa function (2.2) can be expressed by a polynomial expansion in the basis $\{p_i(\omega)\}_{i \in \mathbb{N}}$

$$\alpha(\omega) = \sum_{i=0}^{\infty} c_i p_i(\omega), \quad (2.3)$$

where the coefficients $c_i \in \mathbb{R}$ are evaluated by

$$c_i = \frac{\langle \alpha, p_i \rangle_w}{\|p_i\|_w^2}, \quad i \in \mathbb{N}. \quad (2.4)$$

The w -inner product, used in the above equation, is defined for all $f, g : \Omega \rightarrow \mathbb{R}$ such that

$$\langle f, g \rangle_w = \int_{\Omega} f(\omega) g(\omega) w(\omega) d\omega. \quad (2.5)$$

and the induced w -norm is determined by $\|f\|_w = \sqrt{\langle f, f \rangle_w}$.

In order to explain the parallelism between the polynomial (2.3) and the polynomial chaos expansion, we interpret ω as a realization of a real random vector $\boldsymbol{\omega}$, with probability density function $w(\omega)$. The random variables modeling the uncertainties are denoted with bold letters, e.g. $\boldsymbol{\omega}$, while the normal font indicates their realizations $\omega \in \Omega$. With this notation, $\alpha(\boldsymbol{\omega})$ is a random variable while $\alpha : \Omega \rightarrow \mathbb{R}$, $\omega \mapsto \alpha(\omega)$ is a function depending on the realization $\omega \in \Omega$.

The mean and the variance of the spectral abscissa random variable $\alpha(\boldsymbol{\omega})$, respectively defined by

$$\mathbb{E}(\alpha(\boldsymbol{\omega})) := \int_{\Omega} \alpha(\omega) w(\omega) d\omega, \text{ and } \mathbb{V}(\alpha(\boldsymbol{\omega})) := \int_{\Omega} (\alpha(\omega) - \mathbb{E}(\alpha(\boldsymbol{\omega})))^2 w(\omega) d\omega, \quad (2.6)$$

exist and are finite, since the integrands are continuous functions, as described in the previous section 2.1, and the domain of integration Ω is a compact subset of \mathbb{R}^D . Moreover, the polynomial expansion of $\alpha(\boldsymbol{\omega})$

$$\alpha(\boldsymbol{\omega}) = \sum_{i=0}^{\infty} c_i p_i(\boldsymbol{\omega}), \quad (2.7)$$

corresponds to a polynomial chaos expansion of the spectral abscissa function with germ $\boldsymbol{\omega}$.

The polynomial chaos expansion permits to compactly define a general random variable, through the chaos coefficients c_i , and the germ $\boldsymbol{\omega}$, which also specifies the

w -orthonormal polynomial basis $\{p_i\}_{i \in \mathbb{N}}$. The chaos coefficients c_i convey mean, variance and variance-based sensitivity analysis of the random variable. Indeed, other than for the computation of mean and variance, they permit to decompose the variance into the contribution of individual model parameters and the interaction between each of them (Sobol's sensitivity index) or to measure the total variance due to each single model parameter (total order sensitivity index). For further information on the sensitivity indexes, refer to [34, 82].

THEOREM 2.1 *Given a polynomial chaos expansion (2.7), the following formulas hold:*

1. *Mean:* $\mathbb{E}(\alpha(\omega)) = c_0$.
2. *Variance:* $\mathbb{V}(\alpha(\omega)) = \sum_{i=1}^{\infty} c_i^2 \|p_i\|_w^2$.
3. *If the polynomial basis $\{p_i(\omega)\}_{i \in \mathbb{N}}$ is constructed by a tensor product of univariate polynomial bases $\{p_{i,d}(\omega_d)\}_{i \in \mathbb{N}}^{d \in \{1, \dots, D\}}$ through the bijective D -tupling function $\pi_D : \mathbb{N}^D \rightarrow \mathbb{N}$, $(i_1, \dots, i_D) \mapsto i$ in such a way that*

$$p_i(\omega) = \prod_{d=1}^D p_{i_d, d}(\omega_d), \quad \text{with } (i_1, \dots, i_D) = \pi_D^{-1}(i), \quad (2.8)$$

then, the Sobol's sensitivity index $\mathbb{S}_\mathfrak{d}(\alpha(\omega))$ associated with the non-empty subset of uncertain parameters $\omega_\mathfrak{d}$, with $\mathfrak{d} \subseteq \{1, \dots, D\}$ and $\mathfrak{d} \neq \emptyset$, is determined by

$$\mathbb{S}_\mathfrak{d}(\alpha(\omega)) = \sum_{i \in Q_\mathfrak{d}} \frac{c_i^2 \|p_i\|_w^2}{\mathbb{V}(\alpha(\omega))},$$

where $Q_\mathfrak{d} = \{i \in \mathbb{N} : \pi_D^{-1}(i) = (i_1, \dots, i_D)$, such that, for every $d = 1, \dots, D$, $i_d > 0$ if and only if $d \in \mathfrak{d}\}$. For $d \in \{1, \dots, D\}$, the effect of the d -th parameter ω_d can be quantified by the total order sensitivity index

$$\mathbb{S}_d(\alpha(\omega)) = \sum_{\mathfrak{d} \subseteq \{1, \dots, D\}, d \in \mathfrak{d}} \mathbb{S}_\mathfrak{d}(\alpha(\omega)).$$

Proof. A proof of the first two classical results 1 and 2 can be found in [94], while the last result 3 is derived by [14]. \square

Theorem 2.1 relies on the orthogonality of the polynomial basis $\{p_i\}_{i \in \mathbb{N}}$ with respect to the probability density function $w(\omega)$ of the random vector ω . For example, the Legendre polynomials are orthogonal to the probability density functions of uniform distributions [103, 47].

The polynomial chaos theory and polynomial approximation are closely related and in the following sections we apply the results of the latter into the former context. To

this end, the asymptotic convergence rate of polynomial (chaos) approximation are stated in the L^∞ norm, *i.e.* the supremum norm $\|\cdot\|_s$ for every function $f : \Omega \rightarrow \mathbb{R}$. This represents a novelty in the context of the polynomial chaos theory, where the L^∞ norm is rarely employed, even though it is more stringent than the L^2 and the L^1 norms.

The behavior of the spectral abscissa function (2.2), $\alpha(\omega)$, is fundamental for the accuracy of the truncations of its polynomial expansion (2.3) and the corresponding polynomial expansion (2.7) of $\alpha(\omega)$, as we are going to analyze in the following sections. However, first, we explicit the polynomial (chaos) expansion of the examples introduced in section 2.1.

Example 2.4. We analytically compute the polynomial (chaos) expansion of the spectral abscissa functions given in Examples 2.1–2.3. In the parameter space $\Omega = [-1, 1]$, we consider the Legendre polynomial basis $\{p_i\}_{i \in \mathbb{N}}$, which is orthogonal with respect to $w(\omega) = 1/2$. Indeed, for every $\omega \in [-1, 1]$, and for $i, j \in \mathbb{N}$, the orthogonality of the Legendre polynomial basis is given by

$$\langle p_i, p_j \rangle_w = \int_{\Omega} p_i(\omega) p_j(\omega) w(\omega) d\omega = \begin{cases} \|p_i\|_w^2 = \frac{1}{2i+1} & \text{if } i = j, \\ 0 & \text{otherwise.} \end{cases}$$

The w function corresponds to the probability density function of a random variable uniformly distributed in the interval $[-1, 1]$. Therefore, the polynomial expansion in the Legendre polynomial basis orthogonal to w can be interpreted as a realization of the polynomial chaos expansion, whose germ ω is a uniform random variable.

To analytically express the coefficients c_i in (2.4), we evaluate the w -inner product between the spectral abscissa functions and the i -th Legendre polynomial. We start analyzing the spectral abscissa defined in Example 2.1 and we furnish the corresponding w -inner product iteratively, starting from:

$$\langle \alpha, p_0 \rangle_w = \frac{1}{2} (e - e^{-1}).$$

Set $i \in \mathbb{N} \setminus \{0\}$, by using integration by parts, and the following Legendre polynomial properties

$$p_i(\pm 1) = (\pm 1)^i, \quad \text{and} \quad \frac{dp_{i+1}(\omega)}{d\omega} = \sum_{k=0}^{\lfloor i/2 \rfloor} \frac{p_{i-2k}(\omega)}{\|p_{i-2k}\|_w^2},$$

we get

$$\langle \alpha, p_{i+1} \rangle_w = \frac{1}{2} \left(e + \frac{(-1)^i}{e} - 2 \sum_{k=0}^{\lfloor i/2 \rfloor} \frac{\langle \alpha, p_{i-2k} \rangle_w}{\|p_{i-2k}\|_w^2} \right) = \frac{1}{2} \left(e + \frac{(-1)^i}{e} - 2 \sum_{k=0}^{\lfloor i/2 \rfloor} c_i \right),$$

where c_i indicates the i -th coefficients of polynomial approximation (2.3) for the spectral abscissa function $\alpha(\omega) = e^\omega$, with $\omega \in [-1, 1]$.

By [1, Relations 22.13.8-22.13.9], the w -inner product of the spectral abscissae of Example 2.2 and 2.3 can respectively be expressed for every $i \in \mathbb{N}$ as

$$\langle \alpha, p_i \rangle_w = \begin{cases} \frac{(-1)^j \Gamma(j - \frac{1}{2})}{4\Gamma(-\frac{1}{2})\Gamma(j+2)}, & \text{if } i = 2j, \\ 1/6, & \text{if } i = 1, \\ 0, & \text{otherwise;} \end{cases} \quad \langle \alpha, p_i \rangle_w = \begin{cases} \frac{(-1)^j \Gamma(j - \frac{1}{4})\Gamma(\frac{3}{4})}{4\Gamma(-\frac{1}{4})\Gamma(j + \frac{7}{4})}, & \text{if } i = 2j, \\ \frac{(-1)^j \Gamma(j + \frac{1}{4})\Gamma(\frac{5}{4})}{4\Gamma(\frac{1}{4})\Gamma(j + \frac{9}{4})}, & \text{if } i = 2j + 1, \end{cases}$$

where $\Gamma(\cdot)$ denotes the Gamma function. These inner products are rational numbers, computable without any error via a symbolic software.

Remark 2.1. Close to multiple non-semi-simple dominant characteristic roots the spectral abscissa might present a very large Lipschitz constant. This phenomenon might significantly affect the transient behavior of the polynomial approximation errors, increasing the polynomial degree, but it does not affect the asymptotic convergence behavior of the polynomial approximation.

2.3 UNIVARIATE POLYNOMIAL APPROXIMATION

In practice, for computational reasons, the polynomial expansion (2.3) is approximated by finitely many terms

$$\alpha_P(\omega) = \sum_{i=0}^P \tilde{c}_i p_i(\omega). \quad (2.9)$$

Several methods exist to compute the coefficients \tilde{c}_i ; here we focus on the Galerkin and collocation approaches, analyzed in sections 2.3.1 and 2.3.2, respectively. Both methods are applied to the model problems of section 2.1 by increasing the polynomial degree $P \in \mathbb{N}$, in order to inspect the L^∞ convergence rates of the polynomial approximation (2.9) and compare them with the asymptotic theoretical results.³

2.3.1 Galerkin approximation

Given a finite polynomial basis $\{p_i\}_{i=0}^P$, the Galerkin approach finds an approximation (2.9) of spectral abscissa function (2.2) such that the residual is orthogonal with respect to the polynomial basis, in formula

$$\langle \alpha - \alpha_P, p_i \rangle_w = 0, \quad \text{for every } i = 0, \dots, P. \quad (2.10)$$

³ The reader interested in a fully automated procedure for polynomial approximation, which adaptively select the degree P by monitoring the decrease of the magnitude of the coefficients \tilde{c}_i , is referred to software Chebfun, used for example in the tutorial [23] and in [90].

This leads to $\tilde{c}_i = c_i$, where the coefficients c_i are defined in (2.4). Hence, the Galerkin approach is nothing else than a truncation up to order P of polynomial series (2.3). Moreover, it provides the optimal approximation in the w -norm, *i.e.*

$$\|\alpha - \alpha_P\|_w = \sqrt{\int_{\Omega} (\alpha(\omega) - \alpha_P(\omega))^2 w(\omega) d\omega}$$

is minimized.

This approximation of $\alpha(\omega)$ corresponds to the stochastic Galerkin approximation of $\alpha(\omega)$ in the polynomial chaos theory.

The convergence analyses consider, first of all, the truncation error up to order P of the polynomial expansion, and then, the numerical error to compute coefficient c_i .

Approximation error

If the coefficients c_i are correctly evaluated, the following theorem, derived by [99], determines the error bounds of the polynomial approximation (2.9), obtained by the Galerkin approach with Legendre polynomials $\{p_i\}_{i=0}^P$ (with $w(\omega) = 1/2$ for $\omega \in [-1, 1]$).

THEOREM 2.2 *Let $\alpha, \alpha', \dots, \alpha^{(k-1)}$ be absolutely continuous on $\Omega = [-1, 1]$, with $k > 1$. If $\alpha^{(k)}$ presents bounded variation with respect to the Chebyshev weighting function, *i.e.**

$$\int_{-1}^1 \frac{|\alpha^{(k+1)}(\omega)|}{\sqrt{1-\omega^2}} d\omega = \tilde{V}_k < \infty,$$

then, for each $P > k + 1$, the following relation holds

$$\|\alpha - \alpha_P\|_s \leq \sqrt{\frac{\pi}{2}} \frac{\tilde{V}_k}{(k-1)(P-k)^{k-0.5}}.$$

The level of smoothness, *i.e.* the maximum k satisfying the assumption of Theorem 2.2, heavily determines the convergence behavior of polynomial approximation (2.9). Only the smooth behavior of the spectral abscissa verifies the assumptions of Theorem 2.2, and satisfies them for all $k \in \mathbb{N}$, ensuring a convergence rate faster than $O(P^{-k})$, for all $k \in \mathbb{N}$. In fact, the convergence rate for this case is at least geometric, based on analytic extension of real functions on the complex plane [99]; such extension always exists for a real analytic function.

The truncation error obtained by the Galerkin approach for the spectral abscissa of parametric eigenvalue problem in Example 2.1 presents a spectral convergence, more precisely the order of convergence is $O(e^{-cP})$ with $c \in \mathbb{R}_+ \setminus \{0\}$, as shown in Figure 2.4. The spectral abscissae of Examples 2.2 and 2.3 converge with an order of $O(P^{-1})$, and $O(P^{-0.5})$, respectively. The polynomial approximation coefficients are analytically evaluated in Example 2.4.

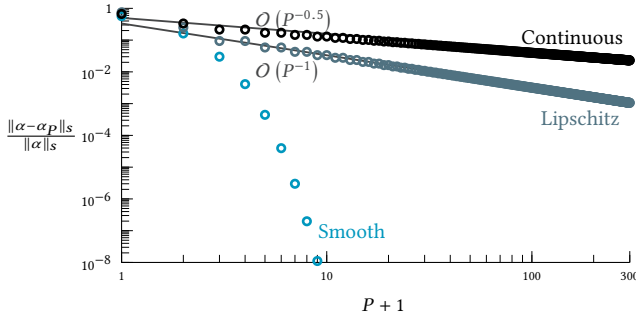


Figure 2.4 Convergence history for Galerkin approach. Relative errors of polynomial approximation (2.9) obtained by the Galerkin approach up to order P for the spectral abscissa functions of Examples 2.1–2.3.

Numerical error

It is not always possible to analytically compute the coefficients $c_i = \tilde{c}_i$ with (2.4), therefore an integration method based on $M + 1$ nodes can approximate the integrals $\langle \alpha, p_i \rangle_w$ and consequently the coefficients, denoted by \tilde{c}_i^M . This type of approach is known as non-intrusive spectral projection in the polynomial chaos framework.

In this section, the coefficients of the Galerkin polynomial approximation α_P^M are approximated by the following integration methods based on $M + 1$ points.

Classical integration methods based on an equally spaced discretization of Ω containing the extremes of Ω : -1 and 1 . In particular, we focus on extended trapezoidal rule and extended Simpson's rule. For the latter method, M is required to be an even number.

Interpolatory quadrature rules approximate an integral by integrating the interpolant of its integrand, where the degree of the polynomial interpolant is at most M . We consider Clenshaw-Curtis and Gauss quadrature rules based on Chebyshev and Legendre points, respectively. (Further information on the interpolatory properties of Chebyshev points are presented in the upcoming section 2.3.2.)

For smooth functions, including the smooth behavior of the spectral abscissa, the extended trapezoidal and Simpson's rules provide an order of convergence $O(M^{-2})$ and $O(M^{-4})$, respectively.

Figure 2.5 shows the numerical errors of classical integration methods to evaluate the first coefficient c_0 of polynomial expansion (2.3) for the examples in section 2.1. The convergence of the spectral abscissa function in Example 2.1 follows the theoretical

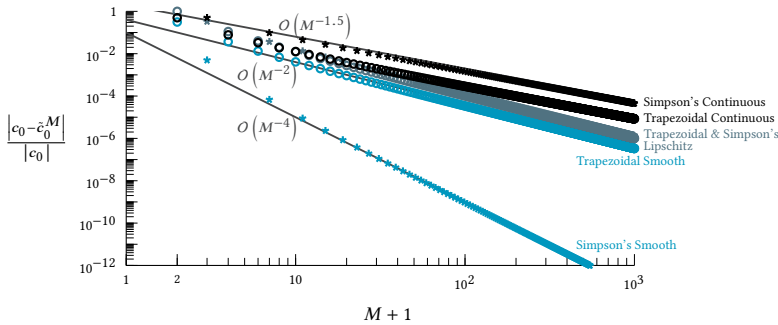


Figure 2.5 Convergence history of \tilde{c}_0^M for classical integration methods. Relative errors to compute the first coefficient \tilde{c}_0^M of (2.9) with extended Trapezoidal and Simpson’s rules based on $M + 1$ equally spaced points for the spectral abscissa functions of Examples 2.1–2.3.

error bounds. For Examples 2.2 and 2.3, the convergence rates for both classical integration methods are $O(M^{-2})$ and $O(M^{-1.5})$, respectively.

Whenever the integrand is smooth enough to be well-approximated by a polynomial, the interpolatory quadrature rules perform better than the classical integration rule; as stated in the following theorem, combining the results of [90, 102, 101].

THEOREM 2.3 For an integer $k \geq 1$, let $\alpha, \alpha', \dots, \alpha^{(k-1)}$ be absolutely continuous on $\Omega = [-1, 1]$ and given $i \in \mathbb{N}$ let $(\alpha(\omega)p_i(\omega))^{(k)}$ present bounded variation, i.e.

$$\int_{-1}^1 \left| (\alpha(\omega)p_i(\omega))^{(k+1)} \right| d\omega = V_{i,k} < \infty.$$

Then, the Clenshaw-Curtis quadrature rule for the approximation of c_i with $M + 1$ points, i.e. \tilde{c}_i^M , satisfies

$$|c_i - \tilde{c}_i^M| \leq \frac{32}{15\pi} \frac{V_{i,k}}{k(M-k)^k}, \quad \text{for } M > k,$$

and $(M + 1)$ -Gauss quadrature satisfies

$$|c_i - \tilde{c}_i^M| \leq \frac{32}{15\pi} \frac{V_{i,k}}{k(2M+1-k)^k}, \quad \text{for } M > 2k + 1.$$

Moreover, for $k = 1$, Clenshaw-Curtis quadrature rule presents a convergence rate of $O(M^{-2})$, while Gauss quadrature error is at most of size $O(M^{-2} \ln(M))$.

The theorem can be applied to smooth behavior of the spectral abscissa, providing a convergence rate faster than $O(M^{-k})$ for all $k \in \mathbb{N}$, for both interpolatory quadrature rules. Moreover, the theorem ensures that if the spectral abscissa is Lipschitz

continuous, and it is hence absolutely continuous, then Clenshaw-Curtis quadrature has a rate of convergence $O(M^{-2})$, while the Gauss quadrature errors converge, at least, as $O(M^{-2} \ln(M))$.

Figure 2.6 illustrates the numerical error induced by the approximation with interpolatory quadrature rules of the first coefficient c_0 of Examples 2.1–2.3. The spectral abscissa of Example 2.1 spectrally converges with order $O(e^{-cM})$ for $c \in \mathbb{R}_+ \setminus \{0\}$, improving the convergence rate of the classical integration methods. For non-smooth cases, Examples 2.2 and 2.3, the convergence rates of interpolatory quadrature rules are like the ones obtained by classical integration methods, Figure 2.5.

From this numerical experiment, Clenshaw-Curtis and Gauss quadrature rules present similar convergence rates. Hence, the bound of Theorem 2.3 for smooth and Lipschitz functions are optimal for Clenshaw-Curtis quadrature rule, and conservative for Gauss quadrature rule (as already observed in [102, 101]).

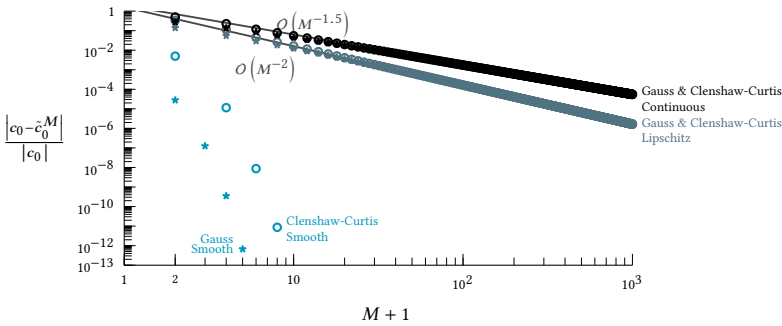


Figure 2.6 Convergence history of \tilde{c}_0^M for interpolatory quadrature rules. Relative errors to compute the first coefficient \tilde{c}_0^M of (2.9) with Clenshaw-Curtis and Gauss quadrature rules with $M + 1$ points for the spectral abscissa functions of Examples 2.1–2.3.

Remark 2.2. When the coefficients \tilde{c}_i^M of α_P^M are approximated by interpolatory quadrature rules, it is advised to set $M \geq P$ as explained with further details at the end of the upcoming section 2.4.1.

Remark 2.3. In the polynomial chaos framework, the first coefficient \tilde{c}_0^M can be interpreted by Theorem 2.1 as the mean of the spectral abscissae in Examples 2.1–2.3, considering ω in these examples a realization of a uniform random variable in $[-1, 1]$. The corresponding convergence rates for the mean (Figures 2.5 and 2.6) provide only insights on the numerical error of the integration method, and are not meaningful for the truncation error of the polynomial approximation.

2.3.2 Collocation approach

The collocation approach determines the coefficients of (2.9) by interpolation on $P + 1$ points, $\{\xi_m\}_{m=0}^P \subset \Omega$:

$$\alpha_P(\xi_m) = \alpha(\xi_m), \quad \text{for all } m \in \{0, \dots, P\}. \quad (2.11)$$

The polynomial coefficients \tilde{c}_i of α_P can be computed by solving a linear system of $P + 1$ equations, and this can be often done with a negligible numerical error.

Remark 2.4. The collocation method is mainly affected by approximation errors, while the Galerkin approach might also present a numerical error, due to numerical computation of the coefficients, as illustrated in the previous section. On the other hand, whereas the Galerkin approach dynamically computes the coefficients, *i.e.* each coefficient is evaluated independently from the others, the collocation approach simultaneously evaluates all $P + 1$ coefficients, solving a linear system of equations.

A widely used choice of interpolating nodes for the interval $[-1, 1]$ are Chebyshev nodes. The polynomial interpolant satisfies error bounds, similar to Theorem 2.2, and provides a near-best approximation in L^∞ sense, as stated in the following theorem, whose proof can be found in [90, Theorems 7.2 and 16.1].

THEOREM 2.4 *If $\alpha, \alpha', \dots, \alpha^{(k-1)}$ are absolutely continuous on $\Omega = [-1, 1]$ and $\alpha^{(k)}$ presents bounded variation V_k , *i.e.**

$$\int_{-1}^1 \left| \alpha^{(k+1)}(\omega) \right| d\omega = V_k < \infty,$$

then the Chebyshev interpolant α_P of degree $P > k$, satisfies

$$\|\alpha - \alpha_P\|_s \leq \frac{4}{\pi} \frac{V_k}{\pi k(P-k)^k}.$$

Moreover, if α_P^\star is the best polynomial approximation of order less than or equal to P , then

$$\|\alpha - \alpha_P\|_s \leq \left(2 + \frac{2}{\pi} \log(P+1) \right) \|\alpha - \alpha_P^\star\|_s.$$

Theorem 2.4 ensures the collocation approach on Chebyshev nodes converges, at least, as $O(P^{-1})$ and faster than $O(P^{-k})$ for all $k \in \mathbb{N}$, for the Lipschitz and smooth behaviors of the spectral abscissa, respectively.

The polynomial interpolant on Chebyshev points can be computed by Fast Fourier Transform based algorithms, mapping interpolating values onto coefficients of a polynomial approximation in the Chebyshev polynomial basis. Chebyshev interpolants for Examples 2.1–2.3, as well as the best L^∞ polynomial approximation

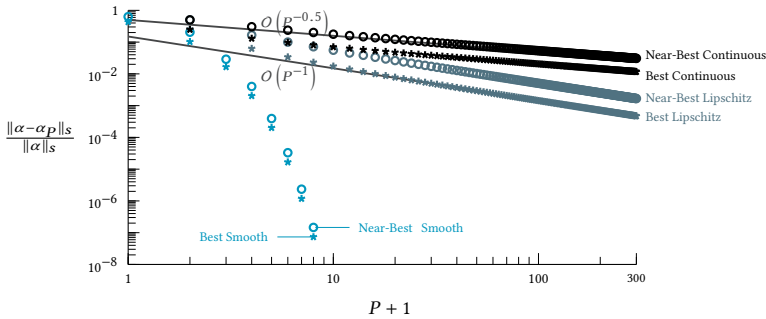


Figure 2.7 Convergence history of best and near-best polynomials. Relative errors of polynomial approximation (2.9) obtained by interpolation on $P + 1$ Chebyshev points (near-best approximation) for the spectral abscissa functions of Examples 2.1–2.3. The relative error for the best polynomial approximation in the L^∞ sense is also shown.

are evaluated by Chebfun [23]. Figure 2.7, other than indicating the interpolating error (near-best polynomial approximation), shows the convergence rates of the best L^∞ polynomial approximation. The convergence rates are analogous to the ones obtained by the Galerkin approach (section 2.3.1, Figure 2.4) and agree with Theorem 2.4 for smooth and Lipschitz behaviors.

Remark 2.5. In order to apply Theorem 2.1, the polynomial approximation in Chebyshev polynomial basis can be recast as a truncated polynomial chaos expansion in the uniformly distributed germ using a polynomial transformation. This transformation converts the Chebyshev expansion coefficients into the Legendre coefficients and does not affect the results shown in Figure 2.7, since the numerical error of the transformation is negligible [88].

2.4 MULTIVARIATE POLYNOMIAL APPROXIMATION

In this section, first of all, we generalize polynomial approximation (2.9) to handle multiple variables, *i.e.* $D > 1$. With this novel generalization, the coefficients \tilde{c}_i can be evaluated by the Galerkin and collocation approaches, through the corresponding formula (2.10) and (2.11). Then, we consider examples of $D = 2$ parametric eigenvalue problems, where spectral abscissa functions present the different behaviors characterized in section 2.1. The Galerkin and collocation approaches are, hence, applied to the latter benchmark in sections 2.4.1 and 2.4.2, respectively.

We focus on polynomial approximation using a degree graded polynomial basis $\{p_i(\omega)\}_{i \in \mathbb{N}}$, constructed by products of univariate degree graded polynomial bases $\{p_{i,d}(\omega_d)\}_{i \in \mathbb{N}}^{d \in \{1, \dots, D\}}$, satisfying hence the assumption of Theorem 2.1 point 3. The

degree grading of the polynomial basis $\{p_i\}_i$ follows a norm $\|\cdot\|$ on \mathbb{N}^D , which is associated with a D -tupling function $\pi_D : \mathbb{N}^D \rightarrow \mathbb{N}$. Therefore, the basis is obtained by formula (2.8), and the generalization of polynomial approximation (2.9) for the multivariate case is given by

$$\alpha_P(\omega) = \sum_{\|\pi_D^{-1}(i)\| \leq P_d, i \in \mathbb{N}} \tilde{c}_i p_i(\omega) = \sum_{i=0}^P \tilde{c}_i p_i(\omega), \quad (2.12)$$

where $P+1$ is equal to the number of polynomials in $\{p_i\}_{i \in \mathbb{N}}$ such that the multivariate degree is less than or equal to $P_d \in \mathbb{N}$.

Remark 2.6. The bijective D -tupling functions $\pi_D : \mathbb{N}^D \rightarrow \mathbb{N}$ provide an ordering with respect to each stochastic dimension of the problem, allowing the extension from the univariate to the multivariate case. Indeed, we are interested in the D -tupling functions such that if for every $i, j \in \mathbb{N}$ with $\pi_D^{-1}(i) = (i_1, \dots, i_D)$ and $\pi_D^{-1}(j) = (j_1, \dots, j_D)$ we have $i_d < j_d$ for all $d = 1, \dots, D$, then $i < j$. Further information on D -tupling functions can be found in [86].

Two popular choices of norms are the 1-norm, $\|\pi_D^{-1}(i)\|_1 = \sum_{d=1}^D i_d$, and the ∞ -norm, $\|\pi_D^{-1}(i)\|_\infty = \max_{d=1, \dots, D} i_d$, which are associated with the total and maximal degrees, respectively. In these cases, the number of coefficients \tilde{c}_i in (2.12) satisfies $P+1 = \binom{P_d+D}{D}$ and $P+1 = (P_d+1)^D$ for the total and maximal degree, respectively. Additional information on the multivariate degree can be found in [91].

If the bases $\{p_{i,d}(\omega_d)\}_{i,d}$ are orthogonal with respect to $w_d(\omega_d)$ with $\omega_d \in \Omega_d \subset \mathbb{R}$, then the D -dimensional polynomial basis $\{p_i(\omega)\}_i$ is orthogonal to the normalized weight function

$$w(\omega) = \prod_{d=1}^D w_d(\omega_d), \quad \omega \in \Omega = \prod_{d=1}^D \Omega_d, \quad \omega_d \in \Omega_d. \quad (2.13)$$

In the polynomial chaos theory, probability density function (2.13) corresponds to the assumption that the random vector ω is constituted by D independent random variables ω_d , $d = 1, \dots, D$. In this framework, the multivariate polynomial degree determines the truncation scheme, and in particular, the total degree corresponds to the standard truncation scheme.

The upcoming sections 2.4.1 and 2.4.2 apply the Galerkin and collocation approaches to the following benchmark examples with $D = 2$ uncertain parameters.

Example 2.5. We consider the spectral abscissa functions associated with the oscillator with feedback delay system

$$\ddot{x}(t) = -\omega_1^2 x(t) - 2\omega_1\omega_2 \dot{x}(t) + K_1 x(t-1) + K_2 \dot{x}(t-1), \quad (2.14)$$

such that $x(t) \in \mathbb{R}$ is the normalized position at time $t \in [-1, \infty)$, $\omega_1 \in \Omega_1 = [0.9, 1.1]$ and $\omega_2 \in \Omega_2 = [0.1, 0.2]$ are respectively angular frequency and damping ratio, while $(K_1, K_2) \in \mathbb{R}^2$ describes the control force which acts with a delay of $\tau = 1$. The control variables, reported in Table 2.1, provide the different behaviors of the spectral abscissa function (section 2.1) for parametric eigenvalue problems with $D = 2$. In particular, the controller, which ensures only the continuous behavior of the spectral abscissa due to a triple non-semi-simple characteristic root, is designed by minimizing the spectral abscissa with the stability optimization method analyzed in section 1.1.4, considering $\omega_1 = 1$ and $\omega_2 = 0.15$. The controller, furnishing a Lipschitz continuous behavior, is obtained by the probabilistic approach introduced in section 1.2.1, minimizing the mean of the spectral abscissa, considering ω_1 and ω_2 independent random variables uniformly distributed in Ω_1 and Ω_2 , respectively. Further details on this example from a stabilization point of view are given in the next chapter, section 3.3.3.

Table 2.1 Numerical values of the control parameters K_1, K_2 for system (2.14), corresponding to different behaviors of the spectral abscissa for $(\omega_1, \omega_2) \in \Omega_1 \times \Omega_2$.

Behavior	Smooth	Lipschitz	Continuous
K_1	0.2	0.5105	0.6179
K_2	0.2	-0.0918	-0.0072

For this problem, the spectral abscissa functions are not known analytically, even though it is possible to compute their values given $\omega \in \Omega = \Omega_1 \times \Omega_2$, as explained in section 1.1.3. In particular, the convergence rates in the L^∞ norm of Figures 2.11 and 2.12 are computed with respect to 10^6 equidistant points in Ω .

Without loss of generality, the linear transformation $[-1, 1]^2 \rightarrow \Omega$ is embedded into the system (2.14), and in the associated parametric eigenvalue problems. Therefore, polynomial bases, interpolation and cubature rules are not shifted and rescaled to Ω .

The degree grading of the polynomial basis, considered in the following sections, are specified by:

Total Degree is determined by the 1-norm, such that $\|(i_1, i_2)\|_1 = i_1 + i_2$. The total degree is associated with a pairing function (i.e. a $D = 2$ -tupling function) assigning consecutive numbers to points along diagonals of $\mathbb{N} \times \mathbb{N}$, as the Cantor pairing function $\pi_{|\cdot|}(i_1, i_2)$ represented in Figure 2.8a and defined by

$$\pi_{|\cdot|}(i_1, i_2) = \frac{i_1^2 + 3i_1 + 2i_1i_2 + i_2 + i_2^2}{2}. \quad (2.15)$$

The polynomial approximation, obtained from the basis corresponding to the pairing function $\pi_{|\cdot|}$, i.e. $\{p_i^{[i]}\}_i$, such that the polynomials $p_i^{[i]}$ have total degree less than or

equal to P_d , is

$$\alpha_P^{[l]}(\omega) = \sum_{\|\pi_{[l]}^{-1}(i)\|_1 \leq P_d, i \in \mathbb{N}} \tilde{c}_i^{[l]} p_i^{[l]}(\omega) = \sum_{i=0}^P \tilde{c}_i^{[l]} p_i^{[l]}(\omega), \quad (2.16)$$

where $P + 1 = \binom{P_d+2}{2} = \frac{(P_d+1)^2}{2} + \frac{(P_d+1)}{2}$. From (2.15), we have $P = \pi_{[l]}(P_d, 0)$.

Maximal Degree is determined by the ∞ -norm, such that $\|(i_1, i_2)\|_\infty = \max\{i_1, i_2\}$. A pairing function, associated with the maximal degree, assigns consecutive numbers to points along the edges of squares of $\mathbb{N} \times \mathbb{N}$, e.g. the Rosenberg-Strong pairing function $\pi_{[m]}(i_1, i_2)$ illustrated in Figure 2.8b and specified by

$$\pi_{[m]}(i_1, i_2) = (\max\{i_1, i_2\})^2 + \max\{i_1, i_2\} + i_1 - i_2. \quad (2.17)$$

The polynomial approximation obtained from the corresponding basis $\{p_i^{[m]}\}_i$, such that the polynomials $p_i^{[m]}$ have maximal degree less than or equal to P_d is

$$\alpha_P^{[m]}(\omega) = \sum_{\|\pi_{[m]}^{-1}(i)\|_\infty \leq P_d, i \in \mathbb{N}} \tilde{c}_i^{[m]} p_i^{[m]}(\omega) = \sum_{i=0}^P \tilde{c}_i^{[m]} p_i^{[m]}(\omega), \quad (2.18)$$

where $P + 1 = (P_d + 1)^2$. From (2.17), we have $P = \pi_{[m]}(P_d, 0)$.

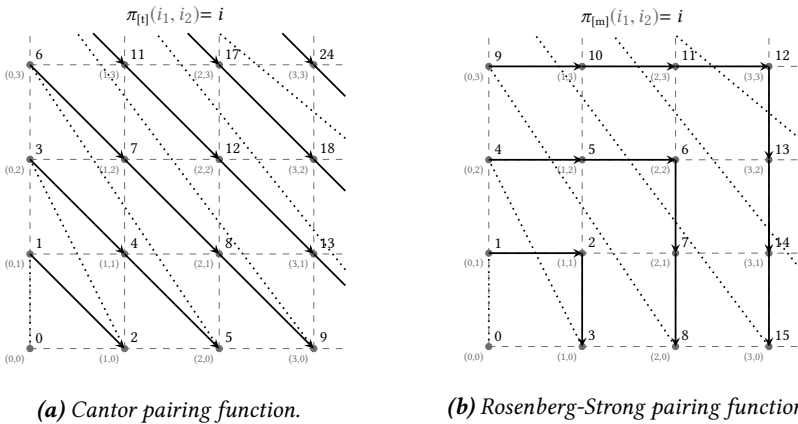


Figure 2.8 Pairing (or 2-tupling) functions associated with the total and maximal degree of bivariate polynomials.

2.4.1 Galerkin approach

In this section, the spectral abscissa functions associated with (2.14) with control parameters of Table 2.1, are approximated by the Galerkin approach on total and

maximal Legendre tensor basis, $\{p_i^{[l]}\}_{i \in \mathbb{N}}$ and $\{p_i^{[m]}\}_{i \in \mathbb{N}}$ with $w(\omega) = 1/4$ for $\omega \in [-1, 1]^2$. Analogously to section 2.3.1, we first consider the approximation error of the Galerkin approach, evaluating the coefficients with a numerical error negligible with respect to the approximation error; then, we approximate the coefficients, \tilde{c}_i^M , via integration methods and analyze the numerical error. At the end of this section, we provide some advice to set the different parameters such that the numerical error does not dominate the approximation error.

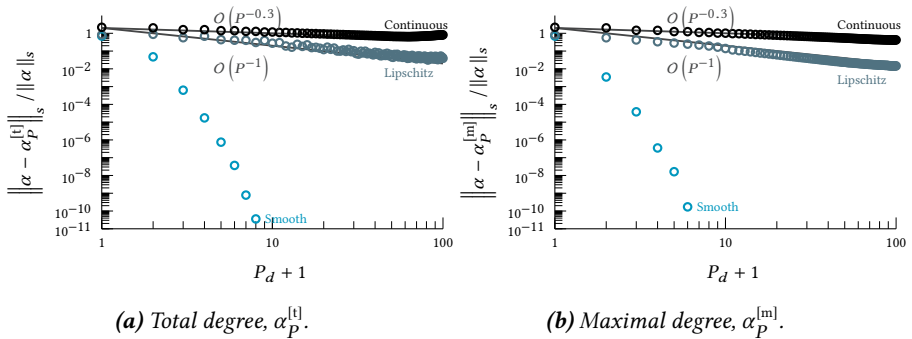


Figure 2.9 Convergence history for Galerkin approach. Relative errors of the Galerkin approach to compute the polynomial approximations $\alpha_p^{[l]}$ and $\alpha_p^{[m]}$, for benchmarks in Example 2.5.

Approximation error

Figure 2.9 shows the convergence rates of the Galerkin approach approximation error. In this simulation, the coefficients have a negligible numerical error compared to the approximation error, thanks to the advice given at the end of this section. For both total and maximal degrees, the converge rates are analogous, and they are of order $O(e^{-cP_d})$ with $c \in \mathbb{R}_+ \setminus \{0\}$, $O(P_d^{-1})$ and $O(P_d^{-0.3})$, for the smooth, Lipschitz continuous, and continuous behaviors of the spectral abscissae function in Example 2.5, respectively.

Numerical error

The coefficients in the Galerkin approach can be approximated by integration methods. To numerically integrate the left-hand side of (2.4), we consider bi-dimension generalizations of the Clenshaw-Curtis quadrature rule, based on Chebyshev points. These integration methods are based on the following set of points:

Tensor product Chebyshev grid is constructed by tensor product of $(M_C + 1)$ unidimensional Chebyshev points. The total number of points is $M + 1 = (M_C + 1)^2$.

Padua points are the self-intersections and boundary contacts of the generating curve $T_{M_P}(x) - T_{M_P+1}(y) = 0$ for $(x, y) \in [-1, 1]^2$, where T_{M_P} is the Chebyshev polynomial of degree M_P . The total number of points is $M + 1 = \binom{M_P+2}{2}$. Refer to [5, 12] for further information on Padua points.

The approximation of an integral, obtained by integrating the interpolant of the integrand, evaluated on the previous sets of points, leads to the following integration methods [83].

Tensorial Clenshaw-Curtis cubature rule based on tensor product Chebyshev grid.

Non-tensorial Clenshaw-Curtis cubature rule relying on Padua points.

These methods approximate the coefficients $\tilde{c}_i^{[t],M}$ and $\tilde{c}_i^{[m],M}$ and, hence, permit to compute the polynomial approximations with respect to total and maximal degrees, i.e. $\alpha_P^{[t],M}$ and $\alpha_P^{[m],M}$, respectively. By the advice furnished in the next section, the coefficients $\tilde{c}_i^{[t],M}$ are computed by non-tensorial Clenshaw-Curtis cubature rules on $M + 1$ Padua points, while $\tilde{c}_i^{[m],M}$ are evaluated by tensorial Clenshaw-Curtis cubature rules on $M + 1$ tensor product Chebyshev grid.

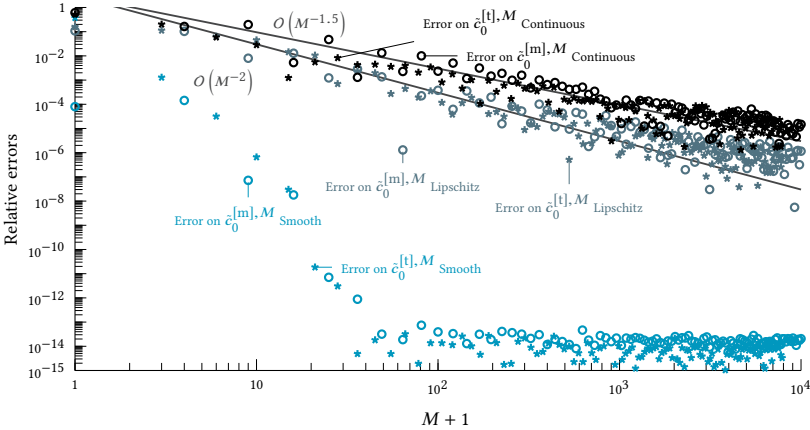


Figure 2.10 Convergence history for Clenshaw-Curtis cubature rules. Relative errors to compute the first coefficient $c_0 = c_0^{[t]} = c_0^{[m]}$ of (2.12) for benchmarks in Example 2.5. The approximations $\tilde{c}_0^{[t],M}$, and $\tilde{c}_0^{[m],M}$ are obtained by non-tensorial and tensorial Clenshaw-Curtis cubature rules, respectively. The reference values are computed by $M^* > 5 \cdot 10^5$ which corresponds to $M_P = 999$ and $M_C = 707$.

In order to compute the numerical errors, $\tilde{c}_i^{[t],M^*}$ and $\tilde{c}_i^{[m],M^*}$ are considered as reference values. These coefficients are computed by the corresponding cubature rules based on $M^* > 5 \cdot 10^5$ points, in particular $M_P = 999$ and $M_C = 707$. Figure 2.10 shows the

error to compute the first coefficient \tilde{c}_0^M , which is independent from the multivariate polynomial degree, since $c_0^{[l]} = c_0^{[m]}$. The cubature rules on tensor product Chebyshev grid and Padua points present similar convergences rates. For Example 2.5, the Lipschitz and continuous behaviors of the spectral abscissae converge as $O(M^{-2})$ and $O(M^{-1.5})$, respectively; while the smooth behavior present a convergence of order $O(e^{-cM})$ with $c \in \mathbb{R}_+ \setminus \{0\}$.

In terms of a polynomial chaos expansion (Theorem 2.1), Figure 2.10 corresponds to the error to compute the mean of the spectral abscissa $\alpha(\omega)$ associated with (2.14), where ω is a realization of ω , random vector uniformly distributed in Ω .

Decoupling numerical error with respect to approximation error

This section is based on numerical examples from which we conclude some novel advice on how to set the number of points in the integration methods to accurately compute the coefficients of the Galerkin approach. Indeed, these integration methods should consider a small number of points, M , which are still sufficiently large to avoid the corruption of the approximation error by the numerical error, due to the approximation of the integrals.

Since the coefficients \tilde{c}_i in (2.9) and (2.12) are determined by integrating $\alpha(\omega)p_i(\omega)\omega(\omega)$ over the domain Ω , we request that the polynomial approximation behind the integration rule is exact for all polynomials $\{p_i\}_{i=0}^P$.

This advice leads in the unidimensional case, section 2.3.1, that the number of nodes, $M+1$, in the interpolatory quadrature rules, *i.e.* Gauss and Clenshaw-Curtis quadrature rules, is greater than the degree, P , of the polynomial approximation α_P^M .

For the bi-dimensional case, the polynomial approximation behind the non-tensorial Clenshaw-Curtis cubature rule, *i.e.* the interpolation on Padua points, is exact for polynomial with total degree less than or equal to M_P . The interpolant on tensor product Chebyshev grid, underling the tensorial Clenshaw-Curtis cubature rule, is exact for all the polynomials with maximal degree less than or equal to M_C . From these properties, the interpolatory cubature rule for $D > 1$ are associated with the polynomial multivariate degree. In particular, non-tensorial and tensorial Clenshaw-Curtis cubature rules are interpolatory cubature rules associated with the total and maximal degrees for $D = 2$, respectively.

Following the advice, $\alpha_P^{[l],M}$ is accurately approximated by non-tensorial Clenshaw-Curtis cubature rule with $M_P \geq P_d$ or by tensorial Clenshaw-Curtis cubature rule with $M_C \geq P_d$. On the other hand, $\alpha_P^{[m],M}$ can be evaluated by tensorial Clenshaw-Curtis with $M_C \geq P_d$ or by non-tensorial Clenshaw-Curtis cubature rule with $M_P \geq 2P_d$. Therefore, the number of nodes in the integration rule is minimized by considering non-tensorial Clenshaw-Curtis cubature rule for approximating the coefficients of

$\alpha_P^{[t],M}$ with $M_P \geq P_d$, and tensorial Clenshaw-Curtis cubature rule for approximating the coefficients of $\alpha_P^{[m],M}$ with $M_C \geq P_d$.

Table 2.2 Advice to compute Galerkin polynomial approximations (2.16) and (2.18), whose coefficients are evaluated by non-tensorial and tensorial Clenshaw-Curtis cubature rule, based on Padua points and tensor product Chebyshev grid, respectively. The natural choices are highlighted.

	Total degree $\alpha_P^{[t],M}$	Maximal degree $\alpha_P^{[m],M}$
Padua points	$M_P \geq P_d$ $M + 1 = \binom{M_P+2}{2} \geq P + 1 = \binom{P_d+2}{2}$	$M_P \geq 2 \cdot P_d$ $M + 1 = \binom{2M_P+2}{2} \gg P + 1 = \binom{P_d+1}{2}$
Tensor product Chebyshev grid	$M_C \geq P_d$ $M + 1 = (M_C + 1)^2 \gg P + 1 = \binom{P_d+2}{2}$	$M_C \geq P_d$ $M + 1 = (M_C + 1)^2 \geq P + 1 = \binom{P_d+1}{2}$

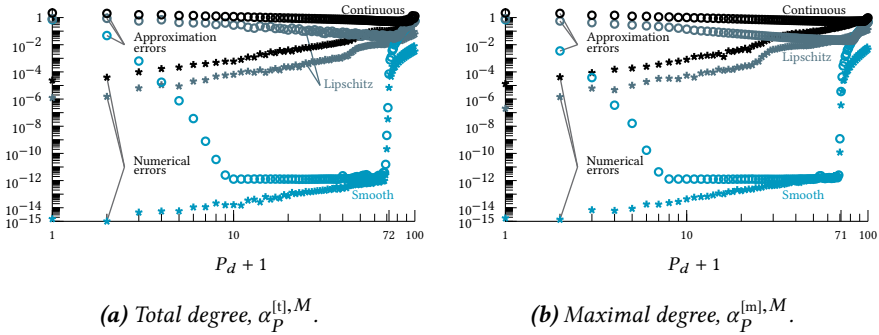


Figure 2.11 Convergence history for Galerkin approach. Numerical and approximation errors on the polynomial approximation for benchmarks in Example 2.5, using the two non-natural choices of Table 2.2. The coefficients $\tilde{c}_i^{[t],M}$ and $\tilde{c}_i^{[m],M}$ are computed by tensorial and non-tensorial Clenshaw-Curtis cubature rules, respectively, where $M > P$ is given by $M_C = 71 < 100$ and $M_P = 140 < 2 \cdot 100$.

Table 2.2 summarizes the advice for the bi-dimensional case, highlighting the natural choices of computing the polynomial approximations $\alpha_P^{[t],M}$ and $\alpha_P^{[m],M}$ through the associated interpolatory cubature rules. These natural choices provide the convergence errors in Figure 2.9, where the coefficients of $\alpha_P^{[t]}$, $\alpha_P^{[m]}$ are evaluated with $M_P = 110$ non-tensorial and $M_C = 110$ tensorial Clenshaw-Curtis cubature rules, respectively. On the other hand, Figure 2.11 shows a counter check of this advice for spectral abscissa polynomial approximations of Example 2.5. The number of points of the cubature rules, M , is greater than the number of coefficients, P ; however, the polynomial approximation $\alpha_P^{[t],M}$ is computed by tensorial Clenshaw-Curtis cubature with $M_C = 71$ while the polynomial approximation $\alpha_P^{[m],M}$ is evaluated by non-tensorial Clenshaw-Curtis cubature rule with $M_P = 140$. The numerical errors

$$\sum_{\|\pi_{[t]}^{-1}(i)\|_1 \leq P_d} \left| \tilde{c}_i^{[t],M^*} - \tilde{c}_i^{[t],M} \right| \quad \text{and} \quad \sum_{\|\pi_{[m]}^{-1}(i)\|_\infty \leq P_d} \left| \tilde{c}_i^{[m],M^*} - \tilde{c}_i^{[m],M} \right|, \quad (2.19)$$

heavily affect the approximation errors as soon as $P_d \gtrsim M_C = 71$ for $\alpha_P^{[l],M}$, and $P_d \gtrsim \frac{M_P}{2} = 70$ for $\alpha_P^{[m],M}$.

2.4.2 Collocation approach

Contrary to the Galerkin approach, where the coefficients can be computed independently one of each other with formula (2.4), in the collocation approach the number of degrees of freedom, *i.e.* the $P + 1$ coefficients, should match the number of interpolation points. Hence the interpolant of total degree P_d , $\alpha_P^{[l]}$, is computed on Padua points with $M_P = P_d$, while the interpolant of maximal degree P_d , $\alpha_P^{[m]}$, is evaluated on tensor products Chebyshev grid with $M_C = P_d$. This connection between interpolant polynomial degrees and the choice of interpolating points is strengthened by the following theorem, which provides the near-best optimal approximation in supremum norm associated with a multivariate polynomial degree.

THEOREM 2.5 *Let $\alpha_P^{[l]\star}$ and $\alpha_P^{[l]}$ be the best polynomial approximation of total degree less than or equal to P_d and the polynomial interpolant on $M_P = P_d$ Padua points, respectively. Then*

$$\|\alpha - \alpha_P^{[l]}\|_s \leq (1 + O(\log^2(P_d))) \|\alpha - \alpha_P^{[l]\star}\|_s.$$

Analogously, if $\alpha_P^{[m]\star}$, and $\alpha_P^{[m]}$, are the best polynomial interpolant of maximal degree less than or equal to P_d and the polynomial interpolant on $M_C = P_d$ tensor product Chebyshev grid, respectively, then

$$\|\alpha - \alpha_P^{[m]}\|_s \leq (1 + O(\log^2(P_d))) \|\alpha - \alpha_P^{[m]\star}\|_s.$$

The near-best optimality is derived by the growth of the Lebesgue constant [5]. Moreover, the following theorem [12] extends the error bounds of Theorem 2.4 for total degree polynomial interpolant evaluated in Padua points.

THEOREM 2.6 *If α is continuous and differentiable up to the k -th derivative in $[-1, 1]^2$, with $k > 0$, then the interpolant $\alpha_P^{[l]}$ on $M_P = P_d$ Padua points satisfies the following relation*

$$\|\alpha - \alpha_P^{[l]}\|_s \leq O\left(P_d^{-k} \log^2(P_d)\right).$$

Theorem 2.6 provides an error bounds only for the smooth behavior of the spectral abscissa, ensuring a convergence faster than $O(P_d^{-k})$ for all $k \in \mathbb{N}$.

The experiments on the spectral abscissa functions of Example 2.5 are shown in Figure 2.12. The convergence rates are analogous to the ones of the Galerkin approach (Figure 2.9), the only difference is that the numerical error is negligible for the collocation approach. The interpolant polynomials for these experiments are

computed by the software Chebfun relying on Chebyshev expansion. Analogously to Remark 2.5, the Chebyshev coefficients can be transformed into Legendre coefficients by the method [88], in order to apply Theorem 2.1.

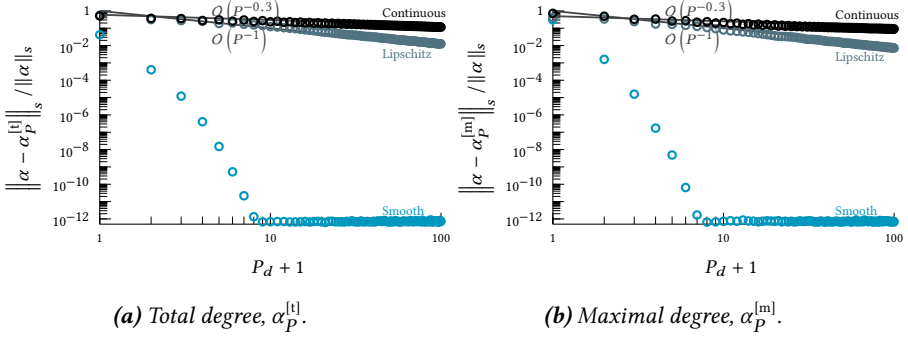


Figure 2.12 Convergence history for collocation approach. Relative errors for benchmarks in Example 2.5 on the interpolant polynomials, based on Padua points for total degree and tensor product Chebyshev grid for maximal degree.

2.5 BEYOND POLYNOMIAL (CHAOS) APPROXIMATIONS

Dominant eigenvalue functions are often unsuitable for polynomial and polynomial chaos approximations, especially in system and control applications where non-differentiable and even non-Lipschitz continuous behaviors are expected or favored, as described in section 2.1 and illustrated by the non-smooth behaviors of Examples 1.4 and 2.5. In this context, also piecewise-polynomial approximation [75] and enriched polynomial approximation [28] are not expected to provide satisfactory solution, since the location of the discontinuities is not known a priori; and for stochastic dimension $D > 1$, the geometry of non-differentiable points within the parameter space Ω is not well understood.

For large-scale eigenvalue problems, obtaining an accurate polynomial (chaos) approximations of non-smooth dominant eigenvalue functions becomes computationally infeasible. Therefore, approximations potentially better tailored to the behavior of dominant eigenvalue functions are constituted by projection methods, in which a large-scale parametric eigenvalue problem is projected into a small one. This has the advantage that the approximation is still in the form of the solution of an eigenvalue problem, inheriting all properties, and able to preserve the non-smooth spectral abscissa behaviors. Projection methods are reliably applied in eigenvalue computations and model order reduction [58], as well as eigenvalue optimization [43]. However, their potential for global approximations of dominant eigenvalue functions

and for the computation of statistical information has been considered only for linear eigenvalue problem with parametric symmetric matrices [72].

In what follows, we project a generalized eigenvalue problem $A(\omega)v = \lambda B(\omega)v$, where $A(\omega), B(\omega)$ are two non-singular parametric matrices, into the subspace formed by left and right eigenvectors associated with the rightmost eigenvalues for given $\omega \in \{\omega_m\}_m \subset \Omega$. The eigenvalues of the projected eigenproblem provide an Hermite interpolation of the dominant eigenvalues of the original problem at $\omega \in \{\omega_m\}_m$, as stated in the following proposition, which extends to generalized eigenvalue problem the results in [73, 43].

PROPOSITION 2.7 *Let V and U be matrices whose column space respectively contains the right and left eigenvectors associated with the dominant eigenvalue of $A(\omega)v = \lambda B(\omega)v$ for $\omega \in \{\omega_m\}_m \subset \Omega$. For each $\omega \in \{\omega_m\}_m$, if the dominant eigenvalue λ_D is simple and the matrices $A(\omega)$, and $B(\omega)$ are differentiable towards ω , then an eigenvalue λ of the projected eigenproblem $U^*A(\omega)V\tilde{v} = \lambda U^*B(\omega)V\tilde{v}$ interpolates the original rightmost eigenvalue, and also its derivative with respect to the elements of parameter vector ω .*

Proof. For notational convenience, set $\omega \in \{\omega_m\}_m$ and consider $A(\omega) = A, B(\omega) = B$. The left and right eigenvectors associated with the dominant eigenvalue λ_D can be rewritten by using the matrices U and V , namely $v_D = V\tilde{v}$ and $u_D = U\tilde{u}$. Therefore, the interpolation of the dominant eigenvalue is given by:

$$\lambda_D U^* B V \tilde{v} = U^* \lambda_D B v_D = U^* A v_D = U^* A V \tilde{v}.$$

Analogous result holds for the derivative of the dominant eigenvalues with respect to an element $\hat{\omega}$ of the parameter ω . Applying Proposition 1.4 to the generalized eigenvalue problem $\Lambda(\lambda; \omega) = \lambda B(\omega) - A(\omega)$, we get

$$\frac{\partial \lambda_D}{\partial \hat{\omega}} = \frac{u_D^* \frac{\partial(\lambda_D B - A)}{\partial \hat{\omega}} v_D}{u_D^* B v_D} = \frac{\tilde{u}^* U^* \left(\lambda_D \frac{\partial B}{\partial \hat{\omega}} - \frac{\partial A}{\partial \hat{\omega}} \right) V \tilde{v}}{\tilde{u}^* U^* B V \tilde{v}} = \frac{\tilde{u}^* \frac{\partial(\lambda_D U^* B V - U^* A V)}{\partial \hat{\omega}} \tilde{v}}{\tilde{u}^* U^* B V \tilde{v}},$$

which concludes the proof. \square

Remark 2.7. For symmetric eigenvalue problems, the interpolation properties hold in a stronger sense, i.e. for $\omega \in \{\omega_m\}_m$ the dominant eigenvalue of the original eigenproblem is also the dominant eigenvalue of the projected eigenproblem [72, Property 1]. However, for general real-valued matrices, $A(\omega), B(\omega)$, the projected eigenproblem may present a dominant eigenvalue that does not correspond to the dominant eigenvalue of the original problem. To stress this concept, the left and right eigenvectors \tilde{u} and \tilde{v} , associated with the eigenvalue λ_D for the projected eigenvalue problem, are denoted without the subscript $_D$ in the proof of Proposition 2.7.

To illustrate the idea, we consider the generalized parametric eigenvalue problem (1.19) obtained from the infinite-dimensional linear eigenvalue problem associated with the

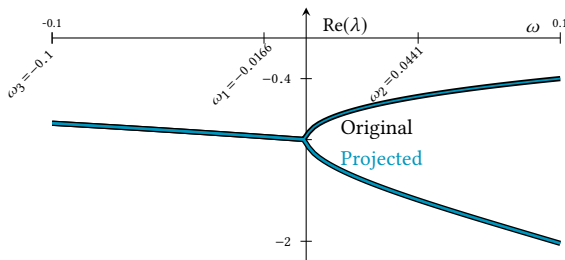


Figure 2.13 Comparison between the dominant eigenvalues' real parts of the eigenproblem (1.19) and of its projection for the hot-shower problem (1.24) with $K = e^{-1}$ and $\omega \in [-0.1, 0.1]$. The eigenproblem (1.19) considers $M = 100$ collocation points, and its 5×5 -projection is based on the left and right eigenvectors of the rightmost eigenvalues in the randomly selected points ω_1 , ω_2 , and ω_3 . The relative error of the projected spectral abscissa function in the L^∞ norm is $5.7835 \cdot 10^{-9}$.

hot shower problem $\dot{x}(t) = -(e^{-1} + \omega)x(t-1)$ with $\omega \in [-0.1, 0.1]$. This generalized eigenvalue problem, obtained considering 100 collocation points, has dimension 100 by 100 and depends on the scalar parameter ω . As observed in Example 1.4, the spectral abscissa function presents a non-Lipschitz continuous behavior, since for $\omega = 0$ there is a non-semi simple dominant characteristic root with multiplicity 2. We project the generalized eigenproblem into the left and right eigenvectors associated with the rightmost eigenvalues in 3 random points of the interval $[-0.1, 0.1]$; the projected 5×5 eigenproblem approximates the behaviors of the rightmost eigenvalues of the delay system, as shown in Figure 2.13. In order to have a real-valued projected eigenvalue problem, if the rightmost characteristic root presents non-zero imaginary part for $\omega \in \{\omega_m\}_m$, the real matrices V and U are constructed considering real as well as imaginary parts of the left and right eigenvectors associated with this dominant characteristic root.

The spectral abscissa L^∞ relative error for the projected eigenproblem is $5.7835 \cdot 10^{-9}$, six orders of magnitude less than the polynomial approximation obtained by the collocation approach with 100 points (the convergence rate of the interpolant polynomial for this example is illustrated in Figure 2.14). In addition, the approximation obtained by the projection is computed faster than evaluating a high degree polynomial approximation; as a result the small size of the projected eigenvalue problem provides a fast surrogate model, which can be used to infer statistical information.

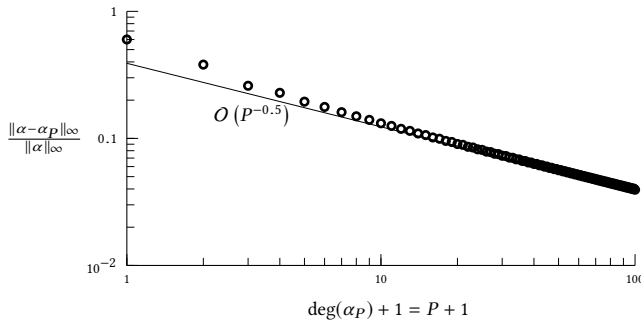


Figure 2.14 Convergence history for the collocation approach. Relative errors to polynomially interpolate on Chebyshev points the spectral abscissa of eigenproblem (1.19), considering $M = 100$ collocation points, for the hot shower problem (1.24) with $K = e^{-1}$ and $\omega \in [-0.1, 0.1]$.

SUMMARY. A non-smooth behavior of the spectral abscissa function is generally due to multiple rightmost eigenvalues, counted with multiplicity. These non-differentiable behaviors, often encountered in control application, heavily affect the polynomial approximation, which is strictly connected to the polynomial chaos theory. Numerical experiments on spectral abscissa non-smooth behaviors systematically show a slow decay rate for the approximation errors of the Galerkin and collocation approaches as well as for the numerical errors due to the integral approximation of the polynomial coefficients. These experiments also suggest that the Galerkin approach numerical errors do not affect the polynomial approximation, if the the integration rule exactly integrates all the polynomials of the truncated polynomial basis.

Extended research results of chapter 2 are presented in section 5.1.1.

PROBABILISTIC STABILITY OPTIMIZATION

This chapter provides a novel stabilization method for linear time-invariant time-delay systems with uncertain parameters modeled by a random vector. The dependence of the system matrices on these uncertain parameters can be nonlinear and the delays can also be subjected to uncertainty. Relying on a minimization of the mean of the spectral abscissa with a variance penalty, the proposed approach provides better robustness properties compared to the spectral abscissa optimization for the nominal model, and more realistic results in contrast to worst-case analysis. The efficacy and applicability of the method is shown by several numerical examples, including an experimental heat-exchanger, and a mechanical system to which a delayed resonator is attached in order to absorb harmonic oscillations.

Analogously to the previous chapter, for simplicity, we deal with linear autonomous time-delay systems (1.4) stated as delay differential algebraic equations

$$E\dot{x}(t) = \sum_{j=0}^h A_j(\omega, \mathbf{K})x(t - \tau_j(\omega)), \quad (3.1)$$

where

- $x(t) \in \mathbb{R}^r$ represents the state at time $t \geq \max_{\omega \in \Omega} \{-\tau_j(\omega) : j = 0, \dots, h\}$;
- $\omega \in \Omega \subset \mathbb{R}^D$ are the possible values of the uncertain parameters, which are described by the continuous real random vector ω with compact support Ω and probability density function

$$w : \Omega \rightarrow \mathbb{R}_+, \quad \omega \mapsto w(\omega).$$

For the sake of simplicity, the probability density function w is smooth, and the support is the D -dimensional unit cube, $\Omega = [0, 1]^D$;

- $\mathbf{K} \in \mathbb{R}^k$ parametrizes the controller;
- $E \in \mathbb{R}^{r \times r}$ is a real matrix, which can be singular;
- For every $j \in \{0, \dots, h\}$, $A_j : \Omega \times \mathbb{R}^k \rightarrow \mathbb{R}^{r \times r}$, $(\omega, \mathbf{K}) \mapsto A_j(\omega, \mathbf{K})$, and $\tau_j : \Omega \rightarrow \mathbb{R}_+$, $\omega \mapsto \tau_j(\omega)$ are functions, which we assume to be smooth.

The delay differential algebraic formulation (3.1) permits to model a wide class of system with feedback control, such that the plant is

$$\begin{cases} \dot{z}(t) = \sum_{j=0}^h F_j(\omega)z(t - \tau_j(\omega)) + \sum_{j=0}^h G_j(\omega)u(t - \tau_j(\omega)), \\ y(t) = \sum_{j=0}^h H_j(\omega)z(t - \tau_j(\omega)) + \sum_{j=0}^h L_j(\omega)u(t - \tau_j(\omega)), \end{cases} \quad (3.2)$$

where $z(t)$, $u(t)$ and $y(t)$ are respectively the state, the input, and the output at time t , and the feedback controller can be either static or dynamic, in formula

$$\text{Static} \quad u(t) = \sum_{j=0}^h \hat{L}_j y(t - \tau_j(\omega)), \quad (3.3a)$$

$$\text{Dynamic} \quad \begin{cases} \dot{z}_c(t) = \sum_{j=0}^h \hat{F}_j z_c(t - \tau_j(\omega)) + \sum_{j=0}^h \hat{G}_j y(t - \tau_j(\omega)), \\ u(t) = \sum_{j=0}^h \hat{H}_j z_c(t - \tau_j(\omega)) + \sum_{j=0}^h \hat{L}_j y(t - \tau_j(\omega)). \end{cases} \quad (3.3b)$$

System (3.2) with feedback controller (3.3) can be recast as a delay differential algebraic equation (3.1), imposing $x = (z^T y^T z_c^T u^T)^T \in \mathbb{R}^r$ and $\mathbf{K} \in \mathbb{R}^k$ the vectorization of the controller matrices \hat{F}_i , \hat{G}_i , \hat{H}_i , and \hat{L}_i .

Assuming that the plant or the controller is strictly proper, *i.e.* either the matrices L_j or \hat{L}_j are zero for every $j = 0, \dots, h$, the resulting delay differential algebraic equation is of retard type, *i.e.* equivalent to the linear time-delay system (1.4). In particular, the delay differential equations (3.1) arising from a strictly proper system (3.2)–(3.3) are always of index 1.⁴ We focus on this particular class of delay differential algebraic equations, since their stability properties are analogous to the autonomous time-delay system, considered in section 1.1.2. Indeed, for a given $(\omega, \mathbf{K}) \in \Omega \times \mathbb{R}^k$ the stability properties of the delay differential algebraic equation of retarded type (3.1) are determined by the characteristic roots $\lambda \in \mathbb{C}$, eigenvalues with finite modulus of the characteristic matrix

$$\mathcal{A}(\lambda; \omega, \mathbf{K}) = \lambda E - \sum_{j=0}^h A_j(\omega, \mathbf{K}) e^{-\lambda \tau_j(\omega)}.$$

Analogously to autonomous time-delay system, delay differential algebraic equations of retarded type always have finitely many characteristic roots in any right half-plane, which can be computed by adapting Algorithm 1.1 to handle the singular leading matrix E , as described in [51, Section 4.1]. Similarly to Proposition 1.2, the delay differential equation equations of retarded type (3.1) are asymptotically stable if and only if the spectral abscissa,

$$\alpha(\omega, \mathbf{K}) := \max_{\lambda \in \mathbb{C}} \{\operatorname{Re}(\lambda) : \det(\mathcal{A}(\lambda; \omega, \mathbf{K})) = 0\},$$

is strictly negative. For every $(\omega, \mathbf{K}) \in \Omega \times \mathbb{R}^k$, we consider the spectral abscissa as the real part of a dominant characteristic root $\lambda_D \in \mathbb{C}$ such that $\operatorname{Re}(\lambda_D) = \alpha(\omega; \mathbf{K})$ and $\operatorname{Im}(\lambda_D) \geq 0$.

⁴ Further information on delay differential algebraic equations can be found in [13, 31, 17].

To develop the novel approach, we need the following assumption on the simplicity of the dominant characteristic root, which is not restrictive from the application point of view.

Assumption 3.1. Given $\mathbf{K} \in \mathbb{R}^k$, the dominant characteristic root is simple for almost all $\omega \in \Omega$; given $\omega \in \Omega$, the dominant characteristic root is simple for almost all $\mathbf{K} \in \mathbb{R}^k$.

Example 3.1. Let us recall the hot shower problem (1.24), analyzed in section 1.2.1. For this autonomous time-delay system, we can make the plant (3.2) and the static feedback controller (3.3a) explicit by rewriting system (1.24) in the form

$$\begin{cases} \dot{z}(t) = -\omega z(t-1) - u(t-1), \\ y(t) = z(t), \\ u(t) = Ky(t), \end{cases} \quad (3.4)$$

where ω models the uncertainty and $K \in \mathbb{R}$ is the feedback gain. Hence, this system can be represented as a delay differential algebraic equation of retarded type (3.1)

$$\begin{pmatrix} 1 & 0 & 0 \\ 0 & 0 & 0 \\ 0 & 0 & 0 \end{pmatrix} \dot{x}(t) = \begin{pmatrix} 0 & 0 & 0 \\ 1 & -1 & 0 \\ 0 & K & 1 \end{pmatrix} x(t) - \begin{pmatrix} \omega & 0 & 1 \\ 0 & 0 & 0 \\ 0 & 0 & 0 \end{pmatrix} x(t-1). \quad (3.5)$$

Formulations (1.24) and (3.5) are almost equivalent, presenting the same characteristic roots $\lambda \in \mathbb{C}$, even though the latter system is not scalar.

Our goal is to generalize the spectrum-based stability optimization considered in section 1.1.4 in order to exploit the probabilistic description of the uncertainty, modeled by the random vector ω . To this end, we minimize a specific linear combination of mean and variance of the spectral abscissa, in formula

$$\min_{\mathbf{K} \in \mathbb{R}^k} f_{\text{obj}}(\mathbf{K}), \quad \text{with } f_{\text{obj}}(\mathbf{K}) = \mathbb{E}(\alpha(\omega, \mathbf{K})) + \kappa \mathbb{V}(\alpha(\omega, \mathbf{K})), \quad (3.6)$$

where $\kappa \in \mathbb{R}_+$ is a given trade off parameter. The mean and the variance of the spectral abscissa, respectively denoted by $\mathbb{E}(\alpha(\omega, \mathbf{K}))$ and $\mathbb{V}(\alpha(\omega, \mathbf{K}))$ exist, as proven in section 2.2 for given $\mathbf{K} \in \mathbb{R}^k$. If the support of ω is a single element of \mathbb{R}^D , i.e. $\Omega = \{\omega\}$ with $\omega \in \mathbb{R}^D$, then the minimization of the objective function (3.6) reduces to the spectral abscissa optimization, described in section 1.1.4, since in this case $\mathbb{E}(\alpha(\omega, \mathbf{K})) = \alpha(\omega, \mathbf{K})$ and $\mathbb{V}(\alpha(\omega, \mathbf{K})) = 0$.

The chapter is structured as follows. In section 3.1, the objective function is analyzed, studying its differentiability and its approximation obtained by integration methods. Then, in section 3.2, we outline the novel stability optimization method, based on approximation and minimization of the objective function (3.6) handled respectively by

quasi-Monte Carlo method and the software HANSO. We end, in section 3.3, with some numerical examples and two engineering applications. Indeed, the novel approach is successfully applied to an experimental heat-transfer set up, in section 3.3.4, and to a mechanical system with active vibration suppression, in section 3.3.5

We remind that, analogously to the notation of chapter 2, the random variables modeling uncertainty are denoted with bold letters, *e.g.* $\boldsymbol{\omega}$, while the normal font is used to indicate their realizations, $\omega \in \Omega$. In this view, given $\mathbf{K} \in \mathbb{R}^k$, $\alpha(\boldsymbol{\omega}, \mathbf{K})$ is a random variable, while $\alpha(\cdot, \mathbf{K}) : \Omega \rightarrow \mathbb{R}$, $\omega \mapsto \alpha(\omega, \mathbf{K})$ is a function with respect to the realization $\omega \in \Omega$.

3.1 OBJECTIVE FUNCTION, ANALYSIS & EVALUATION

The existence of the objective function (3.6) for every $\mathbf{K} \in \mathbb{R}^k$ follows from the existence of the mean and variance, already proved in section 2.2. In this section, we first address the differentiability of the objective function, studying the integrability of the spectral abscissa gradient with respect to controller parameters. Then, we analyze integration methods to approximate the objective function and its gradient.

3.1.1 Differentiability of the objective function

Since we are dealing with a minimization problem, the gradient of the objective function can be used as search direction for the optimization. However, the objective function (3.6) is a linear combination of integrals depending on the spectral abscissa, whose behavior is not always differentiable, as illustrated in section 2.1.

For this reason, we first derive an explicit formula for the gradient of the objective function, under the assumption that the gradient of the spectral abscissa function is integrable over the uncertain domain Ω . Then, we analyze when this latter assumption holds.

PROPOSITION 3.1 *If the gradient of the spectral abscissa with respect to the control parameters \mathbf{K} is an integrable function on Ω , then the gradient of objective function (3.6) exists and it can be expressed by*

$$\nabla_{\mathbf{K}} f_{\text{obj}}(\mathbf{K}) = (1 - 2\kappa \mathbb{E}(\alpha(\boldsymbol{\omega}, \mathbf{K}))) \mathbb{E}(\nabla_{\mathbf{K}} \alpha(\boldsymbol{\omega}, \mathbf{K})) + 2\kappa \mathbb{E}(\alpha(\boldsymbol{\omega}, \mathbf{K}) \nabla_{\mathbf{K}} \alpha(\boldsymbol{\omega}, \mathbf{K})). \quad (3.7)$$

Proof. The objective function is a linear combination of integrals (2.6); therefore its gradient with respect to \mathbf{K} is the gradient of the linear combination of these integrals. By the continuity of the spectral abscissa, section 2.1, and the compactness of the domain Ω , the function $\alpha(\boldsymbol{\omega}, \mathbf{K})$ is integrable over Ω . Providing that $\nabla_{\mathbf{K}} \alpha(\boldsymbol{\omega}, \mathbf{K})$ is also

integrable over Ω , we can differentiate the integrals [87]. Hence, almost everywhere in Ω , the gradient of the mean and of the variance with respect to \mathbf{K} are

$$\begin{aligned}\nabla_{\mathbf{K}}\mathbb{E}(\alpha(\omega, \mathbf{K})) &= \mathbb{E}(\nabla_{\mathbf{K}}\alpha(\omega, \mathbf{K})), \\ \nabla_{\mathbf{K}}\mathbb{V}(\alpha(\omega, \mathbf{K})) &= \int_{\Omega} 2(\alpha(\omega, \mathbf{K}) - \mathbb{E}(\alpha(\omega, \mathbf{K}))) \nabla_{\mathbf{K}}(\alpha(\omega, \mathbf{K}) - \mathbb{E}(\alpha(\omega, \mathbf{K}))) \omega(\omega) d\omega \\ &= 2\mathbb{E}(\alpha(\omega, \mathbf{K})\nabla_{\mathbf{K}}\alpha(\omega, \mathbf{K})) - 2\mathbb{E}(\alpha(\omega, \mathbf{K}))\mathbb{E}(\nabla_{\mathbf{K}}\alpha(\omega, \mathbf{K})).\end{aligned}$$

The gradient of the objective function is well defined and can be expressed by (3.7). \square

The validity of the assumption of Proposition 3.1 for delay differential algebraic equations of retarded type (3.1) is first analyzed in a particular setting and then generalized. Indeed, first, we demonstrate the integrability of the spectral abscissa gradient when the control parameters \mathbf{K} are affected by uncertainties. Then, we consider the general case, proving, under a Lipschitz continuous condition on the spectral abscissa, that the spectral abscissa gradient is integrable. Moreover, we present a case-study, where the spectral abscissa is not Lipschitz continuous, but its gradient is still integrable.

A particular case: the control parameters are uncertain

Let the length of the vector \mathbf{K} be less or equal to the stochastic dimension, i.e. $k \leq D$. The following proposition states that if all control parameters in \mathbf{K} are affected by uncertainty then the hypothesis of Proposition 3.1 is satisfied.

PROPOSITION 3.2 *Let the components of ω be recast as $\omega = (\tilde{\omega}, \hat{\omega})$, where $\tilde{\omega}$ and $\hat{\omega}$ are random vectors with $D - k$ and k components respectively. For $i = 1, \dots, k$, if $\hat{\omega}_i$ occurs only in the coefficients of the matrices $\{A_j(\omega, \mathbf{K})\}_{j=0}^h$ of system (3.1), where K_i occurs, and if these coefficients can be recast as functions of $K_i + \hat{\omega}_i$, then function $\omega \mapsto \nabla_{\mathbf{K}}\alpha(\omega, \mathbf{K})$ is an integrable function on Ω , for all $\mathbf{K} \in \mathbb{R}^k$.*

Proof. By assumption, the spectral abscissa function can be recast as

$$\alpha(\omega, \mathbf{K}) = \beta(\tilde{\omega}, \mathbf{K} + \hat{\omega}),$$

for some continuous function β . We prove the proposition considering the different behaviors of the spectral abscissa analyzed in section 2.1.

If the spectral abscissa presents a smooth behavior, then it is differentiable, and we can apply the chain rule to its partial derivative with respect to K_i

$$\frac{\partial\beta(\tilde{\omega}, \mathbf{K} + \hat{\omega})}{\partial K_i} = \frac{\partial\beta(\tilde{\omega}, \mathbf{K} + \hat{\omega})}{\partial \hat{\omega}_i}, \text{ for all } i = 1, \dots, k. \quad (3.8)$$

Clearly this continuous function is integrable over the compact set Ω .

If the spectral abscissa presents a Lipschitz continuous behavior, then its partial derivate exhibits a discontinuity in a set of measure zero, but it is of bounded variation on Ω . Hence, it is integrable also in this case.

If the spectral abscissa presents a continuous behavior, due to multiple non-semi-simple dominant characteristic roots, we consider the partial derivative of the spectral abscissa with respect to K_i , for all $i = 1, \dots, k$ and we stress only the $\hat{\omega}_i$ -dependency in the characteristic roots. The effects of the uncertainty on K_i can be seen as a real linear perturbation on some matrix coefficients, describing the system. Let $\lambda(\hat{\omega}_i^0)$ be an isolated dominant characteristic root with partial multiplicity (ℓ_1, \dots, ℓ_l) . Then in a neighborhood of $\hat{\omega}_i^0, \Xi$, the spectrum of $\mathcal{A}(\lambda; \omega, \mathbf{K})$ presents $\mathcal{L} = \ell_1 + \dots + \ell_l$ eigenvalues, $\lambda_\ell(\hat{\omega}_i)$ with $\ell = 1, \dots, \mathcal{L}$, counted with multiplicity, such that $\lambda_\ell(\hat{\omega}_i)$ are algebraic functions of $\hat{\omega}_i$ by the Weierstrass preparation theorem, and can be represented by branches of Puiseux series

$$\lambda_g(\hat{\omega}_i) = \lambda(\hat{\omega}_i^0) + c_g(\hat{\omega}_i - \hat{\omega}_i^0)^{1/h_g} + O\left((\hat{\omega}_i - \hat{\omega}_i^0)^{2/h_g}\right), \quad g = 1, \dots, G, \quad \hbar_g \in \mathbb{N}, \quad \hat{\omega}_i \in \Xi,$$

where $c_g \in \mathbb{C}$, $\hbar_1 \geq \dots \geq \hbar_G$ and $\hbar_1 + \dots + \hbar_G = \mathcal{L}$ [36].

In $\Xi \setminus \{\hat{\omega}_i^0\}$, applying (3.8), the partial derivative of the spectral abscissa with respect to K_i behaves as the real part of $\partial \lambda_g(\hat{\omega}_i) / \partial \hat{\omega}_i$ for some $g \in \{1, \dots, G\}$, which are integrable on Ξ . Without loss of generality, Ξ is contained in the $\hat{\omega}_i$ -projection of Ω , and hence $\frac{\partial \alpha(\omega, \mathbf{K})}{\partial K_i}$ is integrable for all $i = 1, \dots, k$. \square

Systems, which satisfy the assumptions of Proposition 3.2, consider uncertainty on the implemented feedback control in the optimization problem. The hot shower problem (1.24), analyzed in section 1.2.1, satisfies the conditions of Proposition 3.2 since the uncertainty ω affects the controller parameter K . However, in applications, the accuracy of the feedback control is usually high with respect to the uncertainty on the other system parameters, and therefore we need to consider the more general case.

General case

In the previous case, summarized in Proposition 3.2, we differentiate $\alpha(\omega, \mathbf{K})$ with respect to the integration variable ω , by applying (3.8). In the more general setting, however, we are differentiating with respect to the controller \mathbf{K} and we are integrating over the uncertain parameters ω on Ω . In this context the following theorem states that, under a Lipschitz condition, $\nabla_{\mathbf{K}} \alpha(\omega, \mathbf{K})$ is integrable on Ω .

THEOREM 3.3 *If for some $L > 0$, the function $\alpha(\omega, \cdot) : \mathbb{R}^k \rightarrow \mathbb{R}$, $\mathbf{K} \mapsto \alpha(\omega, \mathbf{K})$ is locally Lipschitz in \mathbf{K} at $\mathbf{K} = \mathbf{K}_0$, with Lipschitz constant L , for all $\omega \in \Omega$, then the gradient of the spectral abscissa is integrable on Ω at $\mathbf{K} = \mathbf{K}_0$, and, consequently, $\nabla_{\mathbf{K}} f_{\text{obj}}(\mathbf{K})$ exists at $\mathbf{K} = \mathbf{K}_0$.*

Proof. Let $\mathbb{k} \subset \mathbb{R}^k$ denote the neighborhood of \mathbf{K}_0 such that $\alpha(\omega, \cdot)$ restricted to \mathbb{k} is Lipschitz continuous for all $\omega \in \Omega$. In order to obtain the result, we need to prove that $\partial\alpha(\omega, \mathbf{K}_0)/\partial K_i$ is integrable on Ω , for $i = 1, \dots, k$ and then apply Proposition 3.1. Denoting by e_i the i -th column vector of the identity matrix $I_k \in \mathbb{R}^{k \times k}$, for all $\delta \in \mathbb{R}$ such that $\mathbf{K}_0 + \delta e_i \in \mathbb{k}$, the Lipschitz continuity assumption ensures that

$$|\alpha(\omega, \mathbf{K}_0 + \delta e_i) - \alpha(\omega, \mathbf{K}_0)| \leq L|\delta|, \quad \text{for all } \omega \in \Omega.$$

By Assumption 3.1, the spectral abscissa is almost everywhere differentiable on Ω , hence, we obtain

$$\left| \frac{\partial\alpha(\omega, \mathbf{K}_0)}{\partial K_i} \right| = \lim_{\delta \rightarrow 0} \frac{|\alpha(\omega, \mathbf{K}_0 + \delta e_i) - \alpha(\omega, \mathbf{K}_0)|}{|\delta|} \leq L,$$

almost everywhere on Ω . Since $\partial\alpha(\omega, \mathbf{K}_0)/\partial K_i$ exists almost everywhere on the compact set Ω and is bounded on Ω , we arrive at the assertion. \square

We remind that the spectral abscissa is locally Lipschitz in both ω and \mathbf{K} (and hence Theorem 3.3 holds) when the dominant characteristic roots are (semi)-simple, *i.e.* in the smooth and Lipschitz behaviors of the spectral abscissa. However, we are not able to prove for the general continuous behavior of the spectral abscissa that the gradient of the objective function (3.7) always exists, even though we have strong indication that this property holds, as motivated by the following case-study.

Example 3.2. Let us consider a delay system with stochastic dimension $D = 1$ and $\Omega = [-1, 1]$, such that for $\omega = 0$ the rightmost eigenvalue λ_0 is non-semi-simple with algebraic multiplicity $\ell > 1$ and geometric multiplicity equal to 1. Assume moreover that the complete regular splitting property holds for $\omega = 0$, *i.e.* $u_0^* \frac{\partial \mathcal{A}(\lambda_0; 0, \mathbf{K})}{\partial \omega} v_0 \neq 0$, where u_0 and v_0 are the left and the right eigenvectors corresponding to λ_0 , respectively.

By Assumption 3.1, there exists an open interval (a, b) with $a < 0 < b$ where the eigenvalue $\lambda(\omega)$ is isolated, except for $\omega = 0$. If we restrict to the interval $(0, b)$, $\lambda(\omega)$ and its right and left eigenvectors, $v(\omega)$ and $u(\omega)$ respectively, admit a Puiseux expansion at 0 [53], in formula

$$\lambda(\omega) = \lambda_0 + \sum_{i=1}^{\infty} \omega^{i/\ell} \lambda_i, \quad v(\omega) = v_0 + \sum_{i=1}^{\infty} \omega^{i/\ell} v_i, \quad u(\omega) = u_0 + \sum_{i=1}^{\infty} \omega^{i/\ell} u_i.$$

Moreover, the partial derivative with respect to λ of the characteristic matrix, $\partial \mathcal{A}(\lambda; \omega, \mathbf{K})/\partial \lambda$, can be expressed with a Taylor expansion in increasing powers of $\omega^{i/\ell}$, exploiting the Puiseux series of $\lambda(\omega)$,

$$\frac{\partial \mathcal{A}(\lambda; \omega, \mathbf{K})}{\partial \lambda} = \frac{\partial \mathcal{A}(\lambda_0; 0, \mathbf{K})}{\partial \lambda} + \frac{\partial^2 \mathcal{A}(\lambda_0; 0, \mathbf{K})}{\partial \lambda^2} \lambda_1 \omega^{1/\ell} + \mathcal{O}\left(\omega^{2/\ell}\right).$$

By the smoothness properties of the system matrices of (3.1), $\mathcal{A}(\lambda; \omega, \mathbf{K})$ behaves smoothly with respect to \mathbf{K} and then $\partial \mathcal{A}(\lambda; \omega, \mathbf{K}) / \partial K_i$ is bounded for all $i = 1, \dots, k$. Therefore, $u(\omega)^* \frac{\partial \mathcal{A}(\lambda; \omega, \mathbf{K})}{\partial K_j} v(\omega)$ is bounded since u_0 and v_0 are well defined and finite. In addition, since λ_0 is not semi-simple, we get $u_0^* \frac{\partial \mathcal{A}(\lambda_0; 0, \mathbf{K})}{\partial \lambda} v_0 = 0$. Hence, Proposition 1.4 suggests the following behavior for the derivative of the rightmost eigenvalues with respect to K_i for $i = 1, \dots, k$ as a function of $\omega \in (0, b)$:

$$\frac{\partial \lambda(\omega)}{\partial K_i} = \frac{-u(\omega)^* \frac{\partial \mathcal{A}(\lambda; \omega, \mathbf{K})}{\partial K_i} v(\omega)}{\omega^{1/\ell} \left(u_1^* \frac{\partial \mathcal{A}(\lambda_0; 0, \mathbf{K})}{\partial \lambda} v_0 + u_0^* \frac{\partial^2 \mathcal{A}(\lambda_0; 0, \mathbf{K})}{\partial \lambda^2} \lambda_1 v_0 + u_0^* \frac{\partial \mathcal{A}(\lambda_0; 0, \mathbf{K})}{\partial \lambda} v_1 \right) + \mathcal{O}(\omega^{2/\ell})}.$$

Hence, $\partial \alpha(\omega, \mathbf{K}) / \partial K_i$ behaves as $\omega^{-1/\ell}$ in $(0, b)$, if

$$u_1^* \frac{\partial \mathcal{A}(\lambda_0; 0, \mathbf{K})}{\partial \lambda} v_0 + u_0^* \frac{\partial^2 \mathcal{A}(\lambda_0; 0, \mathbf{K})}{\partial \lambda^2} \lambda_1 v_0 + u_0^* \frac{\partial \mathcal{A}(\lambda_0; 0, \mathbf{K})}{\partial \lambda} v_1 \neq 0.$$

Analogous result holds in the interval $(a, 0)$, providing that the gradient of the spectral abscissa with respect to \mathbf{K} is integrable in a neighborhood of $\omega = 0$. Hence, for Proposition 3.1, the gradient of the objective function (3.7) exists.

3.1.2 Approximation of the objective function and its gradient

The objective function (3.6) and its gradient (3.7) are formulated in terms of integrals, whose integrands might be non-differentiable, and might even admit unbounded discontinuities, considering the objective function gradient. This lack of smoothness heavily affects integration methods, as analyzed in chapter 2 and illustrated in Figures 2.6 and 2.10.

In our implementation, the numerical integration to approximate the objective function and its gradient is accomplished by the quasi-Monte Carlo method [15, 62, 11]. Relying on low-discrepancy (or quasi-random) sequences, the quasi-Monte Carlo integration is almost as accurate as the standard Monte Carlo method, based on random or pseudo-random sequence, but it improves the convergence rate of standard Monte Carlo method, if the integrand is of bounded variation [11]. Moreover, compared to interpolatory cubature rules analyzed in section 2.4.1, the number of points considered by quasi-Monte Carlo methods does not depend exponentially with respect to the stochastic dimension D .

We construct a set of M quasi-random points, $\{\xi_m\}_{m=1}^M$, uniformly distributed in the D -dimensional unit cube Ω , using Halton sequences up to stochastic dimension $D = 6$, and the Sobol sequences for higher stochastic dimensions, as suggested by [62]. Given the quasi-random points, $\{\xi_m\}_{m=1}^M \subset \Omega$, the quasi-Monte Carlo approximation of the

objective function evaluated for every $\mathbf{K} \in \mathbb{R}^k$ is given by

$$f_{\text{obj}}(\mathbf{K}) \approx \frac{1}{M} \sum_{m=1}^M (\alpha(\xi_m, \mathbf{K}) + \kappa \alpha(\xi_m, \mathbf{K})^2) w(\xi_m) - \frac{\kappa}{M^2} \left(\sum_{m=1}^M \alpha(\xi_m, \mathbf{K}) w(\xi_m) \right)^2, \quad (3.9)$$

where $\alpha(\xi_m, \mathbf{K})$ is a realization of the random variable $\alpha(\omega, \mathbf{K})$, computed by an adaptation of Algorithm 1.1 to handle a leading matrix E , given $(\xi_m, \mathbf{K}) \in \Omega \times \mathbb{R}^k$.

The spectral abscissa $\alpha(\omega, \mathbf{K})$ is not differentiable in a set of measure zero for $(\omega, \mathbf{K}) \in \Omega \times \mathbb{R}^k$. However, from a computational point of view, we compute the spectral abscissa at only a finite number of points, $\{\xi_m\}_{m=1}^M \subset \Omega$, where we can expect $\alpha(\omega, \mathbf{K})$ to be differentiable. Therefore, analogously to (3.9), the gradient of the objective function (3.7) is approximated by a quasi-Monte Carlo method,

$$\begin{aligned} \nabla_{\mathbf{K}} f_{\text{obj}}(\mathbf{K}) \approx & \left(1 - \frac{2\kappa}{M} \sum_{m=1}^M \alpha(\xi_m, \mathbf{K}) w(\xi_m) \right) \left(\frac{1}{M} \sum_{m=1}^M \nabla_{\mathbf{K}} \alpha(\xi_m, \mathbf{K}) w(\xi_m) \right) + \\ & + \frac{2\kappa}{M} \sum_{m=1}^M \alpha(\xi_m, \mathbf{K}) \nabla_{\mathbf{K}} \alpha(\xi_m, \mathbf{K}) w(\xi_m). \end{aligned}$$

where $\nabla_{\mathbf{K}} \alpha(\xi_m, \mathbf{K})$, given $(\xi_m, \mathbf{K}) \in \{\xi_m\}_{m=1}^M \times \mathbb{R}^k$, is computed by adapting Algorithm 1.2 to handle the leading matrix E .

The gradient of the spectral abscissa is, under mild conditions, integrable over Ω , but if in Ω there are non-semi-simple dominant characteristic roots, then it might not be square integrable. Indeed, in Example 3.2, if the rightmost eigenvalue λ_0 has algebraic multiplicity $\ell = 2$, then $\partial \alpha(\omega, \mathbf{K}) / \partial K_i$ behaves as $\omega^{-1/2}$ for every $i = 1, \dots, k$. The non-square integrability of the integrand represents a difficult case for numerical integration methods, since there is no theoretical convergence bound even for the Monte Carlo method [11]. However, the following experiments on the approximation of the objective function and its gradient by quasi-Monte Carlo method show that for the different behaviors of the spectral abscissa, analyzed in section 2.1, the convergence rate is at least $\mathcal{O}(M^{-0.5})$, which is the usual convergence rate of the Monte Carlo method.

Example 3.3. Analogously to Example 3.1, the oscillator with feedback delay (2.14), considered in Example 2.5, can be rewritten as a system (3.2) with static feedback controller (3.3a)

$$\begin{cases} \dot{z}_1(t) = z_2(t), \\ \dot{z}_2(t) = -\omega_1^2 z_1(t) - 2\omega_1 \omega_2 z_2(t) + u(t-1), \\ u(t) = K_1 z_1(t) + K_2 z_2(t), \end{cases} \quad (3.10)$$

and can be recast as a delay differential algebraic equation of retarded type (3.1).

We consider the angular frequencies ω_1 and the damping ratio ω_2 realizations of independent random variables, uniformly distributed in $[0.9, 1.1]$ and $[0.1, 0.2]$, respectively. For the different behaviors of the spectral abscissa, characterized by the controllers (K_1, K_2) given in Table 2.1, Figure 3.1 shows the convergence rate of quasi-Monte Carlo method to approximate the objective function (3.6) and its gradient (3.7), increasing the number M of quasi-random points $\{\xi_m\}_{m=1}^M$. In particular, for the three different behaviors, the mean and the variance of the spectral abscissa converges as $\mathcal{O}(M^{-1})$. A similar convergence rate is achieved for the gradient of the mean and of the variance, when the spectral abscissa behaves smoothly. On the other hand, when the partial derivative of the spectral abscissa admits bounded and unbounded discontinuities (when the spectral abscissa presents a Lipschitz and continuous behaviors, respectively), the gradient of the mean and of the variance converge as $\mathcal{O}(M^{-0.5})$.

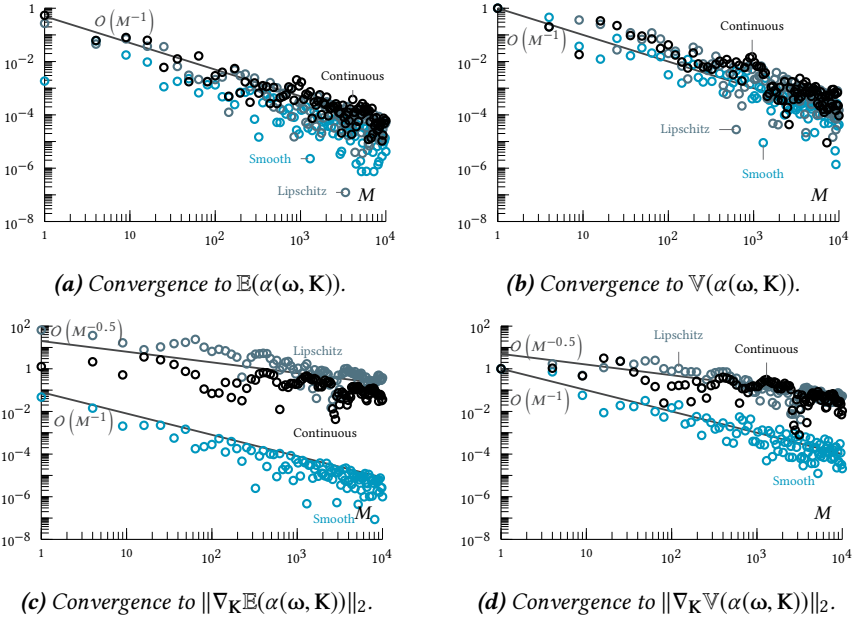


Figure 3.1 Relative errors to approximate by quasi-Monte Carlo method the different quantities, describing the objective function (3.6) and its gradient (3.7), for system (3.10) with feedback controllers given in Table 2.1. The reference values are computed with $M = 5 \cdot 10^5$ quasi-random points.

Remark 3.1. In this section, the objective function (3.6) and its gradient (3.7) are considered as integrals approximated by a quasi-Monte Carlo method. However, they can also be interpreted as linear combination of statistical quantities, like mean and variance. If these underlying statistical moments are approximated by a relative small number of samples, then it is preferable to consider unbiased estimators [15], which

present different formulas with respect to the ones considered in this section, except for the particular case with $\kappa = 0$.

3.2 OPTIMIZATION PROBLEM

A first important property of the objective function (3.6), regarding its optimization, is that it is non-convex and hence may have many local minima. Indeed, the non-convexity is carried over from the deterministic to the stochastic problem; the analysis on the deterministic stability optimization can be found in section 1.1.4.

Moreover, we are theoretically dealing with an objective function which is everywhere differentiable under mild assumptions, hence obtaining a smoother optimization problem than the deterministic spectral abscissa optimization problem. However the quasi-Monte Carlo method, approximating the linear combination of the integrals (2.6) through the formula (3.9), leads to a non-smooth objective function, which is more regular than the spectral abscissa but presents further local minima, as illustrated in Example 3.4 and in Figure 3.2a. Indeed, by the discretization of the integral, the smoothing effect of the integrals is lost.

Example 3.4. Let us consider the hot shower problem (3.5), and let us assume that ω is a realization of a random vector $\boldsymbol{\omega}$ uniformly distributed in $[-0.1, 0.1]$. We analyze the effects on the quasi-Monte Carlo discretization of the mean of the spectral abscissa, $\mathbb{E}(\alpha(\boldsymbol{\omega}, K))$ for $K \in [0.2, 0.6]$, which corresponds to the discretization (3.9) of the objective function (3.6) with trade off-parameter $\kappa = 0$.

Figure 3.2 shows the approximated mean of the spectral abscissa obtained by M spectral abscissa functions $\{\alpha(\xi_m, K)\}_{m=1}^M$ for controller parameter $K \in [0.2, 0.6]$, where $\{\xi_m\}_{m=1}^M$ are M equidistant points in $[-0.1, 0.1]$. The objective function is differentiable for all $K \in [0.2, 0.6]$ while its numerical approximation on $\{\xi_m\}_{m=1}^M$ presents non-differentiable points whenever one of the spectral abscissae $\alpha(\xi_m, K)$ is non-Lipschitz continuous. However, the approximated $f_{\text{obj}}(K)$ is more regular than the associated spectral abscissa functions. Indeed, the non-smooth behaviors of a spectral abscissa function $\alpha(\xi_{\hat{m}}, K)$ is averaged with the smooth behavior of the other spectral abscissa functions $\alpha(\xi_m, K)$, with $m \neq \hat{m}$. Therefore, increasing the number M of sample points $\{\xi_m\}_{m=1}^M$, we expect a smoother behavior of the objective function, as illustrated in Figure 3.2b, similar to the theoretical one, illustrated in Figure 1.7.

It is important to note that this example stresses a pessimistic locally non-Lipschitz behavior of the (discretized) objective function. Indeed, the robust stability optimization (3.6) usually drives the iterations away from non-Lipschitz continuous behavior of the spectral abscissa.

The properties of the optimization problem require software which can deal with non-convex and non-smooth unconstrained minimization, analogous to the deterministic

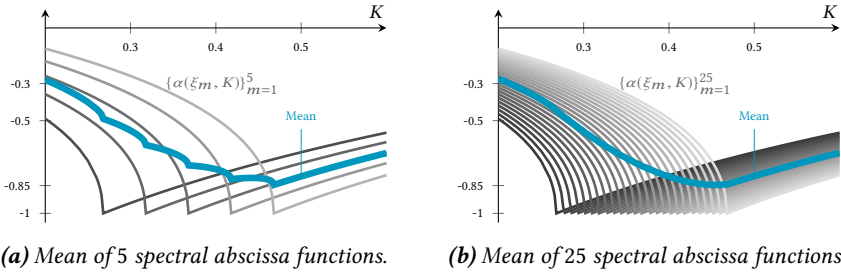


Figure 3.2 *Approximated mean of the spectral abscissa for the hot shower problem (3.5). The approximated mean is obtained by M spectral abscissa functions $\{\alpha(\xi_m, K)\}_{m=1}^M$ for $K \in [0.2, 0.6]$ with $\{\xi_m\}_{m=1}^M$ equidistant points in $[-0.1, 0.1]$.*

case analyzed in section 1.1.4. For this reason, also for the probabilistic objective function (3.6), the optimization is handled by the MATLAB code HANSO (Hybrid Algorithm for Non-Smooth Optimization), described in [64].

However, an accurate approximation of f_{obj} and $\nabla_K f_{\text{obj}}$ is computationally demanding. Therefore, we focus on a deterministic description of the random parameters ω , fixing a set $\{\xi_m\}_{m=1}^{M_{\text{opt}}}$ of M_{opt} realizations in Ω , as explained in section 3.1.2. Hence, the objective function and its gradient are always computed on $\{\xi_m\}_{m=1}^{M_{\text{opt}}}$ during the optimization method, so that the fluctuations induced by the realizations of ω do not affect the accuracy of the solver, and in order to reduce the computational time of the overall algorithm.

To evaluate the optimal gain value $K \in \mathbb{R}^k$, the HANSO algorithm is initialized by default on 10 random starting point. The local optimality of the returned solutions is tested by computing the gradient of the objective function on a refined grid $\{\xi_m\}_{m=1}^{M_{\text{post}}}$, with $M_{\text{post}} \gg M_{\text{opt}}$. If the norm of the gradient is approximately zero in this last step, then the accuracy used to compute the optimal gain value, which depends on M_{opt} , is enough to obtain reliable solutions; otherwise we refine the sample $\{\xi_m\}_{m=1}^{M_{\text{opt}}}$ and we run HANSO again, initialized with the optimal gain value K obtained with the previous rough grid. Indeed, the optimization software might stop in a local minimum arising from the discretization of the objective function, see Figure 3.2a; a refinement of the grid in this case, might hence reveal a better optimal gain value.

To give an overview of the method, we provide a sketch of the overall algorithm, which is publicly available [21].

Algorithm 3.1. *Probabilistic spectrum-based stability optimization.*

1. Construct a set of M_{opt} realizations of ω , $\{\xi_m\}_{m=1}^{M_{\text{opt}}} \subseteq \Omega$, as explained in section 3.1.2.
2. Via HANSO, find the optimal gain value of the system (3.1), giving as inputs the approximation of the objective function and its gradient on $\{\xi_m\}_{m=1}^{M_{\text{opt}}}$.
3. Likewise step 1, construct a set of M_{post} realizations of ω , i.e. $\{\xi_m\}_{m=1}^{M_{\text{post}}}$.
4. Approximate f_{obj} and $\nabla_{\mathbf{K}} f_{\text{obj}}$ on $\{\xi_m\}_{m=1}^{M_{\text{post}}}$.

If $\|\nabla_{\mathbf{K}} f_{\text{obj}}\| \approx 0$ **then** return \mathbf{K} and the approximated statistical quantities $\mathbb{E}(\alpha(\omega; \mathbf{K}))$, and $\mathbb{V}(\alpha(\omega; \mathbf{K}))$.

Else increase M_{opt} and go back to step 1, initializing HANSO at step 2 on the optimal gain value previously found.

Remark 3.2. Algorithm 3.1 can be generalized to systems such that, given $\mathbf{K} \in \mathbb{R}^k$, the stability measure is determined by a finite number of eigenvalues, whose behavior in Ω is continuous and almost everywhere smooth. Therefore, it can be easily generalized to the spectral radius of the monodromy operator associated with linear periodic time-delay system (1.1).

3.3 NUMERICAL EXAMPLES AND APPLICATIONS

In this section, the novel probabilistic stability optimization method, Algorithm 3.1, is tested on three test-cases and two engineering applications. In particular, in section 3.3.1, static and dynamic controllers are designed by the novel approach for a time-delay system with uncertainties affecting the delay and two system coefficients. Section 3.3.2 deals with the probabilistic stability optimization for a time-delay system with a distributed delay. Section 3.3.3 considers the delayed feedback oscillator (3.10) and compares the novel stability optimization method with respect to the deterministic stabilization and worst-case minimization methods. Finally, two engineering applications are considered; in section 3.3.4, Algorithm 3.1 designs a static controller for an experimental heat transfer set up, while in section 3.3.5, we stabilize a mechanical system, which is attached to an active vibration absorber.

All numerical experiments are performed in Matlab version 9.1.0 (R2016b) on a Dell Latitude notebook running an Intel(R) Core(TM) i5-6440HQ CPU @ 2.60GHz quad core processor with 8 GB RAM. Our experiments can be reproduced with the publicly available code of [21].

3.3.1 Static and dynamic controllers

As a first example, we consider the prototype system [51] with stochastic dimension $D = 3$, expressed in the form (3.2)

$$\begin{cases} \dot{z}(t) = A(\omega)z(t) + Bu(t - \tau(\omega)), \\ y(t) = z(t), \end{cases} \quad (3.11)$$

where

$$A(\omega) = \begin{pmatrix} \omega_2 & -0.03 & 0.2 \\ \omega_3 & -0.04 & -0.005 \\ -0.06 & 0.2 & -0.07 \end{pmatrix}, \quad B = \begin{pmatrix} -0.1 \\ -0.2 \\ 0.1 \end{pmatrix}, \quad \begin{aligned} \tau(\omega) &= \omega_1 \sim \mathcal{U}(4.9, 5.1), \\ \omega_2 &\sim \mathcal{U}(-0.09, -0.07), \\ \omega_3 &\sim \mathcal{U}(0.15, 0.25). \end{aligned}$$

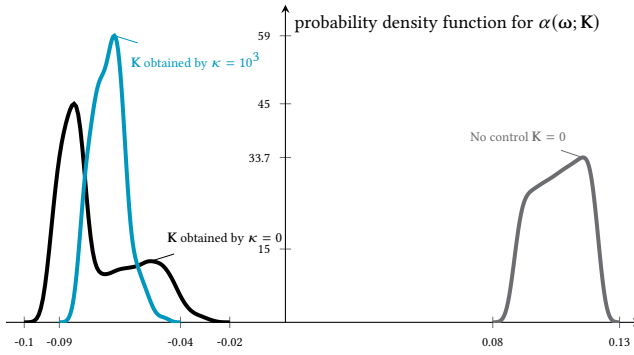


Figure 3.3 Comparison between the probability density functions of the spectral abscissa for system (3.11) with static feedback control, i.e. $r_c = 0$ in (3.12). Without control, i.e. $\mathbf{K} = 0$, the spectral abscissa $\alpha(\omega, 0)$ admits only positive realizations. For the controller \mathbf{K} minimizing the mean with a variance penalty $\kappa = 0$ and $\kappa = 10^3$, the supports of the probability density function are contained in the negative real axis, ensuring the asymptotic stability of the system.

As shown in Figure 3.3, the probability density function of the spectral abscissa with $\mathbf{K} = 0$, i.e. $\alpha(\omega, 0)$, is contained in the positive real line, ensuring the system instability. We design a dynamic controller of the form (3.3)

$$\begin{cases} \dot{z}_c(t) = \hat{F}z_c(t) + \hat{G}y(t), & z_c(t) \in \mathbb{R}^{r_c}, \\ u(t) = \hat{H}z_c(t) + \hat{L}y(t), & u(t) \in \mathbb{R}, \end{cases} \quad (3.12)$$

where \mathbf{K} is the vectorization of the control matrices \hat{F} , \hat{G} , \hat{H} , and \hat{L} , as already shown in the transformation from (3.2) and (3.3) to (3.1).

We apply the optimization approach to objective function (3.6) considering $\kappa = 0, 10^3$ on the system with static control, $r_c = 0$, and with dynamic feedback, $r_c = 1, 2$. The results, obtained with $M_{\text{opt}} = 10^3$ and $M_{\text{post}} = 10^4$, are shown in Table 3.1.

Designing a controller with higher order r_c leads us to a small value of the mean of the spectral abscissa. The supports of the spectral abscissa minimizing (3.6) with static feedback control, illustrated in Figure 3.3, are already contained in the negative real line, ensuring asymptotic stability properties for the system (3.11).

Table 3.1 Comparison between system (3.11) without control and the results of minimizing objective function (3.6) with different controls of the form (3.12).

Control \mathbf{K}	κ	$\alpha(\mathbb{E}(\omega), \mathbf{K})$	$\mathbb{E}(\alpha(\omega, \mathbf{K}))$	$\mathbb{V}(\alpha(\omega, \mathbf{K}))$
Without control $\mathbf{K} = 0$		0.1081	0.1076	$9.1770 \cdot 10^{-5}$
Static control $r_c = 0$	$\kappa = 0$	-0.0895	-0.0739	$2.3655 \cdot 10^{-4}$
	$\kappa = 10^3$	-0.0562	-0.0551	$8.6305 \cdot 10^{-6}$
Dynamic control $r_c = 1$	$\kappa = 0$	-0.1620	-0.1195	$6.9411 \cdot 10^{-4}$
	$\kappa = 10^3$	-0.1157	-0.1133	$1.1774 \cdot 10^{-5}$
Dynamic control $r_c = 2$	$\kappa = 0$	-0.2232	-0.1995	$1.0074 \cdot 10^{-3}$
	$\kappa = 10^3$	-0.1704	-0.1705	$1.2609 \cdot 10^{-5}$

3.3.2 Stabilization problem with distributed delay

As a second example, we consider a plant with a distributed delay term

$$\dot{z}(t) = A_1 z(t) + B(\omega)u(t - \tau_1) + A_2 z(t - \tau_2(\omega)) + \int_{t-\tau_2(\omega)}^t A_3 z(\theta) d\theta, \quad (3.13)$$

where

$$A_1 = \begin{pmatrix} 0.1 & 0 & 0 \\ 0.2 & 0 & -0.2 \\ 0.3 & 0.1 & -0.2 \end{pmatrix}, \quad A_2 = \begin{pmatrix} -0.2 & 0 & 0 \\ -0.4 & -0.2 & 0.4 \\ -0.4 & -0.1 & 0.2 \end{pmatrix},$$

$$A_3 = \begin{pmatrix} 0.1 & -0.2 & 0 \\ 0 & 0.1 & 0.1 \\ -0.1 & 0 & 0.1 \end{pmatrix}, \quad B(\omega) = \begin{pmatrix} \omega_2 \\ 0 \\ 0 \end{pmatrix}, \quad \begin{matrix} \tau_1 = 1, \\ \tau_2(\omega) = \omega_1 \sim \mathcal{U}(5.9, 6.1), \\ \omega_2 \sim \mathcal{U}(0.075, 0.125), \end{matrix}$$

with a static feedback control: $u(t) = \mathbf{K}^T z(t)$. Note that for fixed τ_2 and ω_2 , the system is analyzed in [54]. Setting $h(t)$ equal to the distributed delay term of (3.13), and differentiating $h(t)$, the system (3.13) can be recast as

$$\begin{cases} \dot{z}(t) = A_1 z(t) + B(\omega)u(t - \tau_1) + A_2 z(t - \tau_2(\omega)) + h(t), \\ \dot{h}(t) = A_3 z(t) - A_3 z(t - \tau_2(\omega)). \end{cases} \quad (3.14)$$

Imposing $x = (z^T h^T u^T)^T$, system (3.14) with static feedback can be rewritten as a delay differential algebraic equation of retarded type (3.1)

$$\dot{x}(t) = \begin{pmatrix} A_1 & I & 0 \\ A_3 & 0 & 0 \\ K^T & 0 & -1 \end{pmatrix} x(t) + \begin{pmatrix} 0 & 0 & B(\omega) \\ 0 & 0 & 0 \\ 0 & 0 & 0 \end{pmatrix} x(t - \tau_1) + \begin{pmatrix} A_2 & 0 & 0 \\ -A_3 & 0 & 0 \\ 0 & 0 & 0 \end{pmatrix} x(t - \tau_2(\omega)). \quad (3.15)$$

Formulations (3.13) and (3.14) are almost equivalent; however, the dimension of the latter system is doubled with respect to the dimension of (3.13). As a consequence of differentiating function $h(t)$, (3.14) has 3 additional non-physical zero eigenvalues with respect to the spectrum of (3.13). These additional zero eigenvalues, which also appear in the formulation (3.15), can be removed and the results obtained minimizing objective function (3.6) with $\kappa = 0, 10, 10^2, 10^3$ using $M_{\text{opt}} = 10^3$, and $M_{\text{post}} = 10^4$, are shown in Table 3.2.

Table 3.2 Results of minimizing the objective function (3.6) for system (3.15).

κ	$\alpha(\mathbb{E}(\omega), \mathbf{K})$	$\mathbb{E}(\alpha(\omega, \mathbf{K}))$	$\mathbb{V}(\alpha(\omega, \mathbf{K}))$
$\kappa = 0$	0.1631	0.1845	$2.2629 \cdot 10^{-4}$
$\kappa = 10$	0.1628	0.1846	$2.0903 \cdot 10^{-4}$
$\kappa = 100$	0.1694	0.1866	$1.6418 \cdot 10^{-4}$
$\kappa = 1000$	0.2375	0.2375	$7.0138 \cdot 10^{-6}$

3.3.3 Comparison with deterministic and worst-case stabilization

As a third numerical example, we consider the oscillator with static feedback delay (2.14), whose delay differential algebraic form has been derived in Example 3.3. We recall the system

$$\begin{pmatrix} 1 & & \\ & 1 & \\ & & 0 \end{pmatrix} \begin{pmatrix} \dot{z}_1(t) \\ \dot{z}_2(t) \\ \dot{u}(t) \end{pmatrix} = \begin{pmatrix} 0 & 1 & 0 \\ -\omega_1^2 & -2\omega_1\omega_2 & 0 \\ K_1 & K_2 & -1 \end{pmatrix} \begin{pmatrix} z_1(t) \\ z_2(t) \\ u(t) \end{pmatrix} + \begin{pmatrix} 0 & 0 & 0 \\ 0 & 0 & 1 \\ 0 & 0 & 0 \end{pmatrix} \begin{pmatrix} z_1(t-1) \\ z_2(t-1) \\ u(t-1) \end{pmatrix}. \quad (3.16)$$

We want to design the controller parameters K_1 and K_2 in order to robustly stabilize the system against uncertainty on the angular frequency ω_1 and on the damping ratio ω_2 . To this end, we consider three different stability optimization methods. First, the deterministic spectrum-based stability optimization, described in section 1.1.4, designs the control $\mathbf{K} = (K_1, K_2)$ minimizing the spectral abscissa $\alpha(\omega_1, \omega_2, \mathbf{K})$, setting $\omega_1 = 1$ and $\omega_2 = 0.15$. Second, the novel stabilization method is applied to the system (3.16) where ω_1 and ω_2 are realizations of independent uniform random variables, $\omega_1 \sim \mathcal{U}(0.9, 1.1)$ and $\omega_2 \sim \mathcal{U}(0.1, 0.2)$, respectively. The optimal controllers are achieved by Algorithm 3.1, minimizing the mean of the spectral abscissa with a variance penalty, $\mathbb{E}(\alpha(\omega_1, \omega_2; \mathbf{K})) + \kappa \mathbb{V}(\alpha(\omega_1, \omega_2; \mathbf{K}))$ with $\kappa = 0, 10, 100$. In order

to obtain an accurate result, Algorithm 3.1 is first run with $M_{\text{opt}} = 10^2$, hence the results are refined using $M_{\text{opt}} = 10^3$. The third and last method to stabilize the oscillator with feedback delay is the pseudospectral abscissa minimization [4]. In order to apply this method, the uncertainties on ω_1 and ω_2 must be rewritten as linear perturbations of the original system matrices. Therefore, we consider $\omega_1 = 1 + 0.1 \varepsilon_1$ and $\omega_2 = 0.15 + 0.05 \varepsilon_2$, with $|\varepsilon_1| \leq 1$ and $|\varepsilon_2| \leq 1$. In order to remove the nonlinearity in the uncertainties, two additional slack variables are considered, $\tilde{z}_1(t) = \varepsilon_1 z_1(t)$ and $\tilde{z}_2(t) = \varepsilon_2 z_2(t)$. Carrying out the algebraic manipulations, we can rewrite the delayed feedback oscillator (3.16) considering ω_1 and ω_2 as rank-1 perturbations

$$\begin{pmatrix} \dot{z}_1(t) \\ \dot{z}_2(t) \\ 0 \\ 0 \\ 0 \end{pmatrix} = \begin{pmatrix} 0 & 1 & 0 & 0 & 0 \\ -1 & -0.3 & -2 & -2 & 0 \\ 0 & 0 & -1 & 0 & 0 \\ 0 & 0 & 0 & -1 & 0 \\ K_1 & K_2 & 0 & 0 & -1 \end{pmatrix} + \varepsilon_1 \delta A_1 + \varepsilon_2 \delta A_2 + \varepsilon_3 \delta A_3 \begin{pmatrix} z_1(t) \\ z_2(t) \\ \tilde{z}_1(t) \\ \tilde{z}_2(t) \\ u(t) \end{pmatrix} + \begin{pmatrix} 0 \\ u(t-1) \\ 0 \\ 0 \\ 0 \end{pmatrix},$$

where $|\varepsilon_1| \leq 1$, $|\varepsilon_2| \leq 1$, and the rank-1 matrices are

$$\delta A_1 = \begin{pmatrix} 0 \\ 0.1 \\ 0 \\ 0 \\ 0 \end{pmatrix} \begin{pmatrix} 0 \\ 0.3 \\ -1 \\ -1 \\ 0 \end{pmatrix}^T, \quad \delta A_2 = \begin{pmatrix} 0 \\ 0 \\ 0.1 \\ 0 \\ 0 \end{pmatrix} \begin{pmatrix} 1 \\ 0 \\ 0 \\ 0 \\ 0 \end{pmatrix}^T, \quad \delta A_3 = \begin{pmatrix} 0 \\ 0 \\ 0 \\ 0.05 \\ 0 \end{pmatrix} \begin{pmatrix} 0 \\ 1 \\ 0 \\ 0 \\ 0 \end{pmatrix}^T.$$

For this system, the pseudospectral abscissa corresponds to the worst-case spectral abscissa (in the sense of being the largest) for every ε_1 and ε_2 smaller than 1 in absolute value, in formula

$$\alpha_{\varepsilon_1, \varepsilon_2}(\mathbf{K}) := \sup_{|\varepsilon_1| \leq 1, |\varepsilon_2| \leq 1} \alpha(\varepsilon_1, \varepsilon_2, \mathbf{K}).$$

The comparison results of these three different stabilization methods are summarized in Tables 3.3 and 3.4 and in Figure 3.4. As we would have expected, Table 3.3 shows that the smallest spectral abscissa is attained by the deterministic stability optimization method, the novel approach with a variance penalty $\kappa = 0$ and $\kappa = 100$ leads respectively to the smallest mean and variance of the spectral abscissa random variable, while the smallest pseudospectral abscissa is achieved by the worst-case stability optimization. Interestingly, the numerical results obtained by the novel stabilization method with $\kappa = 10$ are similar to the ones obtained by performing the worst-case stabilization. This similarity is further highlighted in Figure 3.4, by comparing the probability density functions of the spectral abscissa random variables and the pseudospectral abscissae.

The different stabilization methods ensure that the oscillator with feedback delay (3.16) is asymptotically stable against both probabilistic and worst-case uncertainties on the parameters ω_1 and ω_2 . Indeed, in Figure 3.4, the supports of the probability density function and the pseudospectral abscissae are strictly contained in the negative real

Table 3.3 Numerical values of the spectral abscissa $\alpha(\omega_1, \omega_2, \mathbf{K})$ with $\omega_1 = 1$, $\omega_2 = 0.15$, of the pseudospectral abscissa $\alpha_{\varepsilon_1, \varepsilon_2}(\mathbf{K})$, and of the spectral abscissa random variable $\alpha(\omega_1, \omega_2, \mathbf{K})$ mean and variance with $\omega_1 \sim \mathcal{U}(0.9, 1.1)$ and $\omega_2 \sim \mathcal{U}(0.1, 0.2)$ for the oscillator with feedback delay (3.16). The controller parameters are designed with the deterministic stability optimization method, with the novel probabilistic stabilization, and with the worst-case stabilization method, minimizing the pseudospectral abscissa [4].

Control design	κ	$\alpha(\omega_1, \omega_2, \mathbf{K})$	$\alpha_{\varepsilon_1, \varepsilon_2}(\mathbf{K})$	$\mathbb{E}(\alpha(\omega_1, \omega_2, \mathbf{K}))$	$\mathbb{V}(\alpha(\omega_1, \omega_2, \mathbf{K}))$
Deterministic		-1.1388	-0.21089	-0.6699	$5.4061 \cdot 10^{-2}$
Probabilistic	0	-0.8474	-0.37223	-0.7648	$1.5828 \cdot 10^{-2}$
	100	-0.7824	-0.44953	-0.7362	$7.6242 \cdot 10^{-3}$
Worst-case		-0.5811	-0.39645	-0.5531	$1.8166 \cdot 10^{-3}$
		-0.7601	-0.47371	-0.7354	$8.1677 \cdot 10^{-3}$

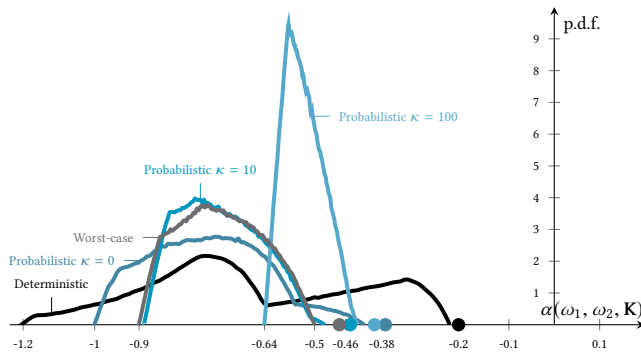


Figure 3.4 Comparison between the probability density functions (p.d.f.) of the spectral abscissa random variables for the oscillator with feedback delay (3.16) with different control parameters \mathbf{K} . These controls are designed by the deterministic stability optimization method, by the novel probabilistic stabilization, and by the worst-case stabilization method, minimizing the pseudospectral abscissa [4]. The dots highlight the value of the pseudospectral abscissae for the different controls.

axis. Moreover, the novel probabilistic approach with $\kappa = 100$ provides a probability density function with the smallest support, guaranteeing the best insensitivity of the stability measure with respect to the uncertainties.

The control parameters achieved by the deterministic stabilization methods and by the novel approach with $\kappa = 0$ respectively lead to a continuous and Lipschitz behaviors of the spectral abscissa. Indeed, the numerical values of K_1 and K_2 in Table 3.4 coincide with the controllers given in Table 2.1 and they are associated with the non-smooth behaviors of the test-cases in Example 2.5.

Table 3.4 furnishes, also, the timings comparison between the different stabilization

methods. The overall time required to the optimization process is hardly comparable, since it is problem dependent and is affected by the computational accuracy of the objective function and its gradient, which might vary during the optimization process; for example, applying Algorithm 3.1, we first considered $M_{\text{opt}} = 10^2$, and hence, we refined the results using $M_{\text{opt}} = 10^3$.

In the last iteration of the optimization process, the computational time to evaluate the objective function and its gradient for the novel approach is approximately M_{opt} divided by the parallelization (in our case $10^3/4$) bigger than the computational time to compute the spectral abscissa and its gradient in the deterministic case. Indeed, the mean and the variance with the novel method are approximated by considering $M_{\text{opt}} = 10^3$ realizations of the spectral abscissa random variable and hence the usage of specialized parallel computer architectures permits to significantly reduce the computational time of the novel approach.⁵

Table 3.4 Numerical values of the controllers K_1 and K_2 for the delayed feedback oscillator (3.16) obtained by the deterministic stability optimization method, by the novel probabilistic stabilization, and by the worst-case stabilization method, minimizing the pseudospectral abscissa [4]. For the different stabilization methods, we present the time request to perform the optimization process by HANSO with 10 random initial values and the time requested to evaluate the objective function and its gradient in the last iteration of the stabilization process.

Control design	κ	K_1	K_2	timings [s]	
				iteration	optimization
Deterministic		0.6179	$-7.1644 \cdot 10^{-3}$	$8.9861 \cdot 10^{-3}$	12.31
	0	0.5105	$-9.1810 \cdot 10^{-2}$	0.9655	208.56
Probabilistic	10	0.4504	-0.1631	0.9246	285.69
	100	0.3633	-0.3988	0.9389	500.71
Worst-case		0.4444	-0.1570	0.2087	192.26

The pseudospectral abscissa computation requires to solve an optimization process in order to reach the largest value of the spectral abscissa among all the possible linear perturbations, for this reason the computational time is highly problem dependent and cannot be easily compared with the other methods. The pseudospectral abscissa is always to the the right of all the possible realizations of the spectral abscissa random variable, Figure 3.4. Therefore, the pseudospectral abscissa represents is a more conservative robust stability measure of the uncertain time-delay system compared to the mean and the variance of the spectral abscissa random variable. Moreover, in order to apply the worst-case stability optimization method, the delayed feedback oscillator has been rewritten in such a way that the uncertainties appear as rank-1

⁵ Let us note that the evaluation of the spectral abscissa, Algorithm 1.1, is problem dependent. In particular, the computational time required to the Newton's correction to reach the requested tolerance cannot be estimated a priori.

linear perturbations, increasing the system dimension from $r = 3$ to $r = 5$. If the uncertainty on the system are highly nonlinear, then it might not be possible to rewrite the system with rank-1 linear perturbations or the final system dimension might be very large and hence computational demanding.⁶

3.3.4 Heating system

The novel optimization approach is tested on the linear model of the experimental heat transfer set up, described in [98]. Feedback controllers for this model are designed by the deterministic spectrum-based stability optimization method in [60, 51].

The mathematical model has system dimension $r = 10$, and involves six different delays in the state and two different delays in the inputs

$$\dot{z}(t) = \sum_{i=0}^5 A_i(\omega, \mathbf{K})z(t - \tau_i) + B_1u(t - \tau_5) + B_2u(t - \tau_6), \quad z(t) \in \mathbb{R}^{10}, \quad (3.17)$$

see [60] for the corresponding matrices and delay values.

We consider system (3.17) with static feedback control: $u(t) = \mathbf{K}^T z(t)$. In order to determine the controller gain $\mathbf{K} \in \mathbb{R}^k$, we first apply to the nominal model (thereby neglecting the uncertainty) the deterministic stabilization method of [51], which adapts the method considered in section 1.1.4 to handle the leading matrix E . Subsequently, we design $\mathbf{K} \in \mathbb{R}^k$ by Algorithm 3.1, considering an uncertainty of 10% on the nominal value of the left-cooler temperature, denoted by T_L , and considering an uncertainty of 10% on the nominal temperatures of both coolers, denoted by T_L and T_R . The temperatures of both coolers depend on the seasonal temperature of the outdoor air; hence, we model T_L and T_R as realizations of independent random variable T_L and T_R uniformly distributed in the intervals [13.5, 16.5] and [15.3, 18.7], respectively.⁷

To obtain the results shown in Table 3.5, we set $\kappa = 0, 10, 10^2, 10^3$ and we first run Algorithm 3.1 using a number of samples $M_{\text{opt}} = 500$ and $M_{\text{post}} = 10^3$. However, due to the presence of local minima that are not global, the results did not always satisfy the following relations:

$$\mathbb{E}(\alpha(\omega, \mathbf{K}_1)) \leq \mathbb{E}(\alpha(\omega, \mathbf{K}_2)), \quad \mathbb{V}(\alpha(\omega, \mathbf{K}_1)) \geq \mathbb{V}(\alpha(\omega, \mathbf{K}_2)), \quad (3.18)$$

where \mathbf{K}_1 and \mathbf{K}_2 are the optimal controller for the objective functions (3.6) with $0 \leq \kappa_1 < \kappa_2$. Hence, for each value of κ , we re-run Algorithm 3.1 initializing

⁶ Further information on the pseudospectral abscissa for time-delay systems can be found in [3], and reference therein.

⁷ The uncertainty T_L affects the (10, 10)-th entry of matrix A_0 , the (10, 9)-th entry of A_2 , and the only non-zero coefficient (10-th entry) of vector B_1 . On the other hand, the uncertainty T_R affects the (6, 6)-th entry of matrix A_0 , and the (6, 5)-th entry of A_2 .

HANSO on all optimal gain values previously found and refining the set of realizations using $M_{\text{opt}} = 10^3$ and $M_{\text{post}} = 10^4$. The latter results, shown in Table 3.5, satisfies criterion (3.18) and the gradient of the objective function, evaluated in the post-processor analysis, is approximatively zero.

Table 3.5 Comparison between the results of minimizing objective function (3.6) for system (3.17) with different system uncertainties. The second row corresponds to optimizing the spectral abscissa for the deterministic case, $T_L = 15$ and $T_R = 17$; the third to the sixth rows show the results of optimizing (3.6) for $\kappa = 0, 10^3$ and imposing different uncertainties. T_L, T_R denotes random variables uniformly distributed in $[13.5, 16.5]$ and $[15.3, 18.7]$, respectively.⁸

Control design	κ	$\alpha(T_L, T_R, \mathbf{K})$	$\mathbb{E}(\alpha(T_L, T_R, \mathbf{K}))$	$\mathbb{V}(\alpha(T_L, T_R, \mathbf{K}))$	$\mathbb{E}(\alpha(T_L, T_R, \mathbf{K}))$	$\mathbb{V}(\alpha(T_L, T_R, \mathbf{K}))$
Deterministic		$-6.4140 \cdot 10^{-2}$	$-6.2668 \cdot 10^{-2}$	$2.6465 \cdot 10^{-6}$	$5.9903 \cdot 10^{-2}$	$8.4117 \cdot 10^{-2}$
Uncertain T_L	0	$-6.3402 \cdot 10^{-2}$	$-6.3331 \cdot 10^{-2}$	$4.9526 \cdot 10^{-8}$	$-5.4113 \cdot 10^{-2}$	$1.4040 \cdot 10^{-5}$
	10^3	$-6.3353 \cdot 10^{-2}$	$-6.3327 \cdot 10^{-2}$	$1.0437 \cdot 10^{-8}$	$-5.7756 \cdot 10^{-2}$	$1.4668 \cdot 10^{-5}$
Uncertain T_L, T_R	0	$-6.3406 \cdot 10^{-2}$	$-6.3209 \cdot 10^{-2}$	$2.7837 \cdot 10^{-7}$	$-6.2981 \cdot 10^{-2}$	$2.8111 \cdot 10^{-7}$
	10^3	$-6.3143 \cdot 10^{-2}$	$-6.3081 \cdot 10^{-2}$	$8.2656 \cdot 10^{-8}$	$-6.2919 \cdot 10^{-2}$	$1.0105 \cdot 10^{-7}$

Table 3.5 shows how the uncertainty on the parameters may affect the optimal gain values and, consequently, the statistical moments of the spectral abscissa. Indeed, increasing the stochastic dimension D , the different optimal gain controllers may change. It is important to notice, that the deterministic solution may lead to unstable system if the temperatures of both coolers are affected by uncertainty, since the mean is positive, see the highlighted cell in Table 3.5.

3.3.5 Mechanical system with active vibration absorber

The mechanical system, shown in Figure 3.5, consists of two parts, a single-degree of freedom primary structure P which is affected by uncertainty and is excited by an external harmonic force f_e , and an absorber A attached to the primary structure with spring, damper and an actuator. The control objective of this example is two-fold. First, the external harmonic force f_e has to be compensated by active feedback, actuating with force f_A . Second, the positioning of the primary structure and robust stability of the induced equilibrium are ensured by a feedback controller designed with the novel approach. This latter feedback controller acts on the primary structure with the input force u and takes into account both the primary structure uncertainty and the absorber dynamics.

The mechanical system is modeled by the following equations

$$\begin{aligned}
 m_A \ddot{z}_A(t) + c_A \dot{z}_A(t) + k_A z_A(t) - c_A \dot{z}_P(t) - k_A z_P(t) &= f_A(t), \\
 m_P \ddot{z}_P(t) + c_A \dot{z}_P(t) + k_A z_P(t) - c_A \dot{z}_A(t) - k_A z_A(t) &= -f_A(t) + f_e(t) + u(t),
 \end{aligned} \tag{3.19}$$

⁸ The results obtained with $\kappa = 10, 10^2$ are similar to the one corresponding to $\kappa = 0$, for this reason they are not reported in Table 3.5.

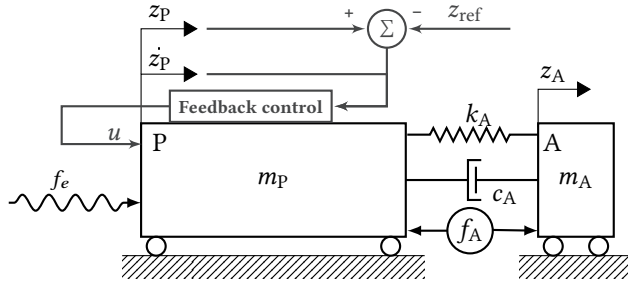


Figure 3.5 Mechanical system with active vibration absorber.

where $z_p(t)$ and $z_A(t)$ are respectively the position of the primary structure and of the absorber at time t , $u(t)$ is the input parameter of the primary structure, f_e is a harmonic force exciting the system with undesirable oscillations of frequency ν_e , and f_A is the force actuating between the primary mass and the absorber, which has a suppressing effect on f_e . The physical parameters of the system are m_A , c_A , k_A denoting the mass, damping and the stiffness of the absorber and m_p denotes the primary structure mass. The parameter of system (3.19) are given in Table 3.6.

Table 3.6 Parameter values for system (3.19). The values are evaluated in [66, 65].

Parameter	Definition	Mean value	Uncertainty	Units
m_p	Primary mass	1.52	$\pm 20\%$	kg
m_A	Absorber mass	0.223		kg
k_A	Spring stiffness	350		N/m
c_A	Damping ratio of the spring	1.273		kg/s
ν_e	Excitation frequency	13π		rad/s

The absorber actively reacts on the external harmonic force with properly tuned feedback. We consider an absorber control with distributed time-delay of the form

$$f_A(t) = \frac{g}{\tau} \int_0^\tau \ddot{z}_A(t - \theta) d\theta, \quad (3.20)$$

where $\tau > 0$ is the length of the delay, and g is the absorber feedback gain [66].

The feedback parameters, τ and g , are tuned in order to turn the absorber to an ideal oscillator with a dominant couple of characteristic roots placed at the imaginary axis at the given excitation frequency. Consequently, the external harmonic force at the given frequency ν_e is suppressed entirely. To this end, the transfer function from f_e to z_p is set equal to zero for the given frequency, *i.e.* it is zero in $\pm \nu_e i$. Splitting real and

imaginary parts, and balancing the magnitudes, as described in [66], the parameter of (3.20) suppressing the external harmonic force are

$$\tau = \frac{2}{v_e} \left(\text{atan} \left(\frac{c_A v_e}{m_A v_e^2 - k_A} \right) + 2(l-1)\pi \right), \quad g = \frac{\tau \left(v_e^2 c_A^2 + (m_A v_e^2 - k_A)^2 \right)}{2v_e^2 c_A}, \quad (3.21)$$

where $l \in \mathbb{N} \setminus \{0\}$ is the branch number denoting a counter associated with phase wrap-around. We consider $l = 1$, since this branch number presents a wide stability region [66]. Considering the values in Table 3.6 and $l = 1$, the delay τ and the absorber feedback gain g in (3.21) are approximated by

$$\tau \approx 5.7355 \cdot 10^{-2} \text{ s}, \quad g \approx 4.3017 \cdot 10^{-2} \text{ kg}. \quad (3.22)$$

For $u \equiv 0$, the spectral abscissa is zero and then the system (3.19) with active vibration absorber (3.20)–(3.22) is not asymptotically stable. To ensure asymptotic stability to the system, we design a feedback control, taking into account the uncertainty contained in the primary mass m_p , which we model by $m_p = 1.52 \text{ kg} + \omega$, where the random variable ω is uniformly distributed in the interval $[-0.304, 0.304]$.

We assume that the measured outputs of the systems are the position and the velocity of the primary structure, *i.e.*

$$y(t) = \begin{pmatrix} z_p(t) \\ \dot{z}_p(t) \end{pmatrix}, \quad (3.23)$$

and we design static and dynamic controllers for the plant (3.19) and output (3.23) of the form

$$\begin{cases} \dot{z}_c(t) = \hat{F}z_c(t) + \hat{G} \left(y(t) - \begin{pmatrix} z_{\text{ref}}(t) \\ 0 \end{pmatrix} \right) \\ u(t) = \hat{H}z_c(t) + \hat{L} \left(y(t) - \begin{pmatrix} z_{\text{ref}}(t) \\ 0 \end{pmatrix} \right) \end{cases}, \quad \begin{matrix} z_c \in \mathbb{R}^{r_c}, \\ u(t) \in \mathbb{R}, \end{matrix} \quad (3.24)$$

where $z_{\text{ref}}(t)$ is the desired position of the primary mass at time t , and the matrices \hat{F} , \hat{G} , \hat{H} and \hat{L} model the feedback control $\mathbf{K} \in \mathbb{R}^k$ analogously to (3.3).

In order to apply Algorithm 3.1, the plant (3.19), output (3.23), and controller equation (3.24) are reformulated as a system of delay differential algebraic equations of retarded type of the form (3.1). To achieve this reformulation, the absorber feedback (3.20) is rewritten as $f_A(t) = g/\tau(\dot{z}_A(t - \tau) - \dot{z}_A(t))$ and the plant (3.19) is rewritten in a first order form so that the state of the delay differential algebraic equation of retarded type is $x = (z_A, z_p, \dot{z}_A, \dot{z}_p, y^T, z_c^T, u)^T$.

In order to determine static ($r_c = 0$) and dynamic controllers ($r_c = 1$), we first apply the deterministic stability optimization method to the nominal model obtained by considering the averaged values of the uncertain parameter, *i.e.* $m_p = 1.52 \text{ kg}$. Secondly, we design the feedback controllers by probabilistic stabilization method,

considering the primary mass of (3.19) affected by uncertainty, *i.e.* $m_p = 1.52 + \omega$ kg, with ω being a realization of the random variable ω uniformly distributed in $[-0.304, 0.304]$. The probabilistic stabilization method, described in Algorithm 3.1, minimizes the approximated objective function (3.9) with trade off parameters $\kappa = 0, 1, 10, 100$, and where $M_{\text{opt}} = 10^3$ and $M_{\text{opt}} = 2 \cdot 10^3$.

The results are given in Table 3.7, and illustrated in Figure 3.6. By increasing parameter κ the mean increases and the variance decreases, improving the robustness against the parameter uncertainties. On the other hand, the spectral abscissa increases and the deterministic system with $m_p = 1.52$ kg presents a slower asymptotically convergence rate to the zero-solution. Evident improvements can be seen with the dynamic controller, as it has more parameters to tune and hence the optimization has more degrees of freedom $k = 6$, with respect to the static controller which presents only $k = 2$ degrees of freedom.

Table 3.7 Numerical value of the spectral abscissa (*i.e.* $\omega = 0$, $m_p = 1.52$ kg), its mean and variance for system (3.19), output (3.23) and static ($r_c = 0$) and dynamic ($r_c = 1$) controllers (3.23). The controllers are designed by deterministic and probabilistic spectrum-based stability optimization, considering respectively the nominal value of the mass, $m_p = 1.52$ kg and the mass affected by 20% of uncertainty, *i.e.* $m_p = 1.52 + \omega$ kg, where ω is a realization of ω uniform random variable in $[-0.304, 0.304]$.

Controller	Control design	κ	$\alpha(0, \mathbf{K})$	$\mathbb{E}(\alpha(\omega, \mathbf{K}))$	$\mathbb{V}(\alpha(\omega, \mathbf{K}))$
Static, $r_c = 0$	Deterministic		-7.4454	-4.9881	0.7812
		0	-6.6502	-5.0992	0.8284
	Probabilistic	1	-5.8202	-4.7553	0.4451
		10	-4.0842	-3.8331	$4.1171 \cdot 10^{-2}$
		100	-2.9593	-2.8894	$3.6837 \cdot 10^{-3}$
Dynamic, $r_c = 1$	Deterministic		-30.6482	-7.0621	99.3767
		0	-9.9397	-10.0416	22.9431
	Probabilistic	1	-8.3575	-7.0698	0.8979
		10	-5.5551	-5.5108	$2.7537 \cdot 10^{-2}$
		100	-4.7510	-4.7474	$4.2727 \cdot 10^{-3}$

It is possible to have some insight on the system dynamics by looking at the spectral abscissa functions on the support of the uncertainty, Figure 3.7. The deterministic controllers lead to spectral abscissa functions with a wider image than the ones obtained with the probabilistic approach. In particular, the spectral abscissa function obtained by the deterministic dynamic controller admits positive values, revealing the system instability for some values of m_p . On the other hand, the dynamic controllers obtained by the novel approach lead to spectral abscissa functions, whose image is contained in the real negative axis, ensuring the system stability and the robustness of the method. Hence, even though, with the deterministic controller the performance is

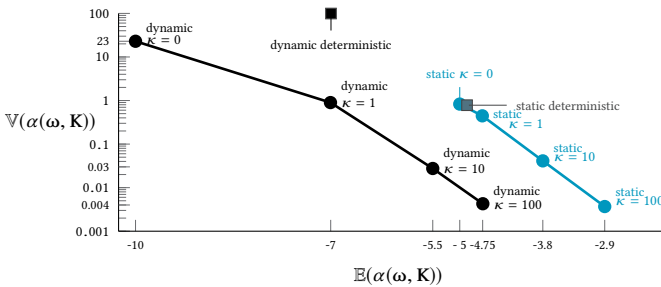


Figure 3.6 Pareto fronts, comparing the results of mean and variance given in Table 3.7.

better at the nominal value, as shown in Table 3.7, with the novel approach we ensure a better convergence rate if the primary mass is affected by uncertainty. In addition, by increasing the value κ , we obtain spectral abscissa function with a small image, ensuring a better insensitivity with respect to the parameter m_p .

Moreover, analogously to the hot shower problem in section 1.2.1, the optimal gain values achieved by the deterministic stabilization methods corresponds to a non-Lipschitz point, sensitive to small perturbation of the parameter m_p . On the other hand, the spectral abscissa functions with optimal controller obtained by the novel probabilistic approach show smoother behaviors.

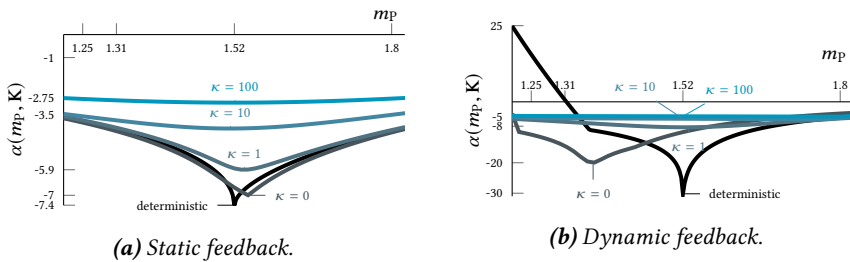


Figure 3.7 Spectral abscissa functions of system (3.19), (3.23), and (3.23) with primary mass $m_p \in [1.216, 1.824]$ for different optimal controllers K , see Table 3.7.

A comparison in the time domain of the primary mass position for the dynamic controllers is illustrated in Figure 3.8.⁹ The undesired oscillations affect the primary structure as the input f_e is exciting the system from $t = 0$ s with amplitude 3 N. The absorber A, with its feedback (3.20)-(3.22), is attached to the primary structure at time $t = 1$ s while the feedback control (3.23)-(3.24) is applied during the whole simulation. Figure 3.8 illustrates that when the absorber is attached, the oscillations affecting

⁹ The dynamics for the system with static controllers are given in [26, Figure 6], together with the time domain simulation of the system with dynamic controller obtained by the novel probabilistic approach with $\kappa = 100$, which is similar to Figure 3.8d.

the primary mass are suppressed entirely, and the primary mass remains stable at the desired position. At time $t = 2.5$ s, the reference position of the primary mass is changed to 10 mm, in formula:

$$z_{\text{ref}}(t) = \begin{cases} 0 \text{ mm}, & t \in [0, 2.5] \text{ s}, \\ 10 \text{ mm}, & t \in [2.5, 4] \text{ s}. \end{cases} \quad (3.25)$$

The system response is shown in Figure 3.8. We observe performance degradation with dynamic controllers in the deterministic case and for low values of κ . In particular, the system with the deterministic dynamic controller is not stable for $m_p < 1.52(1 - 13.65\%) \approx 1.31$ kg, see Figure 3.8a, while the dynamic controllers obtained by the novel approach ensure that the system is stable for $m_p \in [1.52(1 - 20\%), 1.52(1 + 20\%)]$ kg. However, in this latter case, the dynamics vary depending on the parameter κ : for $\kappa = 0$, and $\kappa = 1$ we observe performance degradation and the primary structure for $m_p \approx 1.52(1 - 20\%)$ kg oscillates a lot after the reference position is changed, while for $\kappa = 10$ the dynamics are almost insensitive to primary mass variations, and presents null overshoot.

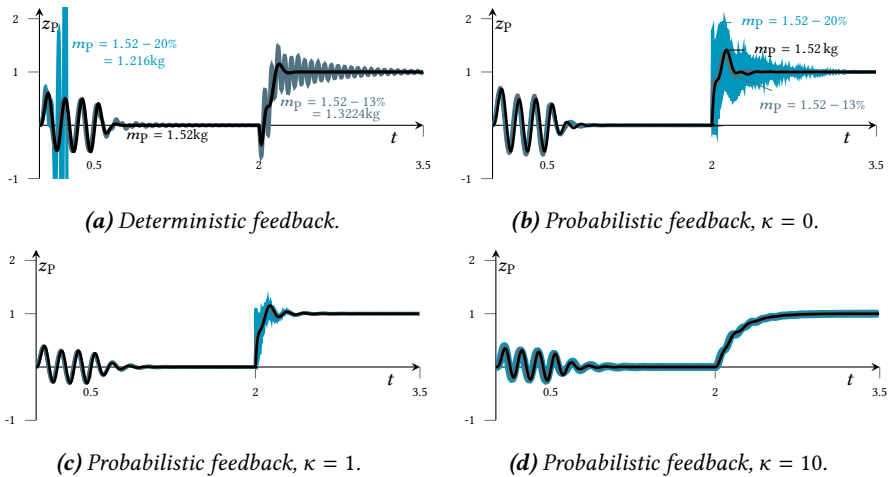


Figure 3.8 Dynamics comparison of the primary structure position for system (3.19), (3.23) and (3.23) with different nominal values of the primary mass m_p . The dynamic controller $r_c = 1$ are designed by deterministic stability optimization, section 1.1.4, and probabilistic stabilization method, Algorithm 3.1. In Figure 3.8a, the dynamic for $m_p = 1.52(1 - 20\%)$ kg is not shown for every $t \in [0, 3.5]$ s, since it is unstable and blows up.

SUMMARY. The novel probabilistic stabilization method, improving the stability properties of uncertain linear interconnected time-delay systems, presents several advantages. A wide class of interconnected systems can be modeled by the delay differential algebraic equation formulation. The uncertainties, described by random variables with given probability function, can affect all the parameters, including the delays. The solutions are more robust and reliable for applications compared to the deterministic design. Different dynamics of stable and robust systems can be achieved by varying the variance penalty in the objective function.

Extended research results of chapter 3 are presented in section 5.1.2.

STABILITY & STABILIZATION FOR PERIODIC DELAY SYSTEMS

This chapter presents novel numerical methods for the stability assessment and the stabilization of linear periodic time-delay systems, where the delays and period are assumed to be commensurable. Under this assumption, the Floquet multipliers are characterized not only as the elements of the monodromy operator spectrum but also as eigenvalues of a characteristic matrix, whose evaluation involves the solution of an initial value problem. This dual interpretation is exploited to compute dominant Floquet multipliers and their associated right eigenvectors, combining a global approximation with local corrections. The left eigenvector is characterized as the right eigenvector of a “transposed” characteristic matrix, or equivalently as the right eigenfunction of the monodromy operator associated with a dual periodic time-delay system. The characteristic matrix also provides an expression for the derivatives of Floquet multipliers, which is applied for the stabilization of the system. Several examples illustrate the efficiency and accuracy of the novel methodologies.

Recall the linear time-periodic time-delay system (1.1),

$$\dot{x}(t) = \sum_{j=0}^h A_j(t)x(t - \tau_j), \quad (4.1)$$

with $h \in \mathbb{N}$, state variable $x(t) \in \mathbb{R}^r$, and the matrix-valued functions $A_j : \mathbb{R} \rightarrow \mathbb{R}^{r \times r}$, $t \mapsto A_j(t)$ are continuous and T -periodic, for $j = 0, \dots, h$. The period is positive, $T > 0$, and the delays are sorted in increasing order, $0 \leq \tau_1 < \tau_2 < \dots < \tau_h$.

We focus on linear periodic time-delay systems (4.1) where the time-delays and period are commensurate. More precisely, we consider the following assumption.

Assumption 4.1. There exist a positive real number $\Delta > 0$, natural numbers N and n_j , for $j = 1, \dots, h$ such that the period and delays satisfy

$$T = N\Delta, \quad \tau_j = n_j\Delta, \quad j = 1, \dots, h. \quad (4.2)$$

Under Assumption 4.1, the Floquet multipliers satisfy not only the infinite-dimensional linear eigenvalue problem (1.3), defined by the monodromy operator, but also a finite-dimensional nonlinear eigenvalue problem. This dual interpretation permits

to develop spectrum-based stability assessment and stabilization for the periodic time-delay system (4.1), analogously to the methods for autonomous time-delay systems, presented in sections 1.1.3-1.1.4, relying on the dual interpretation stated in Theorem 1.3. The novelty of these spectrum-based stability assessment and stabilization methods compared to the state-of-the-art are presented in section 1.2.3.

The chapter is structured as follows. In section 4.1, the spectral properties of system (4.1) are addressed, focusing on the characterization of Floquet multipliers in terms of a nonlinear eigenvalue problem. In section 4.2 algorithms for computing Floquet multipliers are presented. Characterizations of left eigenvectors are presented in section 4.3. Section 4.4 is devoted to the sensitivity analysis of the Floquet multipliers, with application to the design of stabilizing controllers. Section 4.5 illustrates the efficiency of the novel approach using numerical experiments. Additional remarks, beyond the stability assessment and stabilization of periodic time-delay systems (4.1), are presented in section 4.6.

4.1 SPECTRAL PROPERTIES

As mentioned in section 1.1.1, and more precisely in Proposition 1.1, the stability properties of a periodic time-delay system can be inferred from the Floquet multipliers, the non-zero eigenvalues of the monodromy operator. A graphical interpretation of the monodromy operator action and its associated infinite-dimensional linear eigenvalue problem is given in Figure 4.1.

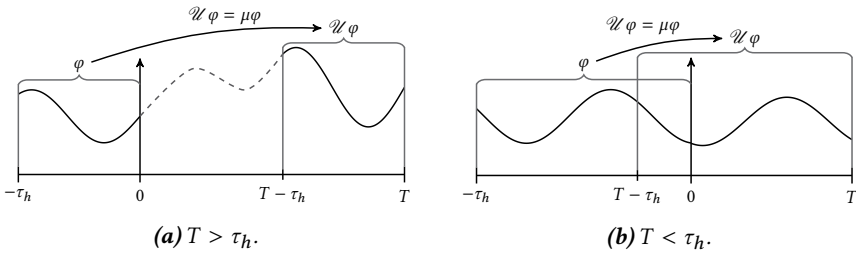


Figure 4.1 The monodromy operator \mathcal{U} translates the continuous function $\varphi : [-\tau_h, 0] \rightarrow \mathbb{C}^r$ along the corresponding solution over a time-interval of length T . In both cases, the depicted initial function φ corresponds to an eigenfunction of the monodromy operator.

We show that the Floquet multipliers can not only be obtained by solving the infinite-dimensional linear eigenvalue problem (1.3), but also from the solutions of a finite-dimensional nonlinear eigenvalue problem. This dual interpretation plays a major role in the subsequent developments of the stability assessment and stability optimization methods. We start with a technical lemma.

LEMMA 4.1 *Number $\mu \in \mathbb{C} \setminus \{0\}$ is a Floquet multiplier of the periodic system (4.1) with period $T = N\Delta$ if and only if there exists a continuous \mathbb{C}^{Nr} -valued function, $\mathbf{q}(s)$ with $\mathbf{q}(0) \neq 0$, which satisfies the boundary value problem*

$$\begin{cases} \dot{\mathbf{q}}(s) = A(s, \mu)\mathbf{q}(s), & s \in [0, 1], \\ \mathbf{q}(1) = B(\mu)\mathbf{q}(0), \end{cases} \quad (4.3)$$

where

$$B(\mu) = \begin{pmatrix} 0 & I_{N-1} \\ \mu & 0 \end{pmatrix} \otimes I_r.$$

The differential equation (4.3) is described by

$$\dot{q}_n(s) = \Delta \sum_{j=0}^h A_j((s+n-1)\Delta) \mu^{a_{n-n_j}} q_{b_{n-n_j}}(s), \quad n = 1, \dots, N, \quad (4.4)$$

with

$$a_k = \left\lfloor \frac{k-1}{N} \right\rfloor, \quad b_k = (k-1) \bmod N + 1,$$

such that $\mathbf{q}(s) = (q_1^T(s) \cdots q_N^T(s))^T$.

Before the detailed proof, we sketch the main idea behind Lemma 4.1, considering the simplest case $h = N = n_1 = \Delta = 1$. The solution $x(t; 0, \varphi)$, emanating at $t = 0$ from an eigenfunction φ corresponding to Floquet multiplier μ , satisfies for $t \in [0, 1]$

$$\begin{aligned} \dot{x}(t; 0, \varphi) &= A_0(t)x(t; 0, \varphi) + A_1\varphi(t) \\ &= A_0(t)x(t; 0, \varphi) + A_1 \frac{x(t; 0, \varphi)}{\mu}, \end{aligned}$$

as well as $x(1; 0, \varphi) = \mu x(0; 0, \varphi)$. Setting $\mathbf{q}(t) = x(t; 0, \varphi)$, we get a boundary value problem of the form (4.3). A graphical illustration of the generalization is given in Figure 4.2. The variable s in (4.3) is a local coordinate inside each interval of length Δ .

Proof. Let (μ, φ) be an eigenpair of \mathcal{U} . Recall the initial value problem (1.2) for system (4.1)

$$\begin{cases} \dot{x}(t) = \sum_{j=0}^h A_j(t)x(t - \tau_j), & t \in [t_0, \infty), \\ x(t) = \varphi(t - t_0), & t \in [t_0 - \tau_h, t_0], \end{cases}$$

and consider its solution in the interval $[-\tau_h, T]$, initialized with φ at $t_0 = 0$, i.e. $x(t; 0, \varphi)$ for $t \in [-\tau_h, T]$. By assumption, we have $x(T + \theta; 0, \varphi) = \mu\varphi(\theta)$ for every $\theta \in [-\tau_h, 0]$. We divide the interval $[-\tau_h, T]$ into Δ -length subintervals and define

$$q_n(s) = x((s+n-1)\Delta; 0, \varphi), \quad s \in [0, 1],$$

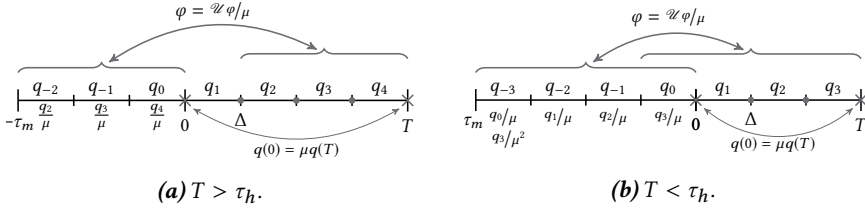


Figure 4.2 Exemplification of Lemma 4.1 proof for two examples. Function φ represents an eigenfunction of the monodromy operator. Functions q_1, \dots, q_N in (4.4) can be interpreted as describing segments of the emanating solution.

for $n = -n_h, \dots, N$. We define $\mathbf{q}(s) = (q_1^T(s) \cdots q_N^T(s))^T$. Since the solution is initialized on an eigenfunction, i.e. $\varphi = \frac{1}{\mu} x_T(\cdot; 0, \varphi)$, functions $\{q_n(s)\}_{n=-n_h+1}^0$ are related to $\{q_n(s)\}_{n=1}^N$ via

$$q_n(s) = \frac{1}{\mu} q_{N+n}(s) = \mu^{\lfloor \frac{n-1}{N} \rfloor} q_{(n-1) \bmod_{N+1}}(s), \quad n = -n_h + 1, \dots, 0. \quad (4.5)$$

Furthermore, for every $n = 1, \dots, N$, we have

$$q_n(s - \tau_j) = x((s + n - n_j - 1)\Delta; 0, \varphi) = q_{n-n_j}(s) = \mu^{a_{n-n_j}} q_{b_{n-n_j}}(s).$$

These properties are illustrated in Figure 4.2.

From the chain rule, it follows that for $n = 1, \dots, N$ and $s \in [0, 1]$

$$\begin{aligned} \dot{q}_n(s) &= \Delta \dot{x}((s + n - 1)\Delta; 0, \varphi) \\ &= \Delta \sum_{j=0}^h A_j((s + n - 1)\Delta) x((s + n - n_j - 1)\Delta; 0, \varphi) \\ &= \Delta \sum_{j=0}^h A_j((s + n - 1)\Delta) q_{n-n_j}(s) \\ &= \Delta \sum_{j=0}^h A_j((s + n - 1)\Delta) \mu^{a_{n-n_j}} q_{b_{n-n_j}}(s), \end{aligned}$$

hence, differential equation in (4.3) is satisfied. The boundary condition is also satisfied, following from the continuity of the solution and the property $x(0; 0, \varphi) = \frac{1}{\mu} x(T; 0, \varphi)$.

Finally, we prove by contradiction that $\mathbf{q}(0) \neq 0$. If $\mathbf{q}(0) = 0$, then the solution of the differential equation in (4.3) would be $\mathbf{q} \equiv 0$, which implies that $x(t; 0, \varphi) \equiv 0$ by the monodromy operator action (4.5). However, this is in contradiction with the property that an eigenfunction is not identically zero.

Let $\mathbf{q}(s)$ be a continuous \mathbb{C}^{Nr} -valued function, satisfying the differential equation (4.3). We construct function $x(t)$, $t \in [-\tau_h, T]$ from \mathbf{q} in the following way,

$$\begin{cases} x(t) = \mu^{an} q_{b_n} \left(\frac{t}{\Delta} - (n-1) \right), & t \in ((n-1)\Delta, n\Delta], \quad n = -n_h + 1, \dots, N, \\ x(-\tau_h) = \mu^{a-n_h+1} q_{b_{-n_h+1}}(0) \end{cases}$$

and show that it corresponds to a solution initialized at an eigenfunction of \mathcal{U} . The construction of x implies

$$x(t) = q_n \left(\frac{t}{\Delta} - (n-1) \right), \quad t \in ((n-1)\Delta, n\Delta], \quad n = 1, \dots, N \quad (4.6)$$

and, for any $j \in \{1, \dots, h\}$,

$$x(t - \tau_j) = \mu^{a-n_j} q_{b_{n-n_j}} \left(\frac{t}{\Delta} - (n-1) \right), \quad t \in ((n-1)\Delta, n\Delta], \quad n = -n_h + 1 + n_j, \dots, N.$$

Following from the construction of x and condition $\mathbf{q}(1) = B(\mu)\mathbf{q}(0)$, we have that x is continuous on $[-\tau_h, T]$ and

$$x(t) = \frac{1}{\mu} x(t + T), \quad t \in [-\tau_h, 0].$$

It remains to show that x is a solution of (4.1). In the time-interval $[(n-1)\Delta, n\Delta]$, for any $n = 1, \dots, N$, we obtain from (4.6) that

$$\begin{aligned} \dot{x}(t) &= \frac{1}{\Delta} \dot{q}_n \left(\frac{t}{\Delta} - (n-1) \right) = \sum_{j=0}^h A_j(t) \mu^{a-n_j} q_{b_{n-n_j}} \left(\frac{t}{\Delta} - (n-1) \right) \\ &= \sum_{j=0}^h A_j(t) x(t - \tau_j), \end{aligned}$$

which completes the proof. \square

Denoting $\mathbf{v} = \mathbf{q}(0)$, conditions (4.3) can be rewritten in the form

$$\mathcal{N}(\mu)\mathbf{v} = 0. \quad (4.7)$$

Here, the function $\mathcal{N} : \mathbb{C} \rightarrow \mathbb{C}^{Nr \times Nr}$ is analytic in $\mathbb{C} \setminus \{0\}$, and for a given value of μ and \mathbf{v} the matrix-vector product $\mathcal{N}(\mu)\mathbf{v}$ is determined as follows,

$$\mathcal{N}(\mu)\mathbf{v} = \mathbf{q}(1) - B(\mu)\mathbf{v}, \quad (4.8)$$

where \mathbf{q} is the solution of initial value problem

$$\begin{cases} \dot{\mathbf{q}}(s) = A(s, \mu)\mathbf{q}(s), & s \in [0, 1], \\ \mathbf{q}(0) = \mathbf{v}. \end{cases} \quad (4.9)$$

Equation (4.7) can be interpreted as a nonlinear eigenvalue problem. The relation with the eigenvalue problem for the monodromy operator is clarified in the following theorem, which generalizes [80, Theorem 2.1] to non-scalar systems with multiple delays.

THEOREM 4.2 *Let $\hat{\mu} \in \mathbb{C} \setminus \{0\}$. If the pair $(\hat{\mu}, \hat{\phi})$ is a solution of the infinite-dimensional linear eigenvalue problem*

$$\mathcal{U}\varphi = \mu\varphi, \quad \mu \in \mathbb{C} \setminus \{0\}, \quad \varphi \in X \setminus \{0\}, \quad (4.10)$$

then $(\hat{\mu}, \hat{\mathbf{v}})$ is a solution of the finite-dimensional nonlinear eigenvalue problem

$$\mathcal{N}(\mu)\mathbf{v} = 0, \quad \mu \in \mathbb{C} \setminus \{0\}, \quad \mathbf{v} \in \mathbb{C}^{Nr} \setminus \{0\}, \quad (4.11)$$

where $\hat{\mathbf{v}} = (v_1^T \cdots v_N^T)^T$ is determined by

$$v_n = x((n-1)\Delta; 0, \hat{\phi}), \quad n = 1, \dots, N.$$

Conversely, if the pair $(\hat{\mu}, \hat{\mathbf{v}})$ is a solution of (4.11), then $(\hat{\mu}, \hat{\phi})$ is a solution of (4.10), where for every $n = -n_h + 1, \dots, 0$,

$$\hat{\phi}(t) = \hat{\mu}^{\lfloor \frac{n-1}{N} \rfloor} q_{(n-1) \bmod N+1} \left(\frac{t}{\Delta} - (n-1) \right), \quad t \in ((n-1)\Delta, n\Delta],$$

with $q(s) = (q_1^T(s) \cdots q_N^T(s))^T$ the solution of initial value problem (4.9) for $\mathbf{v} = \hat{\mathbf{v}}$ and $\mu = \hat{\mu}$.

Proof. The assertions follow from the constructions in the proof of Lemma 4.1. \square

The dimension of nonlinear eigenvalue problem (4.11) does not only depend on the system dimension r but also on the number N of Δ -subintervals of $[0, T]$ (see Assumption 4.1). The latter is minimized if Δ , in (4.2), is chosen as the greatest common divisor of τ_1, \dots, τ_h , and T . We now present an example where $N = 1$.

Example 4.1. We consider system

$$\dot{x}(t) = \sum_{j=0}^h A_j(t)x(t-j\tau) \quad (4.12)$$

with $T = \tau$. When taking $\Delta = \tau$ we can express $\mathcal{N}(\mu)v = q(1) - \mu v$, where q satisfies

$$\begin{cases} \dot{q}(s) = \tau \sum_{j=0}^h A_j(s\tau) \frac{q(s)}{\mu^j}, & s \in [0, 1], \\ q(0) = v. \end{cases} \quad (4.13)$$

Moreover, if system (4.12) is scalar, *i.e.* $r = 1$, $\mathcal{N}(\mu)$ can be explicitly expressed in terms of the coefficients $A_j(t)$ and we can derive a nonlinear equation for the Floquet multipliers. Indeed, if we let

$$\alpha_j = \int_0^1 \tau A_j(s\tau) ds = \int_0^\tau A_j(t) dt,$$

then the solution of the differential equations in (4.13) is

$$q(1) = e^{\sum_{j=0}^h \mu^{-j} \alpha_j} \mathcal{V}.$$

Hence, the Floquet multipliers correspond to the solutions of equation

$$e^{\sum_{j=0}^h \mu^{-j} \alpha_j} - \mu = 0, \quad (4.14)$$

which is in accordance to the characteristic equation for the Floquet exponents as defined in [33, Section 8.1].

4.2 STABILITY ASSESSMENT

This section describes two techniques for computing dominant Floquet multipliers, which are combined in order to accurately infer the stability properties of system (4.1). These two techniques are outlined in Figure 4.3. The first technique, discussed in section 4.2.1, approximates the Floquet multipliers by a spline collocation method, furnishing a global view of the monodromy operator spectrum, and, hence, detecting a guess of the largest Floquet multiplier in modulus. The second technique, analyzed in section 4.2.2, computes the Floquet multiplier in a neighborhood of an initial guess by Broyden's method, a local root-finding method, where the accuracy of the computation depends on evaluating the matrix-vector product $\mathcal{N}(\mu)\mathcal{V}$. Finally, section 4.2.3 discusses an algorithm for the computation of Floquet multipliers based on a combination of these techniques.

4.2.1 Discretization of the infinite-dimensional linear eigenvalue problem

We derive a finite-dimensional linear eigenvalue problem, whose eigenvalues approximate Floquet multipliers. First, we outline how a collocation approach can approximate solutions of (4.1) in the form of a spline. Second, we illustrate how these approximations induce a matrix approximation of the monodromy operator. The derivation is different from [8, Chapter 6], and from [10] for the one-delay case, but the underlying ideas are the same. Third, in the spirit of Theorem 4.2, we show that the corresponding linear eigenvalue problem can also be obtained from a particular approximation of the nonlinear eigenvalue problem (4.11). The latter explains a particular choice of spline, in accordance with the subdivision of the interval $[-\tau_h, T]$ in intervals of length Δ . We conclude with some implementation aspects.

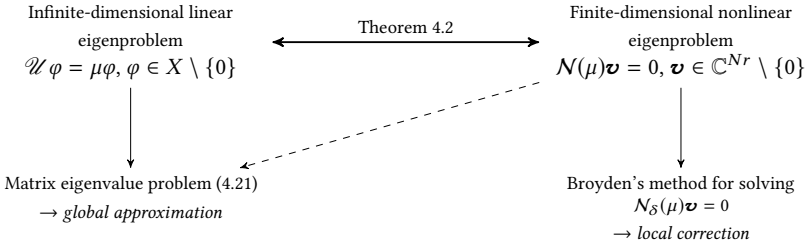


Figure 4.3 Approach for computing dominant Floquet multipliers and stability assessment of (4.1). The upper part illustrates the theoretical results of section 4.1 concerning the dual interpretation of Floquet multipliers in terms of eigenvalue problems. The lower part outlines the Floquet multipliers computation of section 4.2.

Discretization of the initial value problem

We approximate a solution of (4.1) by a spline, which is piecewise defined on Δ -subintervals by M -degree polynomials $\{q_n^M\}_{n=-n_h+1}^N$, where polynomial q_n^M represents the approximation on the interval $[(n-1)\Delta, n\Delta)$. Without loss of generality, we assume that this Δ -interval is scaled and shifted to the interval $[0, 1)$. Given a polynomial basis $\{p_i\}_{i \in \mathbb{N}}$ in the interval $[0, 1]$, this spline approximation is uniquely determined by the coefficients c of the polynomials $\{q_n^M\}_{n=-n_h+1}^N$,

$$c = \begin{pmatrix} c_{-n_h+1} \\ \vdots \\ c_N \end{pmatrix}, \quad c_n = \begin{pmatrix} c_{0,n} \\ \vdots \\ c_{M,n} \end{pmatrix}, \quad n = -n_h + 1, \dots, N,$$

such that

$$q_n^M(s) = \sum_{i=0}^M c_{i,n} p_i(s), \quad s \in [0, 1]. \quad (4.15)$$

We note that the coefficient vector $(c_{-n_h+1}^T \cdots c_0^T)^T$ can be interpreted as a parametrization of the initial condition. Specifying this vector to the value $c_\varphi \in \mathbb{R}^{n_h r(M+1)}$ leads us to the condition

$$Bc = c_\varphi, \quad (4.16)$$

where

$$B = (I_{n_h} \quad 0_{n_h \times N}) \otimes I_{r(M+1)}.$$

We now determine conditions expressing that the vector $(c_1^T \cdots c_N^T)^T$ corresponds to the emanating solution. We first require continuity on $[0, T]$, which can be expressed as

$$q_n^M(0) = q_{n-1}^M(1), \quad n = 1, \dots, N. \quad (4.17)$$

Second, we impose collocation requirements for the time-delay system (4.1) on a mesh $\{\xi_m\}_{m=1}^M$ over the interval $[0, 1]$, which lead to

$$\dot{q}_n^M(\xi_m) = \Delta \sum_{j=0}^h A_j ((\xi_m + n - 1)\Delta) q_{n-n_j}^M(\xi_m), \quad m = 1, \dots, M, \quad n = 1, \dots, N. \quad (4.18)$$

Conditions (4.17) and (4.18) can be stated in matrix form as

$$S c = 0, \quad (4.19)$$

with $S \in \mathbb{C}^{(N \times (n_h + N))r(M+1)}$. Finally, the approximate solution with initial condition parametrized by c_φ can be computed from (4.19) and (4.16), leading to

$$c = \begin{pmatrix} S \\ B \end{pmatrix}^{-1} E^T c_\varphi, \quad (4.20)$$

with

$$E = (0_{n_h \times N} \quad I_{n_h}) \otimes I_{r(M+1)}.$$

Discretization of the monodromy operator

The monodromy operator describes the translation along a solution from the interval $[-\tau_h, 0]$ to the interval $[T - \tau_h, T]$. Considering the previously defined spline approximation of a solution, the monodromy operator action can be approximated by the mapping from vector c_φ , which gives rise to the discretized solution (4.20), into vector $c_T = (c_{N-n_h+1}^T \cdots c_N^T)^T$.

We can express $c_T = E c$, leading to

$$c_T = E \begin{pmatrix} S \\ B \end{pmatrix}^{-1} E^T c_\varphi.$$

Hence, the infinite-dimensional linear eigenvalue problem (4.10) is discretized by

$$\mathcal{U}_M c_\varphi = \mu c_\varphi, \quad (4.21)$$

where \mathcal{U}_M is a matrix approximation of the monodromy operator,

$$\mathcal{U}_M = E \begin{pmatrix} S \\ B \end{pmatrix}^{-1} E^T = (0 \quad I_{n_h r(M+1)}) \begin{pmatrix} S & \\ I_{n_h r(M+1)} & 0 \end{pmatrix}^{-1} \begin{pmatrix} 0 \\ I_{n_h r(M+1)} \end{pmatrix}.$$

Interpretation in terms of the finite-dimensional nonlinear eigenvalue problem

We can alternatively obtain (4.21) from the nonlinear eigenvalue problem (4.11) by a spectral discretization of boundary value problem (4.3). More precisely, approximating q by a M -degree polynomial,

$$q^M(s) = \begin{pmatrix} q_1^M(s) \\ \vdots \\ q_N^M(s) \end{pmatrix}, \quad s \in [0, 1],$$

imposing collocation requirements for the differential equation on the mesh $\{\xi_m\}_{m=1}^M$ and imposing the condition $q^M(1) = B(\mu)q^M(0)$ lead us to (4.19) supplemented with

$$c_\varphi = \mathcal{R}(\mu)c_q, \quad (4.22)$$

where

$$c_\varphi = \begin{pmatrix} c_{-n_h+1} \\ \vdots \\ c_0 \end{pmatrix}, \quad c_q = \begin{pmatrix} c_1 \\ \vdots \\ c_N \end{pmatrix},$$

and

$$\mathcal{R}(\mu) = \begin{cases} \begin{pmatrix} 0_{N-n_h \times n_h} & I_{n_h} \end{pmatrix} \otimes I_{r(M+1)}, & n_h \leq N, \\ \begin{pmatrix} 0 & \frac{I_{n_h \bmod N}}{\mu^{\lceil n_h/N \rceil}} \\ \frac{I_N}{\mu^{\lceil n_h/N \rceil - 1}} \\ \vdots \\ I_N/\mu \end{pmatrix} \otimes I_{r(M+1)}, & n_h > N. \end{cases}$$

As spelled out in the proof of Lemma 4.1, the differential equation (4.3) is derived from equation (4.5) by expressing $x(t; 0, \varphi)$ in the time-interval $[-\tau_h, 0]$ in terms of μ, μ^2, \dots -fractions of $x(t; 0, \varphi)$ at positive time-instants $t \in [0, T]$, where φ is an eigenfunction of \mathcal{U} . The two cases in the expression for $\mathcal{R}(\mu)$ correspond to the situation depicted in Figure 4.2a and Figure 4.2b, respectively.

Partitioning $S = (S_\varphi \ S_q)$, according to the subdivision of c into c_φ and c_q , allows to rewrite (4.19)–(4.22) as

$$\begin{cases} S_\varphi c_\varphi + S_q c_q = 0, \\ c_\varphi = \mathcal{R}(\mu)c_q, \end{cases}$$

which brings us to the polynomial eigenvalue problem

$$\mu^{\lceil n_h/N \rceil} (S_\varphi \mathcal{R}(\mu) + S_q) c_q = 0. \quad (4.23)$$

To establish a connection between this eigenvalue problem and (4.21), we note that (4.22) is equivalent to

$$Bc = \frac{1}{\mu} Ec.$$

Conditions (4.19)-(4.22) can then be rewritten as $\mu S c = 0$ and $\mu B c = E c$, which brings us to the generalized eigenvalue problem

$$\left(\mu \begin{pmatrix} S & \\ I_{n_h r(M+1)} & 0 \end{pmatrix} - \begin{pmatrix} 0_{Nr(M+1)} & 0 \\ 0 & I_{n_h r(M+1)} \end{pmatrix} \right) c = 0. \quad (4.24)$$

From Sylvester's determinant theorem [35, Theorem 1.3.22], the sets of non-zero eigenvalues of (4.24) and of monodromy matrix approximation \mathcal{U}_M are the same.

In conclusion, the non-zero eigenvalues of matrix \mathcal{U}_M , generalized eigenvalue problem (4.24), and polynomial eigenvalue problem (4.23) coincide. The dimensions are $n_h r(M+1)$, $(n_h + N)r(M+1)$, and $Nr(M+1)$ (but the order of the polynomial eigenvalue problem is $\lceil n_h/N \rceil$) while the corresponding eigenvectors, c_φ , c , c_q parametrize segments of the approximate solution emerging from the eigenfunction.

Choice of polynomial basis and collocation points

Generalized eigenvalue problem (4.24) and polynomial eigenvalue problem (4.23) lie at the basis of our algorithm for approximating Floquet multipliers. In our implementation, we express polynomials $\{q_n^M\}_{n=-n_h+1}^N$ in a Chebyshev basis,

$$q_n^M(t) = \sum_{i=0}^M c_{i,n} T_i(2t-1), \quad t \in [0, 1],$$

where T_i is the i -degree Chebyshev polynomial of the first kind, and we take as collocation points $\{\xi_m\}_{m=1}^M$ the Chebyshev nodes shifted and scaled in $[0, 1]$,

$$\xi_m = \frac{1}{2}(\zeta_m + 1), \quad \zeta_m = -\cos \frac{(m-1)\pi}{M}, \quad m = 1, \dots, M. \quad (4.25)$$

As we shall document in section 4.5.1, spectral accuracy (convergence rate faster than $O(M^{-k})$ for any $k \in \mathbb{N}$) is observed for the approximation of a simple Floquet multiplier. This is expected, as the method can be interpreted in terms of a spectral discretization [89] of boundary value problem (4.3), with (4.25) as collocation points.

To conclude the section, we specify matrix S in (4.24) for a particular case.

Example 4.2. We reconsider system (4.12) with $T = \tau$, leading to $\Delta = 1$. We can express

$$S = \begin{pmatrix} 0 & \cdots & 0 & -(1 \ 1 \ \dots \ 1) \otimes I_r & (1 \ (-1) \ \dots \ (-1)^M) \otimes I_r \\ -A_h & \cdots & -A_2 & -A_1 & U \otimes I_r - A_0 \end{pmatrix},$$

where the first r rows are determined by the continuity conditions (4.17), while the other Mr rows are obtained by the collocation conditions (4.18). The block matrices,

determining S , are given by

$$A_j = \Delta \begin{pmatrix} A_j(\xi_1 \Delta) T_0(\zeta_1) & \dots & A_j(\xi_1 \Delta) T_M(\zeta_M) \\ \vdots & & \vdots \\ A_j(\xi_M \Delta) T_0(\zeta_M) & \dots & A_j(\xi_M \Delta) T_M(\zeta_M) \end{pmatrix},$$

for $j = 0, \dots, h$, and

$$U = 2 \begin{pmatrix} 0 & 1U_0(\zeta_1) & \dots & MU_{M-1}(\zeta_1) \\ \vdots & \vdots & & \vdots \\ 0 & 1U_0(\zeta_M) & \dots & MU_{M-1}(\zeta_M) \end{pmatrix},$$

with U_i the i -degree Chebyshev polynomial of the second kind.

4.2.2 Newton's type algorithms for the nonlinear eigenvalue problem

The alternative formulation (4.11) of the eigenvalue problem allows us to compute eigenpairs by applying an iterative solver for nonlinear equations to the system

$$\begin{cases} \mathcal{N}(\mu)\mathbf{v} = 0, \\ \mathbf{w}^* \mathbf{v} = 1, \end{cases}$$

where the second equation, with $\mathbf{w} \in \mathbb{C}^{Nr}$, is a normalization constraint. Letting $y = (\mathbf{v}^\top \mu)^\top$ we can compactly write the system in the form $F(y) = 0$. The application of a damped Newton's method leads us to the basic iteration

$$y_{i+1} = y_i - \gamma_i H_i F(y_i), \quad i \in \mathbb{N},$$

where $\gamma_i \in (0, 1]$ is the damping factor and H_i represents the employed inverse Jacobian approximation.

In the exact Newton's method, the true Jacobian is used, which implies

$$H_i := J(y_i)^{-1} = \begin{pmatrix} \mathcal{N}(\mu_i) & \frac{d\mathcal{N}(\mu_i)}{d\mu} \mathbf{v}_i \\ \mathbf{w}^* & 0 \end{pmatrix}^{-1},$$

and a system of equations needs to be solved to obtain the search direction $H_i F(y_i)$. To compute $\mathcal{N}(\mu_i)$, we have to solve initial value problem (4.9) for Nr independent initial conditions. To compute matrix-vector product $\frac{d\mathcal{N}(\mu_i)}{d\mu} \mathbf{v}_i$ we can use the following proposition.¹⁰

¹⁰ The proposition here presented generalizes the result of [71, Section 3.1], stated in terms of Floquet exponents for a periodic system with a single delay term and this delay equal to the periodicity of the system matrices.

PROPOSITION 4.3 Let (μ, \mathbf{v}) , with $\mu \neq 0$, be an eigenpair of (4.11). Let \mathbf{q} be such that (4.9) is satisfied. Then we can express

$$\frac{d\mathcal{N}(\mu)}{d\mu}\mathbf{v} = \mathbf{q}_\mu(1) - \mathbf{v}_N,$$

where \mathbf{q}_μ is the solution of initial value problem

$$\begin{cases} \dot{\mathbf{q}}_\mu(s) = \frac{\partial A(s, \mu)}{\partial \mu} \mathbf{q}(s) + A(s, \mu) \mathbf{q}_\mu(s), & s \in [0, 1], \\ \mathbf{q}_\mu(0) = 0, \end{cases} \quad (4.26)$$

and $\mathbf{v}_N = (0 \cdots 0 v_1^T)^T$, with $\mathbf{v} = (v_1^T \cdots v_N^T)^T$.

Proof. The solution of (4.9), evaluated at any $s \in [0, 1]$, is a smooth function of μ on $\mathbb{C} \setminus \{0\}$. The assertion follows from differentiating (4.8) and (4.9) with respect to μ , the latter giving rise to equation (4.26). \square

In the Broyden's quasi-Newton's method [2, 39] (for simplicity, we consider only the so-called *good Broyden's method*) an approximation of the Jacobian inverse is updated in every iteration by a rank-one matrix, using the formula

$$H_{i+1} = H_i - \frac{(H_i F(y_{i+1}) - (1 - \gamma_i) H_i F(y_i)) (F(y_i)^* H_i^* H_i)}{F(y_i)^* H_i^* (H_i F(y_{i+1}) - H_i F(y_i))},$$

where in our implementation we use as initialization $H_0 = I$ or

$$H_0 = J(y_0)^{-1}. \quad (4.27)$$

Since characteristic matrix $\mathcal{N}(\mu)$ is not in explicit form, we need to numerically solve the initial value problems (4.9) and (4.26) for evaluating matrix-vector products $\mathcal{N}(\mu)\mathbf{v}$ and $\frac{d\mathcal{N}(\mu)}{d\mu}\mathbf{v}$. The implementation approximates these initial value problems with fixed step-size δ , considering the mixed explicit-implicit trapezoidal rule if the differential equation is stiff, and a Runge-Kutta method of order 4 for non-stiff problems. In this way, the resulting iterative scheme can also be interpreted as applying a Newton's type method to solve the approximate eigenvalue problem

$$\mathcal{N}_\delta(\mu)\mathbf{v} = 0, \quad (4.28)$$

where \mathcal{N}_δ is obtained from \mathcal{N} by replacing the exact solution of (4.9) and (4.26) by the numerical solution. Compared to standard nonlinear eigenvalue problems in explicit form, as (1.12) for autonomous linear system, there is a significant additional cost in evaluating the characteristic matrix $\mathcal{N}(\mu)$, which is needed in every iteration of Newton's method but avoided in Broyden's method.

4.2.3 Floquet multipliers computation

The results in sections 4.2.1-4.2.2 lead us to the following high-level algorithm for computing (part of) the monodromy operator spectrum, which is conceptually similar to Algorithm 1.1, described in section 1.1.3, for computing characteristic roots of linear time-invariant systems with delays.

Algorithm 4.1. *Two-stage approach for computing Floquet multipliers.*

1. Fix $M \in \mathbb{N}$, and compute eigenvalues and eigenvectors of (4.23).
2. Fix $\delta > 0$, and correct the individual Floquet multiplier approximations, and extracted eigenvector approximations of (4.11), by applying Broyden's method to (4.28).

For problems of moderate dimension Nr , we use a direct method to compute all eigenvalues of (4.23) in the first stage, resulting in approximate eigenpairs (μ, c_q) . Recall from (4.15) and the construction in the previous section that $c_q = (c_1^T \cdots c_N^T)^T$ parametrizes the approximate solution corresponding to an eigenfunction of \mathcal{U} . By Lemma 4.1 this allows us to extract an approximation of the eigenvector \mathbf{v} in (4.11),

$$\mathbf{v} = (v_1^T \cdots v_N^T)^T, \quad v_n = \sum_{i=0}^M p_i(0)c_{i,n}, \quad n = 1, \dots, N,$$

that is used in the initialization of the second stage, along with (4.27) as initialization of the inverse Jacobian approximation.

For problems with high dimension Nr , it is computationally infeasible to use a direct method in the first stage of Algorithm 4.1, and iterative eigensolvers are to be preferred. In section 4.5.3, we employ Arnoldi's method to matrix \mathcal{U}_M in (4.21), where every iteration requires solving a system of equation with matrix S_q since

$$\begin{aligned} \mathcal{U}_M c_\varphi &= \begin{pmatrix} 0 & I_{n_r(M+1)} \end{pmatrix} \begin{pmatrix} S_\varphi & S_q \\ I & 0 \end{pmatrix}^{-1} \begin{pmatrix} 0 \\ I_{n_r(M+1)} \end{pmatrix} c_\varphi \\ &= \begin{pmatrix} 0 & I_{n_r(M+1)} \end{pmatrix} \begin{pmatrix} c_\varphi \\ -S_q^{-1} S_\varphi c_\varphi \end{pmatrix}. \end{aligned} \quad (4.29)$$

In this way, eigenvector approximations are obtained in the form of coefficient vector c_φ . The latter can be turned into an eigenvector approximation of (4.11) by numerically solving the initial value problem (1.2) on the interval $[0, T]$, with φ the M -degree spline defined by the coefficients c_φ . The inverse Jacobian in Broyden's method is initialized with the identity matrix, in this case.

Algorithm 4.1 turns out to be very efficient for computing dominant Floquet multipliers. As the first step serves to scan the complex plane, the requirement on M is

that the obtained approximation of the dominant Floquet multiplier and corresponding eigenvector is in the region of attraction of Broyden's method, but M should not be too large, since the eigenvalue problem (4.23) has dimension $\mathcal{O}(r(M+1) \times r(M+1))$.¹¹ As the second step serves for local improvement (and discarding spurious eigenvalues), parameter δ should be chosen sufficiently small not only to effectively take the role of corrector but to be able to reach the desired final accuracy on the Floquet multipliers (recall that modified problem (4.28) is actually solved in the second stage). The fixed step-size δ can be estimated by trials and errors: comparing the results obtained by an adaptive solver with the solution achieved with fixed step-size δ by the trapezoidal rule or by Runge-Kutta method of order 4.

Remark 4.1. As presented in section 4.2.1, the discretized eigenvalue problem (4.23) can also be derived from (4.11) by approximating the solution of the differential equation in (4.9). This approach is based on solving *boundary value problem* (4.3), parametrized by μ , for which the collocation approach is appropriate. In the context of local corrections, we need to solve *initial value problem* (4.9) for specified values of μ and \mathbf{v} , for which a time-stepping method is preferable.

Remark 4.2. If a factorization of matrix S_q or even storing the matrices of the discretized eigenvalue problem would be infeasible, one may be able to apply Broyden's method based on the nonlinear eigenvalue problem formulation (the second stage). In this case, multiple Floquet multiplier approximations can still be obtained, using the deflation technique as presented in [45, 18, 39].

4.3 CHARACTERIZATION OF THE LEFT EIGENVECTORS

We again consider nonlinear eigenvalue problem (4.11), with \mathcal{N} defined by (4.8)-(4.9). Vector $\mathbf{u} \in \mathbb{C}^{Nr} \setminus \{0\}$ is called a left eigenvector of \mathcal{N} , corresponding to eigenvalue μ if

$$\mathbf{u}^* \mathcal{N}(\mu) = 0,$$

or, equivalently, $\mathcal{N}(\mu)^* \mathbf{u} = 0$. In order to give an expression in terms of a right eigenvector, we first define the "transposed" nonlinear eigenvalue problem

$$\check{\mathcal{N}}(\mu) \mathbf{v} = 0, \tag{4.30}$$

where for given $\mu \in \mathbb{C} \setminus \{0\}$ and $\mathbf{v} \in \mathbb{C}^{Nr} \setminus \{0\}$ the matrix vector product $\check{\mathcal{N}}(\mu) \mathbf{v}$ is determined as

$$\check{\mathcal{N}}(\mu) \mathbf{v} = \mathbf{p}(0) - B(\mu)^T \mathbf{v},$$

where \mathbf{p} is the solution of problem

$$\begin{cases} \dot{\mathbf{p}}(s) = -A(s, \mu)^T \mathbf{p}(s), & s \in [0, 1], \\ \mathbf{p}(1) = \mathbf{v}. \end{cases} \tag{4.31}$$

¹¹ Further research directions might address how to determine the number of collocation points M a priori, as explained with further details in the next chapter 5, section 5.2.3.

This brings us to the following result, which is analogous to Proposition 1.5 for autonomous time-delay system.

THEOREM 4.4 *Let $\mathbf{u} \in \mathbb{C}^{Nr}$ and $\mu \in \mathbb{C} \setminus \{0\}$. Vector \mathbf{u} is a left eigenvector of (4.11) corresponding to eigenvalue μ if and only if it is a right eigenvector of problem (4.30) corresponding to eigenvalue $\bar{\mu}$.*

Proof. It suffices to prove that for any $\mu \in \mathbb{C} \setminus \{0\}$ we have $\check{N}(\mu) = N(\bar{\mu})^*$. To this end, take arbitrary vectors $\mathbf{u} \in \mathbb{C}^{Nr}$ and $\mathbf{v} \in \mathbb{C}^{Nr}$. Let $\langle \cdot, \cdot \rangle$ be the Euclidean inner product in \mathbb{C}^{Nr} and let \mathbf{q} satisfy

$$\begin{cases} \dot{\mathbf{q}}(s) = A(s, \bar{\mu})\mathbf{q}(s), & s \in [0, 1], \\ \mathbf{q}(0) = \mathbf{u}. \end{cases}$$

We can derive

$$\begin{aligned} \langle N(\bar{\mu})\mathbf{u}, \mathbf{v} \rangle - \langle \mathbf{u}, \check{N}(\mu)\mathbf{v} \rangle &= \mathbf{q}(1)^*\mathbf{v} - \mathbf{u}^*B(\bar{\mu})^*\mathbf{v} - \mathbf{u}^*\mathbf{p}(0) + \mathbf{u}^*B(\mu)^T\mathbf{v} \\ &= \mathbf{q}(1)^*\mathbf{v} - \mathbf{u}^*\mathbf{p}(0) = \mathbf{q}(1)^*\mathbf{p}(1) - \mathbf{q}(0)^*\mathbf{p}(0) \\ &= \int_0^1 \frac{d\mathbf{q}(s)^*\mathbf{p}(s)}{ds} ds = \int_0^1 \dot{\mathbf{q}}(s)^*\mathbf{p}(s) + \mathbf{q}(s)^*\dot{\mathbf{p}}(s) ds \\ &= \int_0^1 \mathbf{q}(s)^*A(s, \bar{\mu})^*\mathbf{p}(s) - \mathbf{q}(s)^*A(s, \mu)^T\mathbf{p}(s) ds \\ &= 0, \end{aligned}$$

which concludes the proof. \square

Example 4.3. For time-delay system (4.12) with $\tau = T$, we can set $\Delta = \tau$ and $N = 1$. Analogously to Example 4.1, the matrix vector product $\check{N}(\mu)\mathbf{v}$ for $\mu \in \mathbb{C} \setminus \{0\}$ and $\mathbf{v} \in \mathbb{C}^r \setminus \{0\}$ is determined as $\check{N}(\mu)\mathbf{v} = \mathbf{p}(0) - \mu\mathbf{v}$, where

$$\begin{cases} \dot{\mathbf{p}}(s) = -\tau \sum_{j=0}^h A_j(s\tau)^T \frac{\mathbf{p}(s)}{\mu}, & s \in [0, 1]; \\ \mathbf{p}(1) = \mathbf{v}. \end{cases}$$

In the spirit of Theorem 4.2, we now establish, as the main result of this section, a connection between transposed nonlinear eigenvalue problem (4.30) and the monodromy operator corresponding to the following dual time-delay system:

$$\dot{\mathbf{x}}(t) = \sum_{j=0}^h A_j(-t + \tau_j)^T \mathbf{x}(t - \tau_j), \quad (4.32)$$

where the matrix coefficients are not only transposed but they also present a reverse and shift of the time. The following theorem is stated considering the permutation

matrix $R \in \mathbb{R}^{Nr \times Nr}$ defined as

$$R = \begin{pmatrix} & & I_r \\ & \ddots & \\ I_r & & \end{pmatrix}.$$

THEOREM 4.5 *Let $\check{\mathcal{U}}$ be the monodromy matrix corresponding to system (4.32). Let $\hat{\mu} \in \mathbb{C} \setminus \{0\}$. If the pair $(\hat{\mu}, \hat{\varphi})$ is a solution of*

$$\check{\mathcal{U}} \varphi = \mu \varphi, \quad \mu \in \mathbb{C} \setminus \{0\}, \quad \varphi \in X \setminus \{0\}, \quad (4.33)$$

then $(\hat{\mu}, \hat{\mathbf{v}})$ is a solution of

$$\check{\mathcal{N}}(\mu) \mathbf{v} = 0, \quad \mu \in \mathbb{C} \setminus \{0\}, \quad \mathbf{v} \in \mathbb{C}^{Nr} \setminus \{0\}, \quad (4.34)$$

where $\hat{\mathbf{v}} = (v_1^T \cdots v_N^T)^T$ is determined by

$$v_n = x((N-n)\Delta; 0, \hat{\varphi}), \quad n = 1, \dots, N,$$

and $x(t; t_0, \varphi)$ the solution of (4.32) with initial condition φ at time t_0 .

Conversely, if the pair $(\hat{\mu}, \hat{\mathbf{v}})$ is a solution of (4.34), then $(\hat{\mu}, \hat{\varphi})$ is a solution of (4.33), where for every $n = -n_h + 1, \dots, 0$,

$$\hat{\varphi}(t) = \hat{\mu}^{\lfloor \frac{n-1}{N} \rfloor} \hat{p}_{(n-1) \bmod N+1} \left(\frac{t}{\Delta} - (n-1) \right), \quad t \in ((n-1)\Delta, n\Delta],$$

and $\hat{\mathbf{p}}(s) = (\hat{p}_1^T(s) \cdots \hat{p}_N^T(s))^T$ satisfies

$$\hat{\mathbf{p}}(s) = R \mathbf{p}(1-s), \quad (4.35)$$

with \mathbf{p} solution of initial value problem (4.31) for $\mathbf{v} = R \hat{\mathbf{v}}$ and $\mu = \hat{\mu}$.

Proof. Let $\check{\mathcal{N}}(\mu) = R \check{\mathcal{N}}(\mu) R$ and $\check{\mathbf{v}} = R \mathbf{v}$. In these variables, using substitution (4.35) and taking into account $RR = I_{Nr}$, nonlinear eigenvalue problem (4.30)–(4.31) can be rewritten as

$$\check{\mathcal{N}}(\mu) \check{\mathbf{v}} = 0, \quad (4.36)$$

where

$$\check{\mathcal{N}}(\mu) \check{\mathbf{v}} = \check{\mathbf{p}}(1) - (RB(\mu)^T R) \check{\mathbf{v}},$$

and

$$\begin{cases} \dot{\check{\mathbf{p}}}(s) = (RA(1-s, \mu)^T R) \check{\mathbf{p}}(s), & s \in [0, 1], \\ \check{\mathbf{p}}(0) = \check{\mathbf{v}}. \end{cases}$$

We have

$$RB(\mu)^T R = B(\mu),$$

while the $r \times r$ block of $RA(1-s, \mu)^T R$ at position (rn, rm) for $n, m = 1, \dots, N$ is equal to $r \times r$ block of $A(1-s, \mu)^T$ at position $(r(N-m+1), r(N-n+1))$, whose explicit formulation is given by

$$\Delta \sum_{\substack{j=0, \dots, h \\ b_{N-m+1-n_j} = N-n+1}} A_j((1-s+N-m+1-1)\Delta)^T \mu^{a_{N-m+1-n_j}}. \quad (4.37)$$

To conclude the proof, we have to prove that (4.37) is equal to

$$\Delta \sum_{\substack{j=0, \dots, h \\ b_{n-n_j} = m}} A_j(-(s+n-1)\Delta + n_j\Delta)^T \mu^{a_{n-n_j}}, \quad (4.38)$$

so that, by a comparison of this expression with (4.4), the nonlinear eigenvalue problem (4.36) is equivalent to eigenvalue problem (4.33) in the sense of Theorem 4.2. Let us note that $b_{N-m+1-n_j} = N-n+1$ is equivalent to $b_{n-n_j} = m$, since by modular arithmetic we get

$$N-m-n_j \equiv_N N-n \Leftrightarrow m+n_j \equiv_N n \Leftrightarrow n-n_j \equiv_N m,$$

where \equiv_N denotes the congruence modulo N . Moreover, by the last congruence relation, we obtain

$$n-n_j = m + Na_{n-n_j}, \quad \text{with } a_{n-n_j} = \left\lfloor \frac{n-n_j-1}{N} \right\rfloor.$$

Therefore, by the periodicity $T = N\Delta$ of the system matrices $\{A_j(t)\}_{j=0}^h$ we get

$$A_j((1-s+N-m+1-1)\Delta)^T = A_j((1-s-n+n_j+N(1+a_{n-n_j}))\Delta)^T = A_j((1-s-n+n_j)\Delta)^T,$$

and also

$$a_{N-m+1-n_j} = \left\lfloor \frac{N-m-n_j}{N} \right\rfloor = \left\lfloor \frac{N-n+Na_{n-n_j}}{N} \right\rfloor = a_{n-n_j}.$$

Consequently, (4.37) is equivalent to (4.38), which concludes the proof. \square

Based on Theorems 4.4-4.5 the methods for computing right eigenpairs as presented in the previous section can be trivially adapted to compute left eigenpairs.

Remark 4.3. The linear time-periodic system (4.1) admits a dual system, although relations (4.2) might be not satisfied. Indeed, even if Assumption 4.1 does not hold, the monodromy operators \mathcal{U} , and $\check{\mathcal{U}}$ associated respectively with the linear periodic time-delay systems (4.1) and (4.32) satisfy $\sigma(\mathcal{U}) \setminus \{0\} = \sigma(\check{\mathcal{U}}) \setminus \{0\}$, as stated in [56, Theorem 1].

4.4 STABILITY OPTIMIZATION

In this section, analogously to section 1.1.4, we assume that the matrices in (4.1) depend on system or controller parameters $\mathbf{K} = (K_1 \cdots K_k)^T \in \mathbb{R}^k$. More precisely, we consider system

$$\dot{x}(t) = \sum_{j=0}^h A_j(t; \mathbf{K})x(t - \tau_j), \quad (4.39)$$

assuming that functions $A_j : \mathbb{R} \times \mathbb{R}^k \mapsto \mathbb{R}^{r \times r}$, $(t, \mathbf{K}) \mapsto A_j(t; \mathbf{K})$ are continuous and T -periodic in the first argument, for $j = 0, \dots, h$. Accordingly, differential equation (4.3) changes to

$$\dot{\mathbf{q}}(s) = A(s, \mu; \mathbf{K}) \mathbf{q}(s),$$

and we denote the nonlinear eigenvalue problem by $\mathcal{N}(\mu; \mathbf{K})\mathbf{v} = 0$. However, to simplify the notations, we omit the parametric argument whenever it is not essential for the understanding.

Section 4.4.1 addresses the characterization of derivatives of simple Floquet multipliers with respect to parameters \mathbf{K} , inferred from nonlinear eigenvalue problem (4.11), and outlines their computation. These results are at the basis of a method for stability optimization of periodic time-delay systems, presented in section 4.4.2.

4.4.1 Derivatives of Floquet multipliers

The following proposition provides an explicit expression for derivatives of a Floquet multiplier with respect to system parameters.

PROPOSITION 4.6 *Let (μ, \mathbf{v}) be an eigenpair of (4.11), with $\mu \neq 0$ a simple eigenvalue. Let \mathbf{u} be the left eigenvector associated with μ , i.e. $\mathbf{u}^* \mathcal{N}(\mu; \mathbf{K}) = 0$. If \mathbf{q} satisfies (4.9), then, for each $i \in \{1, \dots, k\}$ we can express*

$$\frac{\partial \mu}{\partial K_i} = - \frac{\mathbf{u}^* \mathbf{q}_{K_i}(1)}{\mathbf{u}^* \mathbf{q}_\mu(1) - \mathbf{u}^* \mathbf{v}_N}, \quad (4.40)$$

where \mathbf{q}_μ and \mathbf{q}_{K_i} are solution of initial value problem

$$\begin{cases} \dot{\mathbf{q}}_{K_i}(s) = \frac{\partial A(s, \mu; \mathbf{K})}{\partial K_i} \mathbf{q}(s) + A(s, \mu; \mathbf{K}) \mathbf{q}_{K_i}(s), \\ \dot{\mathbf{q}}_\mu(s) = \frac{\partial A(s, \mu; \mathbf{K})}{\partial \mu} \mathbf{q}(s) + A(s, \mu; \mathbf{K}) \mathbf{q}_\mu(s), \\ \mathbf{q}_{K_i}(0) = 0, \quad \mathbf{q}_\mu(0) = 0, \end{cases}$$

and \mathbf{v}_N is as in Proposition 4.3.

Proof. Applying Proposition 1.4 to the finite-dimensional nonlinear eigenvalue problem (4.11), the formula for a derivative of a simple eigenvalue is

$$\frac{\partial \mu}{\partial K_i} = - \frac{\mathbf{u}^* \frac{\partial N(\mu; \mathbf{K})}{\partial K_i} \mathbf{v}}{\mathbf{u}^* \frac{\partial N(\mu; \mathbf{K})}{\partial \mu} \mathbf{v}}. \quad (4.41)$$

The remainder of the proof is analogous to the proof of Proposition 4.3, relying on the variational equations corresponding to (4.9) and parameters μ and K_i , respectively. \square

Proposition 4.6 bring us to the following algorithm for computing the gradient of a simple Floquet multiplier with respect to parameters vector \mathbf{K} .

Algorithm 4.2. *Computing the gradient of a Floquet multiplier.*

1. Compute a Floquet multiplier μ and its right eigenvector \mathbf{v} by Algorithm 4.1.
2. Compute $\mathbf{u} \in \mathbb{C}^{Nr}$ as the corresponding left eigenvector.
3. Solve initial value problem

$$\begin{cases} \dot{\mathbf{q}}(s) = A(s, \mu; \mathbf{K})\mathbf{q}(s), \\ \dot{\mathbf{q}}_\mu(s) = \frac{\partial A(s, \mu; \mathbf{K})}{\partial \mu} \mathbf{q}(s) + A(s, \mu; \mathbf{K})\mathbf{q}_\mu(s), \\ \dot{\mathbf{q}}_{K_i}(s) = \frac{\partial A(s, \mu; \mathbf{K})}{\partial K_i} \mathbf{q}(s) + A(s, \mu; \mathbf{K})\mathbf{q}_{K_i}(s), \quad i = 1, \dots, k \\ \mathbf{q}(0) = \mathbf{v}, \quad \mathbf{q}_\mu(0) = 0, \quad \mathbf{q}_{K_i}(0) = 0, \quad i = 1, \dots, k, \end{cases} \quad (4.42)$$

on the interval $[0, 1]$ and compute, by formula (4.40), the partial derivatives of the Floquet multiplier with respect to the elements of \mathbf{K} .

If the dimension Nr is small, the vector \mathbf{u} can be computed as singular vector corresponding to the smallest singular value of the matrix N_δ , obtained by solving initial value problem (4.9) with Nr independent initial vectors \mathbf{v} . For problems with high dimension Nr , the construction of the full matrix N_δ for the second step of Algorithm 4.2 has to be avoided. In this situation, we can separately apply Arnoldi's method and, possibly, Broyden's correction initialized with $H_0 = I$, as discussed in the previous section 4.2.3, to the original system (4.1) and to (4.32), followed by a pairing of Floquet multipliers and associated eigenvectors.

Remark 4.4. In our implementation, we use the same integration method with fixed step δ for numerically solving (4.31) and (4.42) as we use for (4.9). In particular, if the left eigenvector is computed as left singular vector of N_δ , we solve (4.9) and (4.42) by either Runge-Kutta of order 4 for non-stiff problems or trapezoidal rule for stiff problems. If the left eigenvector is computed from the discretized monodromy operator of system (4.32), followed by corrections using (4.30), then the initial value problems (4.9), (4.31), and (4.42) are all solved by trapezoidal rule, a symmetric mixed implicit-explicit scheme. The consistency between integration schemes permits to interpret the result of Algorithm 4.2 as the gradient of a eigenvalue of $N_\delta(\mu; \mathbf{K})\mathbf{v} = 0$.

4.4.2 Stability optimization

By Proposition 1.1, the stabilization problem of an unstable system of form (4.39) corresponds to finding controller parameters \mathbf{K} such that the Floquet multipliers are all confined to the open unit disc. This problem, as well as the problem of increasing the decay rate of solutions of a stable system towards the zero equilibrium, lead us to the optimization problem of minimizing the (squared) spectral radius of the monodromy operator as a function of controller parameters \mathbf{K} ,

$$\min_{\mathbf{K}} \rho^2, \quad \text{with } \rho = |\mu_D|; \quad (4.43)$$

where μ_D is a dominant Floquet multiplier, in the sense of being the largest in modulus.

The objective function (4.43) behaves similarly to the spectral abscissa, analyzed in section 2.1. Indeed, the objective function (4.43) is in general non-convex (see Figure 1.4b), and may not be everywhere differentiable, even not everywhere Lipschitz continuous, although a simple Floquet multiplier locally defines a smooth function of parameters \mathbf{K} . The lack of smoothness is related to the occurrence of multiple dominant Floquet multipliers, counted with multiplicity. In general, points of non-differentiability occur on a set with measure zero in the parameter space, meaning that the objective function is smooth almost everywhere. For these reasons, analogously to section 1.1.4, we use the MATLAB code HANSO (Hybrid Algorithm for Non-Smooth Optimization) [64]. The underlying algorithm only requires the evaluation of the objective function and its gradient with respect to the parameters, whenever it is differentiable. This is the case if the dominant Floquet multiplier is isolated and simple, and the objective function gradient is

$$\nabla_{\mathbf{K}} (\rho^2) = 2 \operatorname{Re} (\bar{\mu}_D \nabla_{\mathbf{K}} \mu_D),$$

where $\nabla_{\mathbf{K}} \mu_D$ is obtained by Algorithm 4.2.

The accuracy of the results depends on the resolution of solving initial value problems (4.9), and (4.42). To avoid fluctuations of the objective function and convergence problems, we consider a discretized-first approach analogously to Algorithm 3.1. Indeed, we have always used the same step-size δ for the initial value problems (4.9), and (4.42), and kept it fixed during the optimization process. When using the time-integration schemes described in Remark 4.4, the overall method can be interpreted as stability optimization of discretized eigenvalue problem $\mathcal{N}_\delta(\mu; \mathbf{K})\mathbf{v} = 0$.

4.5 NUMERICAL EXAMPLES

In this section, the novel stability optimization method for periodic time-delay systems is tested on three test-cases. Section 4.5.1 considers a periodic scalar time-delay system,

where the delays are multiple of the period. For this simple system, the numerical results are compared with their analytical values. In section 4.5.2, proportional, derivative, and integral controllers are designed by the novel stabilization method for the Mathieu's equation with delayed input. Section 4.5.3 considers a large scale milling model, describing the interaction between a rotating cutter and a visco-elastic workpiece by a periodic cutting force.

All numerical experiments are performed in Matlab version 9.1.0 (R2016b) on a Dell Latitude notebook running an Intel(R) Core(TM) i5-6440HQ CPU @ 2.60GHz quad core processor with 8 GB RAM. Our experiments can be reproduced with the publicly available code of [25].

4.5.1 Stability and stabilization of a scalar system

For scalar systems of the form (4.12), the nonlinear eigenvalue problem can be explicitly expressed by (4.14). This explicit expression permits to compute the derivative of a simple Floquet multiplier with respect to an element K_i of \mathbf{K} by (4.41),

$$\frac{\partial \mu}{\partial K_i} = \frac{\sum_{j=0}^h \mu^{1-j} \frac{\partial a_j}{\partial K_i}}{1 + \sum_{j=1}^h j \mu^{-j} a_j}, \quad \text{for } i = 1, \dots, k. \quad (4.44)$$

As a first example, we test the proposed methods on a scalar system with $N = 1$, so that the results can be compared with the explicit expressions (4.14) and (4.44). We consider the following system

$$\dot{x}(t) = (K \cos(2t))x(t) + (\sin(2t) + K)x(t - \pi) + 0.1 \cos(2t)e^{\sin(2t)}x(t - 2\pi). \quad (4.45)$$

The Floquet multipliers and their derivatives with respect to controller parameter K can be obtained by (4.14) and (4.44), with $a_0 = a_2 = 0$ and $a_1 = K\pi$,

$$\mu_k = \begin{cases} \frac{K\pi}{W_k(K\pi)}, & \text{if } K \neq 0, \\ 1, & \text{if } K = 0, \end{cases} \quad \frac{\partial \mu}{\partial K} = \begin{cases} \frac{\pi}{1+W_k(K\pi)}, & \text{if } K \neq 0, \\ \pi, & \text{if } K = 0, \end{cases} \quad (4.46)$$

where we remind from Example 1.3 that W_k denotes the k -th branch of the Lambert W function.

For $K = e/\pi$, the largest Floquet multiplier in modulus is simple, $\mu = e$, and its derivative satisfies $\frac{\partial \mu}{\partial K} = \frac{\pi}{2}$. Analogously to Figure 1.3, the approximation errors of Algorithm 4.1 are illustrated in Figure 4.4. In particular, Figure 4.4a depicts the relative error induced by the discretization of the monodromy operator (the first stage of Algorithm 4.1), increasing the number of collocation points M , and illustrates the expected spectral convergence. In Figure 4.4b, a few steps of Broyden's method permit to reach a tolerance error equal to machine precision, however the approximated Floquet multipliers accuracy crucially relies on the step-size δ to solve (4.28).

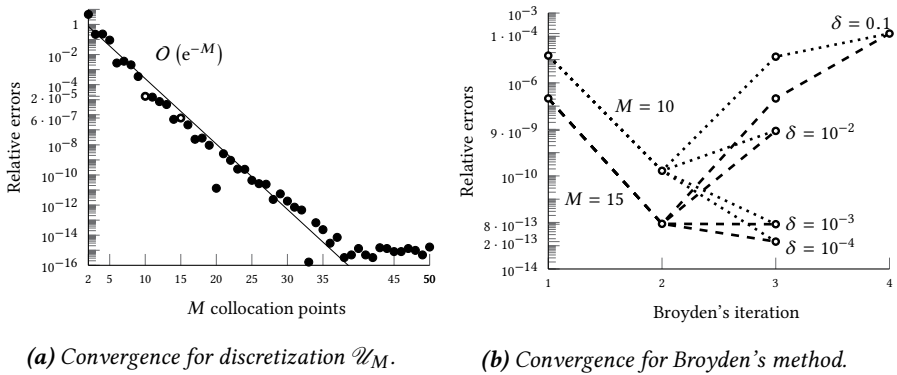


Figure 4.4 Relative errors to evaluate the dominant Floquet multiplier with Algorithm 1.1 for system (4.45) with $K = e/\pi$. Broyden's method is initialized on the largest eigenvalues in modulus of \mathcal{U}_M with $M = 10$ and $M = 15$ collocation points, and its accuracy relies on the step-size δ to approximate the characteristic matrix $\mathcal{N}(\mu)$ with Runge-Kutta method of order 4.

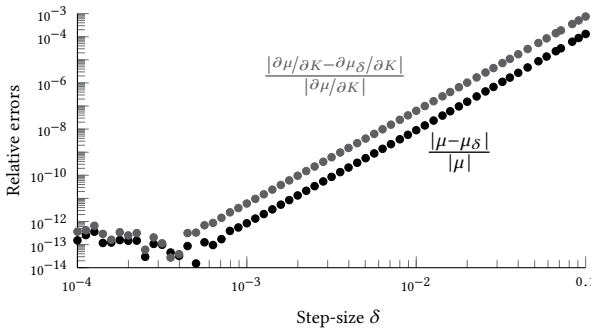


Figure 4.5 Relative errors to compute the dominant Floquet multiplier and its derivative by Algorithms 4.1-4.2. These errors are induced by approximating $\mathcal{N}(\mu)$ with $\mathcal{N}_\delta(\mu)$, for system (4.45).

In contrast to Algorithm 1.1 for autonomous time-delay system, where the second step approximates the characteristic roots up to machine precision by the explicit characteristic matrix formulation, in the second step of Algorithm 4.1, the approximated Floquet multiplier converges to an eigenvalue of $\mathcal{N}_\delta(\mu)$, since the solutions of the initial value problem (4.9) are approximated by an integration method with step-size δ . If δ is not sufficiently small, then Broyden's method might even furnish approximations which are less accurate than the ones obtained by the monodromy operator discretization, considered for the initialization, see the errors for $\delta = 0.1$ in Figure 4.4b. The approximation with step-size δ of the characteristic matrix $\mathcal{N}(\mu)$, i.e. $\mathcal{N}_\delta(\mu)$, does not only affect the computation of the Floquet multiplier but also of its derivative, as illustrated in Figure 4.5 where the initial value problems (4.9) and (4.42)

are computed by Runge-Kutta method of order 4.

System (4.45) is unstable for $K = e/\pi$, since the dominant Floquet multiplier $\mu = e$ does not lie within the unit circle. Computing the dominant Floquet multipliers by a monodromy operator discretization with $M = 15$ collocation points and by Broyden's correction with 4-th order Runge-Kutta method and $\delta = 2 \cdot 10^{-4}$ step-size, the stability optimization approach of section 4.4.2 yields the stabilizing controller parameter $K = -0.1295$, for which the spectral radius is $\rho = 0.3935$. Figure 4.6 displays the iterates generated by the optimization routine. The final controller parameter found is very close to the minimizer $K = -(e\pi)^{-1}$, for which the dominant Floquet multiplier $\mu = e^{-1}$ corresponds to a double non-semi-simple eigenvalue. Finally, Figure 4.7 shows the eigenvalues of (4.23) in the first and last iteration of the stability optimization procedure.

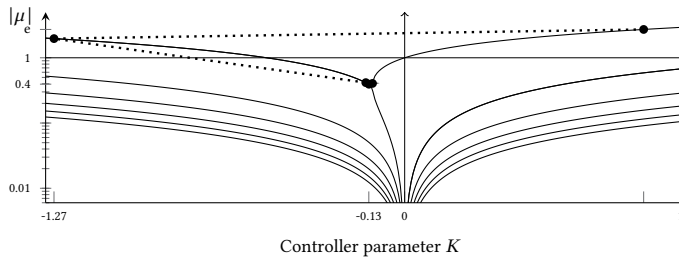


Figure 4.6 The stability optimization path for system (4.45) is compared with the exact modulus of the 10 largest Floquet multipliers, varying the controller parameter K . The stability optimization provides a stabilizing controller already at the third iteration.

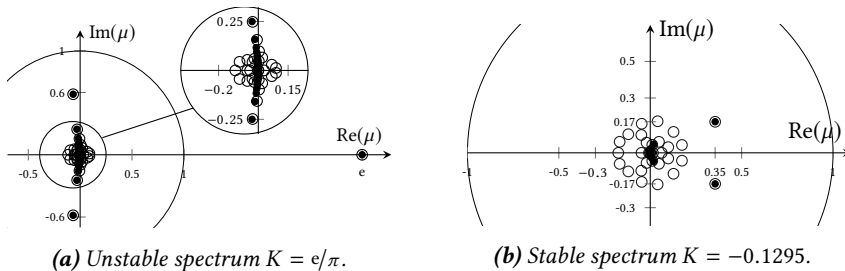


Figure 4.7 The Floquet multiplier approximations obtained as eigenvalues of (4.23) with $M = 20$ (circles) and their analytical value computed by (4.46) (dots) are shown at the beginning and at the end of the stability optimization process.

4.5.2 Delayed Mathieu's equation

As second example, we consider a variant of Mathieu's equation with delayed input and PID controller,

$$\begin{aligned} \ddot{z}(t) + (v + \varepsilon \cos 2t)z(t) &= -u(t - \tau), \\ u(t) &= K_I \int_0^t z(\theta) d\theta + K_P z(t) + K_D \dot{z}(t), \end{aligned}$$

where K_I , K_P and K_D are respectively integral (I), proportional (P) and derivative (D) gain. The Mathieu's equation with delayed PI and PD feedback controllers is analyzed in [77], and arises as model for the stick balancing problem in [37, Section 5.4].

The Floquet multipliers of the Mathieu's equation with delayed PID controller can be inferred from the spectrum of the following linear periodic time-delay system

$$\dot{x}(t) = \begin{pmatrix} 0 & 1 & 0 \\ 0 & 0 & 1 \\ 0 & -v - \varepsilon \cos 2t & 0 \end{pmatrix} x(t) - \begin{pmatrix} 0 & 0 & 0 \\ 0 & 0 & 0 \\ K_I & K_P & K_D \end{pmatrix} x(t - \tau). \quad (4.47)$$

If $K_I = 0$, Mathieu's equation with PD feedback controller can be rewritten as a linear periodic time-delay system of dimension $r = 2$, which presents the same spectrum of system (4.47), except for a non-physical Floquet multiplier of (4.47) equal to one.

For $v = 4$ and $\varepsilon = 2$ the system without controller is unstable. Therefore, we design PI, PD, and PID controllers in the presence of input delay $\tau = 3\pi/4$. In order to minimize the dimension of the nonlinear eigenvalue problem we consider Δ as the greatest common divisor of τ and of the period $T = \pi$, so that $\Delta = \pi/4$ and $N = 4$. Table 4.1 summarizes the results of the stability optimization, with $M = 10$ collocation points and a Runge-Kutta method of order 4 with step-size $\delta = 2 \cdot 10^{-3}$. As expected, increasing the number of controller parameters results in smaller spectral radii.

Table 4.1 Results of the stability optimization algorithm for Mathieu's equation with delayed feedback controller (4.47), where $v = 4$, $\varepsilon = 2$, $\tau = 3\pi/4$. All the designed controllers stabilize the system, since the spectral radii ρ are smaller than 1.

	ρ	K_I	K_P	K_D
PI controller	0.5339	0.3215	0.7541	
PD controller	0.2858		0.7012	0.0231
PID controller	0.2376	1.8035	1.1270	0.5313

The dimension of the characteristic matrix $\mathcal{N}(\mu)$ and of the discretized eigenvalue problem (4.23) are 12×12 and 132×132 , respectively. In the stability optimization we apply both the small and the large scale strategies for the computation of the dominant Floquet multiplier and of its gradient. The small scale strategy solves the discretized eigenvalue problem (4.23) by a direct method, initialize the Jacobian

inverse in Broyden's method with (4.27), and extracts the left eigenvector by explicitly constructing the matrix $\mathcal{N}_\delta(\mu)$. The large scale strategy applies Arnoldi's method and Broyden's correction initialized with $H_0 = I$ to the original system (4.47) and to its dual time-delay system. Both strategies lead to the same results given in Table 4.1; however, their computation time differs, Table 4.2. The fine discretization accuracy of Runge-Kutta method, $\delta = 2 \cdot 10^{-3}$, heavily affects the timings of the small scale strategy, which requires to explicitly compute the characteristic matrix $\mathcal{N}_\delta(\mu)$ both in the initialization (4.27) of the Broyden's method and in the left eigenvector extraction.

Table 4.2 Timings to evaluate the largest in modulus Floquet multiplier and the last iteration of the of the stabilization method at the designed controllers for the delayed feedback Mathieu's equation (4.47) with $\nu = 4$, $\varepsilon = 2$, and $\tau = 3\pi/4$. The required time to design the different controllers with the novel stabilization method is also shown. The small scale strategy, explicitly computing the characteristic matrix $\mathcal{N}_\delta(\mu)$ both in (4.27) and for the extraction of the left eigenvector, is computationally slower than the large scale strategy, which computes the left eigenvector with the dual time-delay system (4.32).

Timings [s] Strategy	Eigenpairs		Iteration		Optimization	
	Small	Large	Small	Large	Small	Large
PI controller	3.3689	0.7091	5.5439	1.3701	1734.7	424.3
PD controller	3.6210	0.8854	6.1812	2.0463	1286.8	492.3
PID controller	5.1067	0.9601	9.0045	2.6682	2398.4	1434.8

4.5.3 A PDE model for a milling problem in machining

The last numerical example considers a milling model, described in [71]. Some Floquet multipliers of this system are computed by deflated Broyden's method in [39]. This milling model describes the interaction between a rotating cutter and a visco-elastic workpiece by a periodic cutting-force f . The rotating cutter is attached to a spring, and modeled by

$$\ddot{z}(t) + 2K\dot{z}(t) + z(t) = -f(t),$$

where K is the damping parameter to be designed in order to improve the stability properties of the overall system. The workpiece is modeled by Kelvin-Voigt material leading to the following partial differential equation (PDE),

$$\begin{cases} \frac{\partial u(t,\ell)}{\partial t^2} - \frac{\partial u(t,\ell)}{\partial \ell^2} - \frac{\partial u(t,\ell)}{\partial \ell^2 \partial t} = 0, & \ell \in [0, 1], \\ u(t, 0) \equiv 0, & \frac{\partial u(t,1)}{\partial \ell} + \frac{\partial u(t,1)}{\partial t \partial \ell} = -f(t). \end{cases}$$

This PDE is discretized in space using n linear finite elements defined on an equidistant grid. By applying Galerkin finite element method, we get a system of ordinary differential equations,

$$P_n \ddot{U}(t) + D_n U(t) + D_n \dot{U}(t) = -f(t)e_n,$$

where $U(t) \in \mathbb{R}^n$ and

$$P_n = \frac{1}{6n} \begin{pmatrix} 4 & 1 & & & \\ 1 & \ddots & \ddots & & \\ & \ddots & & 4 & 1 \\ & & & 1 & 2 \end{pmatrix}, \quad D_n = n \begin{pmatrix} 2 & -1 & & & \\ -1 & \ddots & \ddots & & \\ & \ddots & & 2 & -1 \\ & & & -1 & 1 \end{pmatrix}, \quad e_n = \begin{pmatrix} 0 \\ \vdots \\ 0 \\ 1 \end{pmatrix}.$$

The periodic cutting-force couples the rotating cutter and workpiece dynamics, and is influenced by the previous cut, occurring with delay $\tau = 1$; it is modeled by

$$f(t) = g(t)(z(t) - z(t - \tau)) + g(t)(u(t, 1) - u(t - \tau, 1)),$$

where $u(t, 1)$ is discretized by $e_n^T U(t)$, and $g(t)$ is a function with period 1, defined on the interval $[0, 1]$ as

$$g(t) = \begin{cases} \sin^2(2\pi t) + 0.5 \sin(4\pi t), & t \in [0, 1/2], \\ 0, & t \in (1/2, 1]. \end{cases} \quad (4.48)$$

Setting $y(t) = (U^T z \dot{U}^T \dot{z})^T$, we can rewrite the milling model as a periodic linear time-delay system, whose dimension $r = 2(n + 1)$ depends on the PDE discretization based on n linear elements,

$$E\dot{x}(t) = (A(K) - F \cdot g(t))x(t) + F \cdot g(t)x(t - \tau), \quad (4.49)$$

where

$$E = \begin{pmatrix} I_n & & & \\ & 1 & & \\ & & P_n & \\ & & & 1 \end{pmatrix}, \quad A(K) = - \begin{pmatrix} & -I_n & & \\ & & -1 & \\ D_n & & D_n & \\ & 1 & & 2K \end{pmatrix}, \quad F = \begin{pmatrix} & & & \\ & & & \\ e_n e_n^T & e_n & & \\ e_n^T & 1 & & \end{pmatrix}.$$

System (4.49) can be reformulated into (4.1) by pre-multiplication with matrix E^{-1} . However, as this reduces the sparsity of the matrices, we rely instead on a slight extension of the presented results to periodic time-delay system with a constant non-singular leading coefficient matrix E , as described in the following section 4.6.1.

Let us consider a PDE discretization with $n = 250$, leading to a system dimension $r = 502$. The largest Floquet multipliers in modulus are iteratively approximated by the Arnoldi's method, and their accuracy is then refined by Broyden's method, as explained in section 4.2.3. To compute a left eigenvector, appearing in the expression for the Floquet multiplier derivative with respect to K , we separately apply Arnoldi's and Broyden's methods to the model (4.49) and corresponding model (4.32), followed by a pairing of Floquet multiplier approximations (see section 4.4.1). In order to consistently solve the problem (see Remark 4.4), the initial value problems (4.9), (4.42),

and (4.31) are solved by trapezoidal rule with step-size $\delta = 0.01$. The usage of the trapezoidal rule permits also to tackle the stiffness to numerical solve the initial value problems.

The milling model (4.49) is periodic with $T = \tau_1 = 1$. However, differently from the previous examples, the periodic system matrices are not smooth, presenting a non-differentiable point at $t = 1/2 + kT$ for every integer k , due to (4.48). Consequently, the solutions exhibit a discontinuity in the second derivative at these time-instants. The presence of such a discontinuity decreases the discretization accuracy by the collocation approach if it occurs in an interior point of the domain of a polynomials (4.15), defining the spline approximation. This can be overcome by taking $\Delta = 1/2n$ with $n \in \mathbb{N} \setminus \{0\}$, so the discontinuity is located at the endpoints of the support of two M -degree polynomials.

For $n_1 = N = 2$, the system (4.49) requires a high number of collocation points $M = 250$, to reliably approximate the dominant Floquet multipliers by Arnoldi's method. Therefore, we increase the sparsity of the matrices S_q and S_φ used in the Arnoldi's iteration (4.29) by setting $M = 20$ and $n_1 = N = 26$, which is beneficial in the employed sparse LU factorization of S_q . Indeed, the spline approximation of the eigenfunction is achieved by 26 polynomials of degree $M = 20$, instead of 2 polynomials of degree 250. The resulting S_q and S_φ matrices in (4.29) present a block diagonal structure where each of the 26 blocks has dimension $21r \times 21r$.

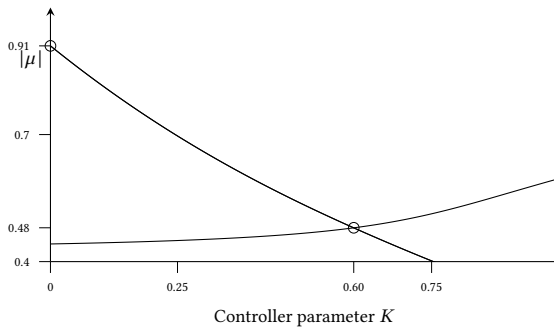
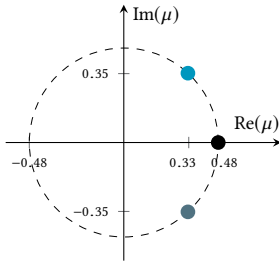
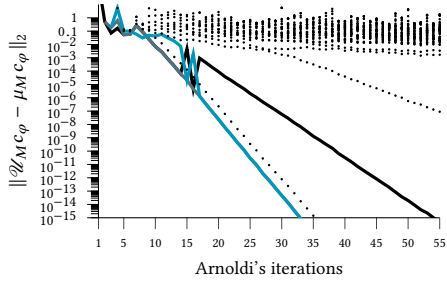


Figure 4.8 Modulus of the largest in modulus Floquet multipliers as a function of K for system (4.49). The initial and final iterations of the optimization process are indicated by circles.

The stability optimization almost halves the modulus of the dominant Floquet multiplier, from $\rho = 0.9095$ at initial gain $K = 0$ to $\rho = 0.4799$ for $K = 0.5968$. The designed controller is close to a minimizer of the spectral radius, as illustrated in Figure 4.8. The minimum is characterized by a real and a conjugate pair of Floquet multipliers having the same modulus, Figure 4.8. The approximations of the largest Floquet multipliers requires few Arnoldi's iterations to converge, for example for the final controller gain the residual norm of the approximated conjugate pair of



(a) Dominant Floquet multipliers.



(b) Convergence for Arnoldi's method.

Figure 4.9 Convergence history of the dominant Floquet multipliers for Arnoldi's method applied to \mathcal{U}_M for $M = 20$, $N = 26$, and $K = 0.5968$

Floquet multipliers reach machine precision within 35 iterations, compared to 55 for the dominant real Floquet multiplier, see Figure 4.9b.

4.6 FURTHER REMARKS

We further develop the arguments previously presented in this chapter with respect to three different research directions. Firstly, in section 4.6.1, we discuss the generalization to linear periodic time-delay system with arbitrary non-singular leading matrix. Then, we generalize the results to deal with the eigenvalues of the solution operator. To conclude, we address for autonomous time-delay system with commensurate delays the link between the nonlinear eigenvalue problems associated with the infinitesimal generator (Theorem 1.3) and to a particular monodromy operator (Theorem 4.2).

4.6.1 Arbitrary non-singular leading matrix

Let us consider a linear-periodic time-delay system, satisfying Assumption 4.1, of the form

$$E\dot{x}(t) = \sum_{j=0}^h A_j(t; \mathbf{K})x(t - \tau_j), \tag{4.50}$$

where E is a non-singular $\mathbb{R}^{r \times r}$ -valued matrix. We briefly discuss the generalization of the previous results to system (4.50), without (explicitly) using the inverse of the leading matrix E . This generalization is considered in the numerical example of section 4.5.3 to preserve the sparsity patterns of the system matrices.

The characteristic matrix $\mathcal{N}(\mu; \mathbf{K})$ associated with (4.50) is defined by its action on $\mathbf{v} \in \mathbb{C}^{Nr}$ as $\mathcal{N}(\mu; \mathbf{K})\mathbf{v} = \mathbf{q}(1) - B(\mu)\mathbf{v}$, with \mathbf{q} solution of the initial value problem

$$\begin{cases} (E \otimes I_N) \dot{\mathbf{q}}(s) = A(s, \mu; \mathbf{K})\mathbf{q}(s), & s \in [0, 1], \\ \mathbf{q}(0) = \mathbf{v}. \end{cases}$$

Its “transposed” problem (4.31) changes to $\check{\mathcal{N}}(\mu)\mathbf{v} = (E^T \otimes I_N)\mathbf{p}(0) - B(\mu)^T\mathbf{v}$, where \mathbf{p} satisfies

$$\begin{cases} (E^T \otimes I_N) \dot{\mathbf{p}}(s) = -A(s, \mu; \mathbf{K})^T\mathbf{p}(s), & s \in [0, 1], \\ (E^T \otimes I_N)\mathbf{p}(1) = \mathbf{v}. \end{cases}$$

Moreover, the dual time-delay system associated with (4.50) is

$$E^T \dot{x}(t) = \sum_{j=0}^h A_j(-t + \tau_j; \mathbf{K})^T x(t - \tau_j).$$

Indeed, Theorem 4.5 can be generalized to time-delay system with non-singular leading matrix E , where condition (4.35) changes to

$$\hat{\mathbf{p}}(s) = R(E^T \otimes I_N)\mathbf{p}(s) = \begin{pmatrix} & & E^T \\ & \ddots & \\ E^T & & \end{pmatrix} \mathbf{p}(s).$$

4.6.2 Characteristic matrix for the solution operator

The Floquet multipliers are eigenvalues of the monodromy operator \mathcal{U} , which is defined as the solution operator $\mathcal{T}(T, 0)$, where $T > 0$ is the period of the system matrices $\{A_j(t)\}_{j=0}^h$ of system (4.1). In this section, we extend the theory behind Algorithms 4.1 and 4.2 dealing with Floquet multipliers, to the more general case of the eigenvalues of the solution operator associated with a time-delay system

$$\dot{x}(t) = \sum_{j=0}^h A_j(t; \mathbf{K})x(t - \tau_j), \quad t \geq t_0 \in \mathbb{R}, \quad (4.51)$$

where the system matrices are not restricted to be time-periodic. System (4.51) admits a unique forward solution of the initial value problem (1.2), then we can define a family of solution operators $\{\mathcal{T}(t_1, t_0)\}_{\substack{t_0 \in \mathbb{R} \\ t_1 \in \mathbb{R}_+}}$. Analogously to Assumption 4.1, we consider system (4.51) and its associated solution operators $\mathcal{T}(t_1, t_0)$, with $t_1 > 0$ and $t_0 \in \mathbb{R}$, such that the parameter t_1 and the delays τ_j are commensurable, *i.e.* $t_1 = N\Delta$, and for every $j \in \{0, \dots, h\}$ $\tau_j = n_j\Delta$ with $N, n_j \in \mathbb{N}$ and $\Delta \in \mathbb{R}_+ \setminus \{0\}$.

Generalizing Theorem 4.2, the non-zero eigenvalues of the solution operator $\mathcal{T}(t_1, t_0)$, *i.e.* $\mu \in \mathbb{C} \setminus \{0\}$, such that

$$\mathcal{T}(t_1, t_0)\varphi = x_{t_1+t_0}(\cdot; t_0, \varphi) = \mu\varphi, \quad \varphi \in X \setminus \{0\},$$

can be alternatively characterized as eigenvalues of the finite-dimensional nonlinear eigenvalue problem $\mathcal{N}(\mu; \mathbf{K})\mathbf{v} = 0$ with $\mathbf{v} \in \mathbb{C}^{Nr} \setminus \{0\}$. The matrix-valued function $\mathcal{N}(\mu; \mathbf{K})$ is implicitly defined as solution of a boundary value problem (4.8)–(4.9), where the differential equation (4.4) changes to

$$\dot{q}_n(s) = \Delta \sum_{j=0}^h A_j(t_0 + (s + n - 1)\Delta; \mathbf{K})\mu^{a_{n-n_j}} q_{n-n_j}(s),$$

for $s \in [0, 1]$ and $n = 1, \dots, N$. A similar formulation can also be obtained for the “transposed” problem (4.31).

Since the system matrices $\{A_j(t; \mathbf{K})\}_{j=0}^h$ are not assumed to be time-periodic in the t -variable, Theorem 4.5 cannot be easily generalized except when $T = \Delta$, *i.e.* $N = 1$. Indeed, the dual time-delay system for $\mathcal{T}(\Delta, t_0)$ associated with (4.51) is

$$\dot{x}(t) = \sum_{j=0}^h A_j(t_0 + \Delta - t; \mathbf{K})^T x(t - \tau_j).$$

This last result generalizes the dual time-delay system (4.32) associated with (4.12),

$$\dot{x}(t) = \sum_{j=0}^h A_j(-t; \mathbf{K})^T x(t - \tau_j).$$

Indeed, the monodromy operator associated with system (4.12) is $\mathcal{U} = \mathcal{T}(\Delta, 0)$, and the system matrices of (4.12) are $T = \Delta$ -periodic.

4.6.3 Characteristic matrices relations for autonomous time-delay system

Let us consider the following autonomous linear time-delay system

$$\dot{x}(t) = \sum_{j=0}^h A_j x(t - \tau_j), \tag{4.52}$$

where the delays are commensurate, *i.e.* for any $j \in \{0, \dots, h\}$, $\tau_j = n_j \Delta$ with $n_j \in \mathbb{N}$ and $\Delta \in \mathbb{R}_+ \setminus \{0\}$. Since system (4.52) is time-periodic for any period $T > 0$, then every solution operator $\mathcal{T}(T, 0)$ is a monodromy operator associated with (4.52). For simplicity, we consider $\mathcal{U} = \mathcal{T}(\Delta, 0)$.

By Theorem 4.2, the Floquet multipliers of the monodromy operator \mathcal{U} associated with (4.52) satisfy the nonlinear eigenvalue problem $\mathcal{N}(\mu)v = 0$ with $v \in \mathbb{C}^r$. In this case, the matrix $\mathcal{N}(\mu)$ admits an explicit formulation, since the solution of the initial value problem (4.13) is

$$q(s) = \exp\left(s\Delta \sum_{j=0}^h A_j \mu^{-n_j}\right) v, \quad s \in [0, 1].$$

Therefore, the nonlinear eigenvalue problem $\mathcal{N}(\mu)v = 0$ is

$$\left(\exp\left(\Delta \sum_{j=0}^h A_j \mu^{-n_j}\right) - \mu I_r\right) v = 0.$$

By this explicit formulation, we can establish the connection between the characteristic matrices associated with the infinitesimal generator and to the monodromy operator, respectively $\mathcal{A}(\lambda)$ and $\mathcal{N}(\mu)$. Let $\lambda \in \mathbb{C}$ and $v \in \mathbb{C}^r \setminus \{0\}$, then

$$\begin{aligned} \mathcal{A}(\lambda)v = 0 &\Leftrightarrow \left(\left(\sum_{j=0}^h A_j e^{-\lambda \tau_j}\right) - \lambda I_r\right) v = 0 \\ &\Leftrightarrow (\lambda, v) \text{ is an eigenpair of the matrix } \left(\sum_{j=0}^h A_j e^{-\lambda \tau_j}\right) \\ &\Leftrightarrow (e^{\lambda \Delta}, v) \text{ is an eigenpair of the matrix } \exp\left(\Delta \sum_{j=0}^h A_j e^{-\lambda n_j \Delta}\right) \\ &\Leftrightarrow \left(\exp\left(\Delta \sum_{j=0}^h A_j e^{-\lambda \Delta n_j}\right) - e^{\lambda \Delta} I_r\right) v = 0 \\ &\Leftrightarrow \mathcal{N}\left(e^{\lambda \Delta}\right) v = 0, \end{aligned}$$

where the third equivalence follows from the spectral mapping theorem.

The relation between the nonlinear eigenvalue problems, $\mathcal{A}(\lambda)v = 0$ and $\mathcal{N}(\mu)v = 0$, is in agreement with the relation (1.9) between the spectra of the infinitesimal generator \mathcal{A} and of the monodromy operator $\mathcal{U} = \mathcal{T}(\Delta, 0)$. Moreover, the relation between the eigenvalues of $\mathcal{A}(\lambda)$ and $\mathcal{N}(\mu)$, can be also derived by (1.9) and Theorems 1.3 and 4.2, which state the equivalence between the infinite-dimensional linear eigenvalue problems and their associated finite-dimensional nonlinear eigenvalue problems.

SUMMARY. The Floquet multipliers of a periodic time-delay system, with commensurable period and delays, are interpreted as eigenvalues of either the monodromy operator or a finite-dimensional characteristic matrix. This dual interpretation is computationally exploited: the characteristic matrix formulation permits to improve the accuracy of Floquet multiplier estimates, obtained by discretizing the monodromy operator. In addition, the derivatives of the Floquet multipliers are explicitly expressed in terms of the characteristic matrix and left and right eigenpairs. The formula for the derivative is used in a novel stabilization method, which is also applicable to large scale system, since the characteristic matrix left eigenpairs are related to the characteristic matrix right eigenpairs of a dual periodic time-delay system.

Extended research results of chapter 4 are presented in section 5.1.3.

CONCLUSIONS

This last chapter summarizes the original contributions of this thesis on spectrum-based stability assessment and stabilization of linear time-delay systems. Based upon these results, further research directions are suggested.

In this dissertation, we have proposed novel numerical methods, advancing the classical spectrum-based stability assessment and stabilization of time-delay systems, briefly reviewed in chapter 1. In particular, we have developed in chapter 3 a stabilization method for time-delay systems, which takes into account uncertainty, modeled by the realizations of a random vector, affecting delays and other system parameters. Moreover, in chapter 4, we have presented a novel spectrum-based stability assessment and stabilization methods for a class of periodic system, whose monodromy operator can be associated with a characteristic matrix, evaluated by solving an initial value problem. The development of these methods relies on the analysis of the smoothness properties considered in chapter 2.

This chapter is organized as follows. Firstly, section 5.1 briefly reviews the main contributions of each chapter. Then, in section 5.2, we outline possible future research directions.

5.1 RESEARCH RESULTS

We present a chapter by chapter summary of the main original contributions.

5.1.1 Chapter 2: Smoothness properties of the stability measure

Chapter 2, other than explaining the parallelism between polynomial approximation and polynomial chaos theory, analyzes the approximation of polynomial series (2.3) of $\alpha(\omega)$ (and its polynomial chaos expansion (2.7) of $\alpha(\omega)$) with respect to the behavior of spectral abscissa function (2.2). The analyses show that the lack of smoothness properties of the spectral abscissa function heavily affects the approximation errors of the Galerkin and collocation approaches, as well as the numerical errors in the approximation of the polynomial coefficients c_i with integration methods.

The convergence rates of the Galerkin and collocation approaches are comparable, whenever numerical errors in the Galerkin approach are negligible. These errors can be neglected by following the advices given at the end of section 2.3.1, which correlate the polynomial degree of α_P^M with the number of points $M + 1$ of the integration methods. In this way, the quality of the Galerkin approach approximation is not affected by the numerical errors of the integration methods.

The test-examples, Examples 2.1–2.3 and 2.5, reveal that if the spectral abscissa behaves smoothly, then the polynomial approximation convergences with spectral accuracy for both approaches, *i.e.* with a convergence rate faster than $O\left(P_d^{-k}\right)$ for any $k \in \mathbb{N}$, where $P_d = P$ for the univariate case $D = 1$. However, if the spectral abscissa is non-differentiable and even non-Lipschitz continuous, then the orders of convergence in the univariate case are respectively $O\left(P^{-1}\right)$ and $O\left(P^{-0.5}\right)$, while in the bivariate case they converge approximately as $O\left(P_d^{-1}\right)$ and $O\left(P_d^{-0.3}\right)$, respectively. These latter cases are not deeply studied in the literature on the spectral abscissa approximation, even though they easily occur when applying stability optimization methods, as presented in chapter 3.

Chapter 2 reviews the main theorems on univariate and bivariate polynomial approximation on Chebyshev and Legendre bases for differentiable functions, and provides convergence rates for real-valued non-differentiable and non-Lipschitz continuous functions. Exploiting the parallelism, the L^∞ error bounds are considered in the polynomial chaos framework, providing a novelty in this context. Indeed, the results in polynomial chaos theory are commonly stated in terms of the L^2 norm, or equivalently, in terms of the second order moment, a weaker measure than the L^∞ norm.

5.1.2 Chapter 3: Probabilistic stability optimization

We have presented a novel stability optimization method for uncertain linear interconnected time-delay systems, modeled by delay differential algebraic equations of retarded type where some coefficients are determined by the realizations of a random vector. The novel approach presents several advantages. First, the system description (3.1) allows to model a wide class of interconnected systems, without any restriction on the number of constant and distributed delays, with the possibility to design static and dynamic feedback controllers. Second, all coefficients of the time-delay system, including the delays, can be affected by uncertainty, *i.e.*, they can be described by random variables with a given probability density function. Third, the solutions are more robust and reliable for realistic applications compared to the associated deterministic design. As shown in the engineering models in sections 3.3.4 and 3.3.5, small perturbations on some parameters, may render stable solutions in the deterministic setting unstable. On the other hand, the solutions can be stabilized and robustified also in these latter cases by the novel probabilistic approach.

Fourth, the novel approach permits to obtain different dynamics of stable and robust systems varying the parameter κ of the objective function (3.6) and order r_c of the controller, as presented in the mechanical system with active vibration absorber in section 3.3.5. In this way, the user, regarding his/her application, may choose the controller based on the different time-evolution behaviors and robustness property of the resulting system.

The presented approach is complementary to the approaches grounded in the pseudospectral abscissa optimization, see the numerical comparison in section 3.3.3. First, while the former adopts a probabilistic setting in describing the uncertainty and in the robust stability criterion, the latter takes a worst-case setting, using only upper bounds on the uncertainty. Second, in the pseudospectral setting, typically matrix-valued perturbations are considered, hence, many parameters are subject to uncertainty. Very efficient algorithms to compute the pseudospectral abscissa are available, but it remains difficult to consider a given structure of the uncertainty, in particular if the characteristic matrix nonlinearly depends on the uncertain parameters. In applications, this issue, combined with the worst-case treatment, may lead to an over bounding on the actual uncertainty and a safe but conservative design. On the contrary, with the adopted approach, the parametric dependence and structure of the uncertainty can be easily taken into account, but from a computational view, only a small number of uncertain parameters can be considered, following from the multivariate integrals involving eigenvalue functions that are not always smooth. This is the currently main limitation of the approach. It should be said, however, that the overall approach concerns an off-line controller design.

5.1.3 Chapter 4: Stability and stabilization for a class of periodic delay system

Central in chapter 4 is the dual interpretation of Floquet multipliers as solutions of either an operator eigenvalue problem or a finite-dimensional nonlinear eigenvalue problem. The related one-to-one mapping can not only be expressed in terms of right eigenpairs (Theorem 4.2), but also in terms of left eigenpairs (Theorem 4.5), where surprisingly the time-shifts in (4.32) depend on the delays. The dual interpretation is computationally exploited, as the nonlinear eigenvalue problem formulation lays at the basis of local corrections to improve the accuracy of (multiple) Floquet multiplier estimates obtained by discretizing the monodromy operator. This results in a robust method for accurately computing dominant Floquet multipliers. In addition, computationally tractable expressions for derivatives can be obtained from the nonlinear eigenvalue problem formulation that are useful in the context of stability optimization. The derived results are also generalized to deal with periodic time-delay systems with a non-singular leading matrix, and to compute the eigenvalues of the solution operator if the integration time is different from T or if the matrices are not periodically varying.

Finally, Assumption 4.1 describes the most general situation where Floquet multipliers can be related to a boundary value problem in terms of an ordinary differential equation. If the assumption is not satisfied (or if the minimum N would be prohibitively large), one can still do the stability analysis and stabilization on the (parametrized) matrix \mathcal{U}_M , discretizing the monodromy operator by the collocation approach.

5.2 FUTURE PERSPECTIVES

The results presented in this thesis disclose possible future research directions. Some possible topics concern the analysis of neutral time-delay system, described in section 5.2.1, the extensions of the probabilistic stability optimization method, presented in section 5.2.2, and the development of an heuristic method to determine the number of collocation points to accurately approximate the dominant Floquet multiplier, explained in section 5.2.3. Moreover, other than the previously mentioned future perspectives, it would be desirable to validate the developed numerical methods against experimental results, in order to boost their usage in various applications of time-delay systems.

5.2.1 Neutral time-delay systems

The analysis conducted in chapters 2 and 3 for autonomous linear time-delay systems of retarded type, can be extended to general eigenvalue problems presenting a finite number of dominant eigenvalues in the uncertain domain Ω . However, this property does not hold in general for the spectrum associated with an autonomous neutral time-delay system. The evolution of these neutral systems not only depends on the solution in the past, as the retarded delay differential equations (1.4), but also on the derivative of the solution at past time-instants. An important issue in extending the aforementioned analysis to neutral time-delay system concerns the possible non-continuity of the spectral abscissa, which might not be a continuous function of the delay parameters, as shown in [51, Example 1]. Since the spectral abscissa is not continuous, stable neutral time-delay systems might become unstable with infinitesimal changes of parameters.

When there is only one delay or when delays are not affected by uncertainty, the spectral abscissa is continuous. Still, the spectrum associated with a neutral time-delay system can present an infinite number of eigenvalues in a given right half-plane; therefore, the spectral abscissa might correspond to the supremum of the rightmost eigenvalues real parts, which is not a maximum. For example, the neutral time-delay system

$$\dot{x}(t) + \dot{x}(t-1) = -2x(t) - x(t-1), \quad (5.1)$$

which can be rewritten as a delay differential algebraic equation of neutral type

$$\begin{pmatrix} 1 & 0 \\ 1 & 0 \end{pmatrix} \dot{z}(t) = \begin{pmatrix} -2 & 0 \\ 0 & 1 \end{pmatrix} z(t) - \begin{pmatrix} 1 & 1 \\ 0 & 0 \end{pmatrix} z(t-1),$$

has all the eigenvalues in the open left half-plane, however the spectral abscissa, defined by the supremum, is zero; this spectrum, analyzed in [95], is illustrated in Figure 5.1. Therefore, for neutral systems, the spectral abscissa may not be described by the rightmost eigenvalues behavior, like in section 2.1; and branches of infinitely many rightmost eigenvalues might cross each other in the complex plane.

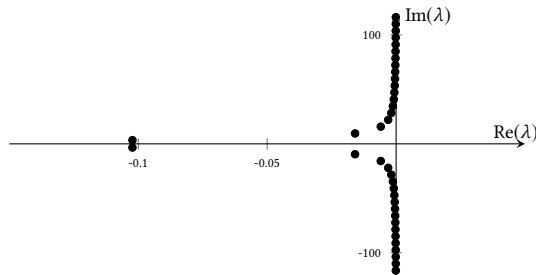


Figure 5.1 Spectrum of the neutral autonomous time-delay system (5.1). In this case, the spectral abscissa corresponds to the supremum of the eigenvalue real parts, and not to the maximum.

For neutral time-delay system, a more robust concept of stability is often considered, the so-called strong stability, such that infinitesimal changes of parameters do not affect the stability assessment [59, Section 1.2]. Analogously to Proposition 1.2 for time-delay systems of retarded type, the strong stability of a neutral time-delay systems can be inferred from a stability measure, known as robust spectral abscissa, which behaves continuously with respect to infinitesimal changes of parameters. Therefore, we could generalize the probabilistic stability optimization method to neutral time-delay systems, if we extend the theoretical background, developed in chapter 3, and the Algorithm 3.1, to deal with the robust spectral abscissa.

5.2.2 Extension of the probabilistic stability optimization

In the light of the discussion in section 5.1.2, further investigations are focusing on the refinement of the novel approach to larger scale problems with higher stochastic dimension. In particular, to tackle the large system dimension, projection methods are currently considered and analyzed, since they reduce the system dimension, preserving the spectral abscissa behaviors, as briefly presented in section 2.5.

In addition, the developed software [21] could be extended to consider periodic time-delay systems, uncertainty modeled by a general random vector, and further statistical moments in the objective function. Even though these extensions are trivial from

a theoretical point of view, they can be useful in applications. In what follows, we further describe these possible software developments.

Periodic time-delay systems. The extension to periodic time-delay system would generalize the spectrum-based stability assessment and stabilization methods developed in chapter 4 to deal with system affected by uncertainties, modeled by the realizations of a random vector. To consider the uncertainties of the periodic time-delay system, the objective function of the stabilization methods should be defined by a linear combination of statistical moments of the squared spectral radius.

General random variables as uncertainty. In chapter 3, the random vector ω , whose realizations affect the time-delay system (3.1), is assumed to be continuous with support the D -dimensional unit cube, $\Omega = [0, 1]^D$. However, we could extend the approach to discrete, continuous, or mixed random vector ω , if there exist numerical methods to randomly sample from ω accordingly to the probability density function w . Indeed, if it is possible to obtain the random realization from the general random vector ω , then we could approximate the objective function and its gradient by Monte Carlo integration method [29, Chapter 6].

Further statistical moments in the objective function. In the probabilistic stability optimization method, we tune parameters in order to shape the probability density function of the spectral abscissa by considering only mean and variance in the objective function (3.6). However, if the stabilization method considers further statistical moments, appropriately weighted, then we could drive the probability density function of the spectral abscissa to have determined features. For example, considering the third and fourth statistical moments, *i.e.* the skewness and kurtosis, as in [61], we could force the spectral abscissa probability function to be symmetric, skewed to the left, or to rarely have realizations far away from the mean. This generalization requires small additional effort compared to the mean-variance minimization, since the major computational cost to approximate the statistical moments relies on the computation of the spectral abscissa and its gradient for every realization of the uncertainty $\{\xi_m\}_{m=1}^M \subset \Omega$.

5.2.3 Reliable computation of the dominant Floquet multipliers

The eigenvalue problem for the discretized monodromy operator \mathcal{U}_M can also be obtained from a spectral discretization of boundary value problem (4.3). In this latter view, the dependence of matrix $A(s, \mu)$ on μ in the ordinary differential equations is in terms of negative integer powers, suggesting a smoothing effect for the solution, if the Floquet multipliers are large in modulus. Further research can try to clarify whether this implies that for sufficiently large M , outside a given circle in the complex plane, the number of Floquet multipliers match the number of eigenvalues of \mathcal{U}_M . Indeed, as observed in following numerical example, the negative powers of μ in $A(s, \mu)$ seem to be related with the approximation accuracy of the Floquet multipliers by eigenvalues of \mathcal{U}_M .

Example 5.1. Let us consider the scalar system (4.45) with $K = -0.1295$. If $M = 20$, the eigenvalues of \mathcal{U}_M accurately approximate the Floquet multipliers outside a circle of radius 0.15 as illustrated in Figure 5.2a. Squaring the number of collocation points $M = 400$, the Floquet multipliers approximations are accurate outside a circle of radius 0.07, which is approximately half of the initial radius, as shown in Figure 5.2b.

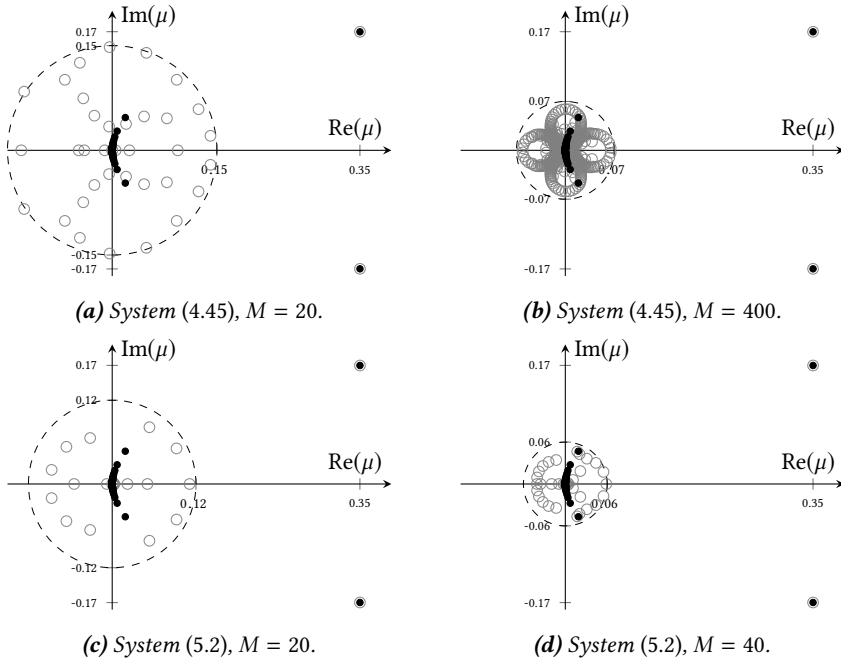


Figure 5.2 The Floquet multiplier approximations obtained as eigenvalues of \mathcal{U}_M (circles) and their analytical value computed by (4.46) (dots). Within the dashed circles, the Floquet multipliers are not approximated by the eigenvalues of the discretized monodromy operator \mathcal{U}_M .

The scalar system, obtained from (4.45) neglecting the $x(t - 2\pi)$ term,

$$\dot{x}(t) = (K \cos(2t))x(t) + (\sin(2t) + K)x(t - \pi), \text{ with } K = -0.1295, \quad (5.2)$$

admits the same Floquet multipliers of (4.45), but the matrix $A(s, \mu)$ in the boundary value problem (4.3) depends on μ only by its inverse, μ^{-1} , and does not present anymore the term μ^{-2} . In this case, if we double the number of collocation points, from $M = 20$ to $M = 40$, the radius of the circle, out of which the Floquet multipliers are accurately approximated by the eigenvalues of \mathcal{U}_M , is halved, from 0.12 to 0.06 as illustrated in the Figures 5.2c and 5.2d.

This investigation could form a theoretical foundation of a heuristic method to robustly determine the number of collocation points M , such that the dominant

Floquet multipliers are accurately approximated by the eigenvalues of \mathcal{U}_M . Moreover, this heuristic method could also permit to locate the rightmost characteristic roots for autonomous time-delay systems, by the relation between the characteristic matrices described in section 4.6.3.

BIBLIOGRAPHY

- [1] ABRAMOWITZ, M., AND STEGUN, I. A., Eds. *Handbook of Mathematical Functions*. Dover Publications Inc., 1965.
- [2] AL-BAALI, M., SPEDICATO, E., AND MAGGIONI, F. Broyden's quasi-Newton methods for a nonlinear system of equations and unconstrained optimization: a review and open problems. *Optim. Methods Softw.* 29 (2013), 937–954.
- [3] BORGIOLO, F. *Spectrum-based Methods and Algorithms for the Robustness Stability Analysis of Delay Systems*. PhD thesis, KU Leuven, 2020.
- [4] BORGIOLO, F., AND MICHIELS, W. Robust stabilisation of linear time-delay systems with uncertainties in the system matrices and in the delay terms. *IFAC Proc. Vol.* 51 (2018), 312–317.
- [5] BOS, L., CALIARI, M., DE MARCHI, S., VIANELLO, M., AND XU, Y. Bivariate Lagrange interpolation at the Padua points: the generating curve approach. *J. Approx. Theory* 143 (2006), 15–25.
- [6] BOUSSAADA, I., TLIBA, S., AND NICULESCU, S. I. A delayed feedback controller for active vibration control: A rightmost-characteristic root assignment based approach. In *2017 21st International Conference on System Theory, Control and Computing (ICSTCC) (2017)*, IEEE.
- [7] BOUSSAADA, I., TLIBA, S., NICULESCU, S. I., ÜNAL, H. U., AND VYHLÍDAL, T. Further remarks on the effect of multiple spectral values on the dynamics of time-delay systems. application to the control of a mechanical system. *Linear Algebra Appl.* 542 (2018), 589–604.
- [8] BREDÁ, D., MASET, S., AND VERMIGLIO, R. *Stability of Linear Delay Differential Equations*. Springer-Verlag New York, 2014.
- [9] BURKE, J. V., LEWIS, A. S., AND OVERTON, M. L. A robust gradient sampling algorithm for nonsmooth, nonconvex optimization. *SIAM J. Optim.* 15 (2005), 751–779.
- [10] BUTCHER, E. A., AND BOBRENKOV, O. A. On the Chebyshev spectral continuous time approximation for constant and periodic delay differential equations. *Commun. Nonlinear Sci. Numer. Simul.* 16 (2011), 1541–1554.
- [11] CAFLISCH, R. E. Monte Carlo and quasi-Monte Carlo methods. *Acta Numer.* 7 (1988), 1–49.
- [12] CALIARI, M., DE MARCHI, S., AND VIANELLO, M. Bivariate Lagrange interpolation at the Padua points: computational aspects. *J. Comput. Appl. Math.* 221 (2008), 284–292.

- [13] CAMPBELL, S. L. Singular linear systems of differential equations with delays. *Appl. Anal.* 11 (1980), 129–136.
- [14] CRESTAUX, T., LE MAÎTRE, O., AND MARTINEZ, J. M. Polynomial chaos expansion for sensitivity analysis. *Reliab. Eng. Syst. Saf.* 94 (2009), 1161–1172.
- [15] DICK, J., KUO, F. Y., AND SLOAN, I. High-dimensional integration: The quasi-Monte Carlo way. *Acta Numer.* 22 (2013), 133–288.
- [16] DRISCOLL, T. A., HALE, N., AND TREFETHEN, L. N., Eds. *Chebfun Guide*. Pafnuty Publications, 2014.
- [17] DU, N. H., LINH, V. H., MEHRMANN, V., AND THUAN, D. D. Stability and robust stability of linear time-invariant delay differential-algebraic equations. *SIAM J. Matrix Anal. Appl.* 34 (2013), 1631–1654.
- [18] EFFENBERGER, C. Robust successive computation of eigenpairs for nonlinear eigenvalue problems. *SIAM J. Matrix Anal. Appl.* 34 (2013), 1231–1256.
- [19] ELMAN, H. C., AND SU, T. Low-rank solution methods for stochastic eigenvalue problems. *SIAM J. Sci. Comput.* 41 (2019), A2657–A2680.
- [20] ERNEUX, T. *Applied Delay Differential Equations*. Springer-Verlag New York, 2009.
- [21] FENZI, L., AND MICHIELS, W. A MATLAB tool for the stabilization of uncertain time-delay systems. lucafe.github.io/Software, 2016.
- [22] FENZI, L., AND MICHIELS, W. Robust stability optimization for linear delay systems in a probabilistic framework. *Linear Algebra Appl.* 526 (2017), 1–26.
- [23] FENZI, L., AND MICHIELS, W. Experiments on polynomial (chaos) approximation of maximum eigenvalue functions: Tutorial. Tech. rep., TW 688, KU Leuven, 2018.
- [24] FENZI, L., AND MICHIELS, W. Polynomial (chaos) approximation of maximum eigenvalue functions. *Numer. Algorithms* 82 (2019), 1143–1169.
- [25] FENZI, L., AND MICHIELS, W. A MATLAB tool for the stability and stabilization of periodic time-delay systems. lucafe.github.io/Software, 2020.
- [26] FENZI, L., PILBAUER, D., MICHIELS, W., AND VYHLÍDAL, T. A probabilistic approach towards robust stability optimization, with application to vibration control. In *Proceedings of the 9th European Nonlinear Dynamics Conference* (2017), F. Stépán and G. Csernák, Eds.
- [27] GHANEM, R., AND GHOSH, D. Efficient characterization of the random eigenvalue problem in a polynomial chaos decomposition. *Int. J. Numer. Methods Eng.* 72 (2007), 486–504.

- [28] GHOSH, D., AND GHANEM, R. Stochastic convergence acceleration through basis enrichment of polynomial chaos expansions. *Int. J. Numer. Methods Eng.* 73 (2007), 162–184.
- [29] GIVENS, G. H., AND HOETING, J. H. *Computational Statistics*. John Wiley & Sons, 2012.
- [30] GUMUSSOY, S., HENRION, D., MILLSTONE, M., AND OVERTON, M. L. Multiobjective robust control with HIFOO 2.0. *IFAC Proc. Vol. 42* (2009), 144–149.
- [31] GUMUSSOY, S., AND MICHIELS, W. Fixed-order H -infinity control for interconnected systems using delay differential algebraic equations. *SIAM J. Control Optim.* 49 (2011), 2212–2238.
- [32] HAKULA, H., KAARNIOJA, V., AND LAAKSONEN, M. Approximate methods for stochastic eigenvalue problems. *Appl. Math. Comput.* 267 (2015), 664–681.
- [33] HALE, J. K. *Theory of Functional Differential Equations*. Springer-Verlag New York, 1977.
- [34] HOMMA, T., AND SALTELLI, A. Importance measures in global sensitivity analysis of nonlinear models. *Reliab. Eng. Syst. Saf.* 52 (1996), 1–17.
- [35] HORN, R. A., AND JOHNSON, C. R. *Matrix Analysis*. Cambridge University Press, 2013.
- [36] HRYNIV, R., AND LANCASTER, P. On the perturbation of analytic matrix functions. *Integr. Equat. Oper. Th.* 34 (1999), 325–338.
- [37] INSPERGER, T., AND STÉPÁN, G. *Semi-Discretization for Time-Delay Systems*. Springer-Verlag New York, 2011.
- [38] JARLEBRING, E. *The Spectrum of Delay-Differential Equations: Numerical Methods, Stability and Perturbations*. PhD thesis, Technische Universität Braunschweig, 2008.
- [39] JARLEBRING, E. Broyden’s method for nonlinear eigenproblems. *SIAM J. Sci. Comput.* 41 (2019), A989–A1012.
- [40] JARLEBRING, E., MEERBERGEN, K., AND MICHIELS, W. Computing a partial Schur factorization of nonlinear eigenvalue problems using the infinite Arnoldi method. *SIAM J. Matrix Anal. Appl.* 35 (2014), 411–436.
- [41] JARLEBRING, E., MICHIELS, W., AND MEERBERGEN, K. A linear eigenvalue algorithm for the nonlinear eigenvalue problem. *Numer. Math.* 122 (2012), 169–195.
- [42] JUST, W. On the eigenvalue spectrum for time-delayed Floquet problems. *Physica D* 142 (2000), 153–165.

- [43] KANGAL, F., MEERBERGEN, K., MENGI, E., AND MICHIELS, W. A subspace method for large-scale eigenvalue optimization. *SIAM J. Matrix Anal. Appl.* 39 (2018), 48–82.
- [44] KATO, T. *Perturbation Theory for Linear Operators*. Springer-Verlag Berlin Heidelberg, 1995.
- [45] KRESSNER, D. A block Newton method for nonlinear eigenvalue problems. *Numer. Math.* 114 (2009), 355–372.
- [46] LAN, J. C., DONG, X. J., PENG, Z. K., ZHANG, W. M., AND MENG, G. Uncertain eigenvalue analysis by the sparse grid stochastic collocation method. *Acta Mech. Sin.* 31 (2015), 545–557.
- [47] LE MAÎTRE, O. P., AND KNIO, O. M. *Spectral Methods for Uncertainty Quantification*. Springer Netherlands, 2010.
- [48] LEWIS, A. S., AND OVERTON, M. L. Nonsmooth optimization via quasi-Newton methods. *Math. Program.* 141 (2013), 135–163.
- [49] LÓPEZ, K., MONDIÉ, S., AND GARRIDO, R. A tuning procedure for the cascade proportional integral retarded controller. *IFAC Proc. Vol.* 51 (2018), 61–65.
- [50] MARELLI, S., AND SUDRET, B. UQLab user manual – polynomial chaos expansions. Tech. rep., Risk, Safety & Uncertainty Quantification, ETH Zurich, 2017.
- [51] MICHIELS, W. Spectrum-based stability analysis and stabilisation of systems described by delay differential algebraic equations. *IET Control Theory Appl.* 5 (2011), 1829–1842.
- [52] MICHIELS, W. Delays effects in dynamical systems and networks: Analysis and control interpretations. In *Nonlinear Systems*. Springer Cham, 2016, pp. 123–136.
- [53] MICHIELS, W., BOUSSAADA, I., AND NICULESCU, S. I. An explicit formula for the splitting of multiple eigenvalues for nonlinear eigenvalue problems and connections with the linearization for the delay eigenvalue problem. *SIAM J. Matrix Anal. Appl.* 38 (2017), 599–620.
- [54] MICHIELS, W., ENGELBORGH, K., VANSEVENANT, P., AND ROOSE, D. Continuous pole placement for delay equations. *Automatica* 38 (2002), 747–761.
- [55] MICHIELS, W., AND FENZI, L. Spectrum-based stability analysis and stabilization of a class of time-periodic time delay systems. *Submitted to SIAM J. Matrix Anal. Appl.*, available at [arXiv 1908.10280](https://arxiv.org/abs/1908.10280), 2019.
- [56] MICHIELS, W., AND GOMEZ, M. A. On the dual linear periodic time-delay system: Spectrum and Lyapunov matrices, with application to \mathcal{H}_2 analysis and balancing. *Submitted for publication*, 2019.

- [57] MICHIELS, W., AND GUGLIELMI, N. An iterative method for computing the pseudospectral abscissa for a class of nonlinear eigenvalue problems. *SIAM J. Sci. Comput.* 34 (2012), A2366–A2393.
- [58] MICHIELS, W., JARLEBRING, E., AND MEERBERGEN, K. Krylov-based model order reduction of time-delay systems. *SIAM J. Matrix Anal. Appl.* 32 (2011), 1399–1421.
- [59] MICHIELS, W., AND NICULESCU, S. I. *Stability, Control and Computation for Time-Delay Systems*. SIAM Society for Industrial and Applied Mathematics, 2014.
- [60] MICHIELS, W., VYHLÍDAL, T., AND ZÍTEK, P. Control design for time-delay systems based on quasi-direct pole placement. *J. Process Control* 20 (2010), 337–343.
- [61] MOHAMMADI, B. Controlling first four moments for robust optimization. *Optim. Eng.* 18 (2016), 561–585.
- [62] MOROKOFF, W. J., AND CAFLISCH, R. E. Quasi-Monte Carlo integration. *J. Comput. Phys.* 122 (1995), 218–230.
- [63] NAZARI, M., BUTCHER, E. A., AND BOBRENKOV, O. A. Optimal feedback control strategies for periodic delayed systems. *Int. J. Dyn. Control* 2 (2014), 102–118.
- [64] OVERTON, M. L. Stability optimization for polynomials and matrices. In *Nonlinear Physical Systems*. John Wiley & Sons, 2014, pp. 351–375.
- [65] PILBAUER, D., BUŠEK, J., KUČERA, V., AND VYHLÍDAL, T. Laboratory set-up design for testing vibration suppression algorithms with time delays. *Trans. VŠB 60* (2014), 87–95.
- [66] PILBAUER, D., VYHLÍDAL, T., AND OLGAC, N. Delayed resonator with distributed delay in acceleration feedback: Design and experimental verification. *IEEE/ASME Trans. Mechatron.* 21 (2016), 2120–2131.
- [67] RAHMAN, S., AND YADAV, V. Orthogonal polynomial expansion for solving random eigenvalue problems. *Int. J. Uncertain. Quan.* 1 (2011), 163–187.
- [68] RAMIREZ, A., MONDIÉ, S., GARRIDO, R., AND SIPAHI, R. Design of proportional-integral-retarded (PIR) controllers for second-order LTI systems. *IEEE Trans. Autom. Control* 61 (2016), 1688–1693.
- [69] RAMÍREZ, A., SIPAHI, R., MONDIÉ, S., AND GARRIDO, R. An analytical approach to tuning of delay-based controllers for LTI-SISO systems. *SIAM J. Control Optim.* 55 (2017), 397–412.

- [70] ROSTAMI, M. W. New algorithms for computing the real structured pseudospectral abscissa and the real stability radius of large and sparse matrices. *SIAM J. Sci. Comput.* 37 (2015), S447–S471.
- [71] ROTT, O., AND JARLEBRING, E. An iterative method for the multipliers of periodic delay-differential equations and the analysis of a PDE milling model. *IFAC Proc. Vol.* 43 (2010), 120–125.
- [72] RUYMBEEK, K., MEERBERGEN, K., AND MICHIELS, W. Calculating the minimal/maximal eigenvalue of symmetric parameterized matrices using projection. *Numer. Linear Algebra Appl.* 26 (2019), 1–17.
- [73] SAADVANDI, M., MEERBERGEN, K., AND DESMET, W. Parametric dominant pole algorithm for parametric model order reduction. *J. Comput. Appl. Math.* 259 (2014), 259–280.
- [74] SARROUY, E., DESSOMBZ, O., AND SINOUE, J. J. Stochastic analysis of the eigenvalue problem for mechanical systems using polynomial chaos expansion - Application to a finite element rotor. *J. Vib. Acoust.* 134 (2012), 1–12.
- [75] SARROUY, E., DESSOMBZ, O., AND SINOUE, J. J. Piecewise polynomial chaos expansion with an application to brake squeal of a linear brake system. *J. Sound Vib.* 332 (2013), 577–594.
- [76] SCHREIBER, K. *Nonlinear Eigenvalue Problems: Newton-Type Methods and Nonlinear Rayleigh Functionals*. PhD thesis, Technische Universität Berlin, 2008.
- [77] SHENG, J., AND SUN, J. Q. Feedback controls and optimal gain design of delayed periodic linear systems. *J. Vib. Control* 11 (2005), 277–294.
- [78] SIEBER, J., ENGELBORGH, K., LUZYANINA, T., SAMAËY, G., AND ROOSE, D. DDE-BIFTOOL manual - Bifurcation analysis of delay differential equations. *arXiv 1406.7144* (2014).
- [79] SIEBER, J., AND SZALAI, R. Characteristic matrices for linear periodic delay differential equations. *SIAM J. Appl. Dyn. Syst.* 10 (2011), 129–147.
- [80] SKUBACHEVSKII, A. L., AND WALTHER, H. O. On the Floquet multipliers of periodic solutions to non-linear functional differential equations. *J. Dynam. Differ. Equations* 18 (2006), 257–355.
- [81] SMITH, H. *An Introduction to Delay Differential Equations with Applications to the Life Sciences*. Springer-Verlag New York, 2011.
- [82] SOBOL, I. M. Global sensitivity indices for nonlinear mathematical models and their Monte Carlo estimates. *Math. Comput. Simulat.* 55 (2001), 271–280.

- [83] SOMMARIVA, A., VIANELLO, M., AND ZANOVELLO, R. Nontensorial Clenshaw-Curtis cubature. *Numer. Algorithms* 49 (2008), 409–427.
- [84] SZALAI, R., AND STÉPÁN, G. Lobes and lenses in the stability chart of interrupted turning. *J. Comput. Nonlin. Dyn.* 1 (2003), 205–211.
- [85] SZALAI, R., STÉPÁN, G., AND HOGAN, S. J. Continuation of bifurcations in periodic delay-differential equations using characteristic matrices. *SIAM J. Sci. Comput.* 28 (2006), 1301–1317.
- [86] SZUDZIK, M. P. The Rosenberg-Strong pairing function. *arXiv 1706.04129* (2017).
- [87] TALVILA, E. Necessary and sufficient conditions for differentiating under the integral sign. *Am. Math. Mon.* 108 (2001), 544–548.
- [88] TOWNSEND, A., WEBB, M., AND OLVER, S. Fast polynomial transforms based on Toeplitz and Hankel matrices. *Math. Comput.* 87 (2018), 1913–1934.
- [89] TREFETHEN, L. N. *Spectral Methods in MATLAB*. SIAM Society for Industrial and Applied Mathematics, 2000.
- [90] TREFETHEN, L. N. *Approximation Theory and Approximation Practice*. Cambridge University Press, 2012.
- [91] TREFETHEN, L. N. Cubature, approximation, and isotropy in the hypercube. *SIAM Rev.* 59 (2017), 469–491.
- [92] VAN BEEUMEN, R., MEERBERGEN, K., AND MICHIELS, W. Compact rational Krylov methods for nonlinear eigenvalue problems. *SIAM J. Matrix Anal. Appl.* 36 (2015), 820–838.
- [93] VANBIERVLIET, J., VERHEYDEN, K., MICHIELS, W., AND VANDEWALLE, S. A nonsmooth optimisation approach for the stabilisation of time-delay systems. *ESAIM: COCV* 14 (2007), 478–493.
- [94] VERMIGLIO, R. Polynomial chaos expansions for the stability analysis of uncertain delay differential equations. *SIAM/ASA J. Uncertain. Quant.* 5 (2017), 278–303.
- [95] VERRIEST, E. I., AND MICHIELS, W. Inverse Routh table construction and stability of delay equations. *Syst. Control Lett.* 55 (2006), 711–718.
- [96] VILLAFUERTE, R., MONDIÉ, S., AND GARRIDO, R. Tuning of proportional retarded controllers: Theory and experiments. *IEEE Trans. Control Syst. Technol.* 21 (2013), 983–990.
- [97] VYHLIDAL, T., AND ZITEK, P. Mapping based algorithm for large-scale computation of quasi-polynomial zeros. *IEEE Trans. Autom. Control* 54 (2009), 171–177.

- [98] VYHLÍDAL, T., ZÍTEK, P., AND PAULŮ, K. Design, modelling and control of the experimental heat transfer set-up. In *Topics in Time Delay Systems*. Springer-Verlag Berlin Heidelberg, 2009, pp. 303–313.
- [99] WANG, H., AND XIANG, S. On the convergence rates of Legendre approximation. *Math. Comput.* 81 (2011), 861–877.
- [100] WILLIAMS, M. M. R. A method for solving stochastic eigenvalue problems II. *Appl. Math. Comput.* 219 (2013), 4729–4744.
- [101] XIANG, S. An improved error bound on Gauss quadrature. *Appl. Math. Lett.* 58 (2016), 42–48.
- [102] XIANG, S., AND BORNEMANN, F. On the convergence rates of Gauss and Clenshaw-Curtis quadrature for functions of limited regularity. *SIAM J. Numer. Anal.* 50 (2012), 2581–2587.
- [103] XIU, D. *Numerical Methods for Stochastic Computations*. Princeton University Press, 2010.

CURRICULUM VITAE

Personal information

Name	Luca Fenzi
Date of birth	24 February 1991
Place of birth	Verona (Italy)
e-mail	fenzi.luca@gmail.com
Website	lucafe.github.io

Curriculum studiorum

Ph.D. Candidate Department of Computer Science, KU Leuven, Belgium.	2015–2020
Master of Mathematics Università degli Studi di Udine, Italy	2013–2015
Scuola Superiore Università degli Studi di Udine, Italy	2010–2015
Erasmus exchange program NTNU, Trondheim, Norway	2015
Bachelor of Mathematics Università degli Studi di Udine, Italy	2010–2013

Honors and Awards

Datathon Best pitch and Second-best Ph.D. team Department of Computer Science, KU Leuven, Belgium.	2019
Giulio Chiesi memorial prize for the best master's thesis with engineering applications Università degli Studi di Udine, Italy	2016
Best graduate student in Mathematics Università degli Studi di Udine, Italy	2016

PUBLICATIONS & SOFTWARES

INTERNATIONAL JOURNAL PAPERS

W. Michiels & Luca Fenzi. *Spectrum-based stability analysis and stabilization of a class of time-periodic time-delay systems*, Submitted to SIAM Journal on Matrix Analysis and Applications, preprint available at arXiv:1908.10280 (2019).

Luca Fenzi & W. Michiels. *Polynomial (chaos) approximation of maximum eigenvalue functions*, Numerical Algorithms, 82:1143–1169 (2019).

Luca Fenzi & W. Michiels. *Robust stability optimization for linear delay systems in a probabilistic framework*, Linear Algebra and its Application, 526:1–26 (2017).

INTERNATIONAL CONFERENCES PROCEEDINGS - FULL PAPERS

Luca Fenzi, D. Pilbauer, W. Michiels & T. Vyhlídal. *A probabilistic approach towards robust stability optimization*, Proceedings of the 9th European Nonlinear Dynamics Conference (ENOC), Budapest (2017).

SOFTWARES AND TUTORIAL

AVAILABLE AT [LUCAFE.GITHUB.IO/SOFTWARE](https://lucafe.github.io/software)

Luca Fenzi & W. Michiels. *Stability and stabilization of periodic time-delay systems*, (2020).

Luca Fenzi & W. Michiels. *Tutorial on polynomial (chaos) eigenvalue functions*, (2018).

Luca Fenzi & W. Michiels. *Stability optimization of uncertain delay equations*, (2016).

INTERNATIONAL CONFERENCES PROCEEDINGS - ABSTRACTS

Luca Fenzi & W. Michiels. *Polynomial (chaos) approximation of the spectral abscissa: Efficiency and limitations*, Time Delay Systems (TDS), Budapest (2018).

Luca Fenzi & W. Michiels. *Robust stability optimization for delay differential algebraic equations in a probabilistic framework*, European Conference on Computational Optimization (EUCCO), Leuven (2016).

FACULTY OF ENGINEERING SCIENCE
DEPARTMENT OF COMPUTER SCIENCE
NUMERICAL ANALYSIS & APPLIED MATHEMATICS

Celestijnenlaan 200A box 2402

B-3001 Leuven

fenzi.luca@gmail.com

lucafe.github.io

